Precipitation
in
Iron-Chromium-Nitrogen Alloys

with an appendix on the crystal structure
of manganese carbide ($Mn_{22}C_6$)

A dissertation submitted for the degree of
Doctor of Philosophy
of the University of Newcastle upon Tyne.

by

Brian Mortimer

Department of Metallurgy,
University of Newcastle upon Tyne.

September, 1971

Preface

This dissertation describes original work which has not been submitted for a degree at any other university.

The investigations were carried out in the Department of Metallurgy of the University of Newcastle upon Tyne during the period October, 1968 to September, 1971 under the supervision of Professor K.H. Jack and Dr. P. Grieveson.

The major part of the thesis describes a study of the nitriding of iron-chromium alloys and is part of a wider investigation being carried out at Newcastle on the effect of substitutional alloying elements on the behaviour of interstitial solutes in iron. A subsidiary topic describing work on the crystallography of some interstitial alloys is discussed in an appendix.

Acknowledgements

I wish to thank Professor K.H. Jack and Dr. P. Grieveson for their advice, discussion, encouragement and general supervision of the work.

I also wish to thank:

Professor N.J. Petch for providing facilities in the Department of Metallurgy of the University of Newcastle upon Tyne;

The Science Research Council for the award of a maintenance grant;

Dr. L. Mercer and his staff at the Gas Council Engineering Research Station, Killingworth, Newcastle upon Tyne for the use of electron microscopy facilities. In particular I wish to thank Mr. P. Rodgerson;

Professor H.M. Thirsk and his staff in the Electron Microscopy Section, Chemistry Department, of the University of Newcastle upon Tyne for electron microscopy facilities;

Many colleagues in the Department of Metallurgy of the University of Newcastle upon Tyne, for stimulating discussion and advice. The assistance of the technical staff of the Department is greatly appreciated;

My wife for typing the script.

Brian Mortimer

September, 1971

Abstract

Precipitation reactions in iron-chromium alloys containing nitrogen are studied by X-ray methods and by optical and electron microscopy.

By experimental control of reaction conditions, seven different phases are identified in iron alloys containing up to 40wt.% chromium nitrided at 450 - 1050°C. The precipitation of chromium nitrides is shown to be consistent with the thermodynamic properties of these phases.

Quench-aging observations on nitrogen-ferrites show that precipitation of iron nitrides below 400°C is markedly affected by the presence of chromium in solution. The results are explicable when the effect of chromium in decreasing the activity coefficient of dissolved nitrogen is taken into account. These observations are compared with recent work on precipitation of iron nitrides in iron-molybdenum-nitrogen and iron-silicon-nitrogen alloys.

Previous observations at Newcastle, of homogeneous precipitation in the iron-nitrogen system and in ternary iron-alloy element-nitrogen alloys containing molybdenum, niobium, titanium or silicon are extended to the technologically important Fe-Cr-N system. The precipitation reactions, which go through the stages well-recognised in face-centred cubic alloys i.e.

Guinier-Preston zones ⟶ metastable intermediate precipitate ⟶ equilibrium precipitate,

are discussed and compared with the observations in the present investigation. In addition, the effects of chromium content and nitrogen potential on the kinetics of nitriding are reported.

The crystal structure and X-ray line broadening of the manganese carbide, $Mn_{22}C_6$, are discussed in an appendix.

Contents

Introduction

Until recently, little systematic work has been carried out on the characterization of nitride phases precipitated from iron containing nitrogen and a substitutional alloying element. Small amounts of manganese and nitrogen added to iron (Baird & Jamieson, 1963; Forrest & Hopkin, 1963; Baird & Mackenzie, 1964; Hopkin, 1965; Baird & Jamieson, 1966) were shown about ten years ago to give improvements in tensile strength and creep resistance, and subsequent research at Newcastle (see Pipkin, 1967) showed that these are due, at least in part, to the precipitation of manganese nitrides.

More recently in this laboratory, exceptionally hard materials containing mixed substitutional-interstitial solute-atom clusters have been observed by nitriding iron-molybdenum (see Spiers, 1969) and iron-niobium alloys (see Roberts, 1970) at 450 - 600°C.

Because chromium is a major constituent of steel used for case hardening by nitriding, a similar systematic investigation of the iron-chromium-nitrogen system was considered desirable. Further, it seemed worthwhile to carry out a detailed examination of the precipitation processes under conditions similar to those used industrially.

As the subsidiary binary systems are well established, only a limited amount of work has been carried out to confirm the main features of the chromium-nitrogen system. The previous investigations provide reliable data on which to base a study of the ternary system.

Experimental methods include X-ray diffraction and electron microscopy as well as the usual physico-metallurgical and physico--chemical techniques. During the course of the work, the application of thermodynamic principles was found to be essential for the interpretation of the precipitation results and in the use of gas-metal equilibration.

Chapter I

Previous Work

I.1 The iron-nitrogen phase diagram

In the iron-nitrogen phase diagram shown in Figure I.1 (Jack, 1951a) there are five stable phases (α - nitrogen ferrite, γ - nitrogen austenite, γ' - Fe_4N, ε -"Fe_3N" and ζ - Fe_2N) and two metastable phases (α' - nitrogen martensite and α'' - $Fe_{16}N_2$). The solubilities of γ' - Fe_4N and α'' - $Fe_{16}N_2$ in body-centred cubic ferrite are of particular interest for the present work and are shown in Figure I.2 with the nitrogen solubility at one atmosphere pressure of molecular nitrogen included for comparison. Face-centred cubic nitrogen-austenite is isostructural with carbon-austenite but has a wider range of homogeneity and exist down to 590°C. At this eutectoid temperature the nitrogen concentration of γ is 2.35wt.% and that of α is 0.1wt.%.

γ' - Fe N has a face-centred cubic metal-atom arrangement like austenite but the nitrogen atoms are fully ordered and occupy one fourth of the number of octahedral interstices (see Figure I.3).

The ε -phase extends from about 5 to 11.1 wt.%N, i.e. approximately from Fe_4N to Fe_2N, and has a close-packed hexagonal iron-atom lattice. The orthorhombic ζ - Fe_2N is a slightly distorted modification of ε resulting from a change in the nitrogen-atom ordering. The occupation of interstices in ε is ordered over its whole homogeneity range and the $\varepsilon \rightarrow \zeta$ transition occurs by a change from one ordered nitrogen-atom arrangement to a different but equally ordered arrangement which causes an anisotropic expansion of the iron-atom lattice. Relationships between the hexagonal ε unit cell dimension a_ε and c_ε and the orthorhombic ζ dimensions a_ζ, b_ζ and c_ζ are:

$$a_\zeta \approx \sqrt{3}\, a_\varepsilon \; ; \; b_\zeta \approx 2\, a_\varepsilon \; ; \; c_\zeta \approx c_\varepsilon$$

Fig.I.1

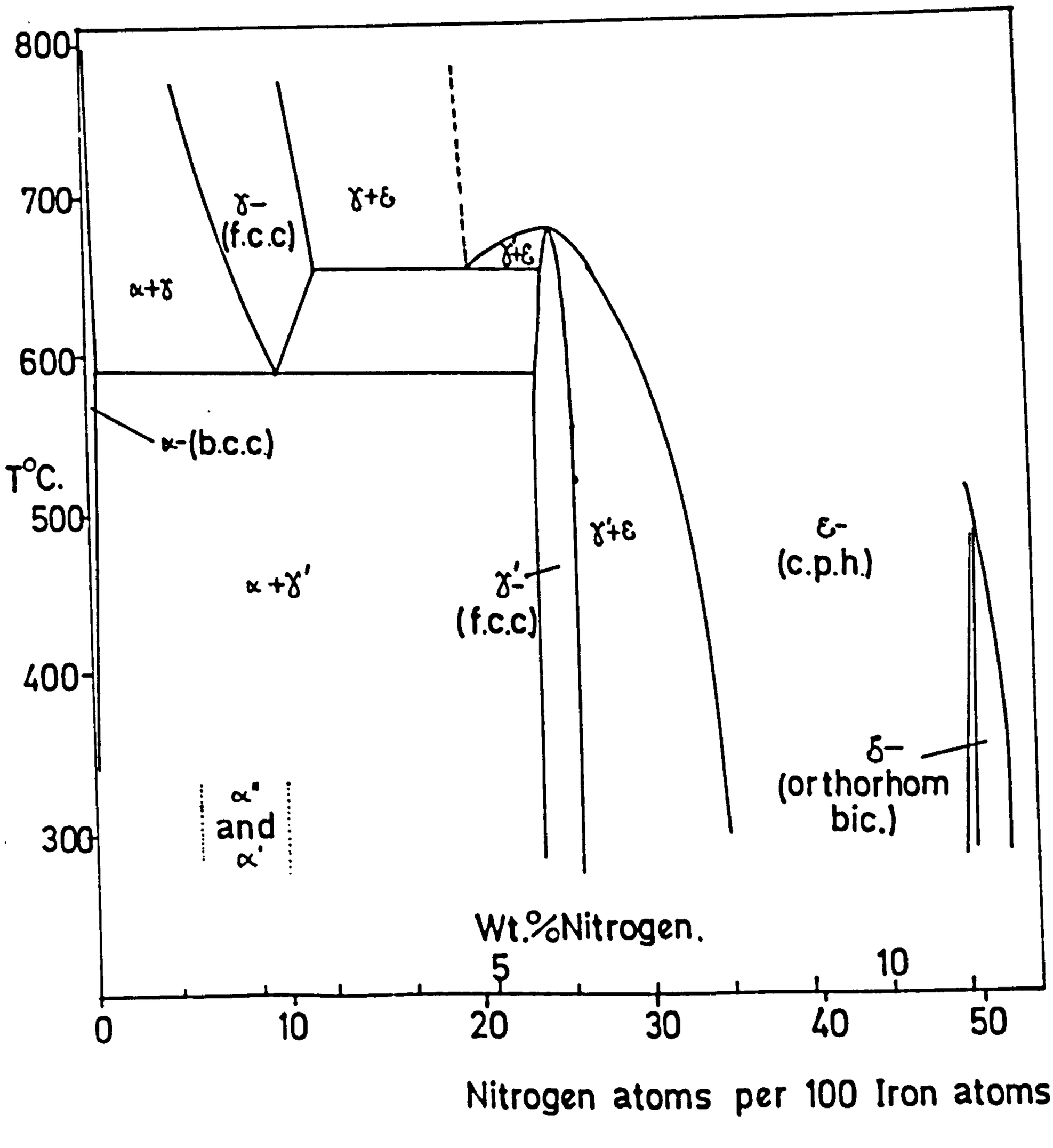

THE IRON-NITROGEN PHASE DIAGRAM.[After Jack, 1951].

Fig. I.2

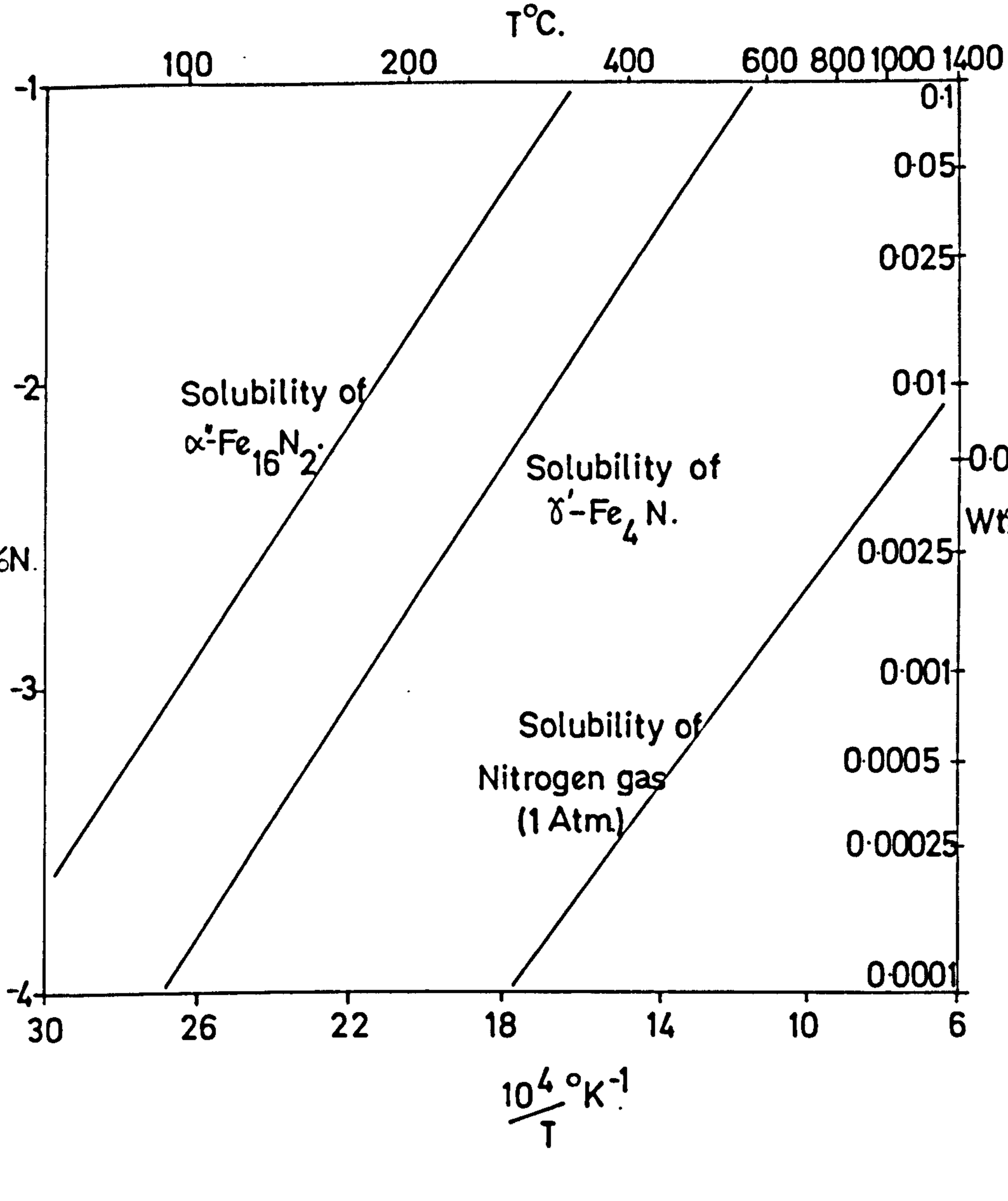

THE SOLUBILITY OF NITROGEN AND IRON NITRIDES IN α-IRON.

Fig.I.3

γ

nitrogen austenite

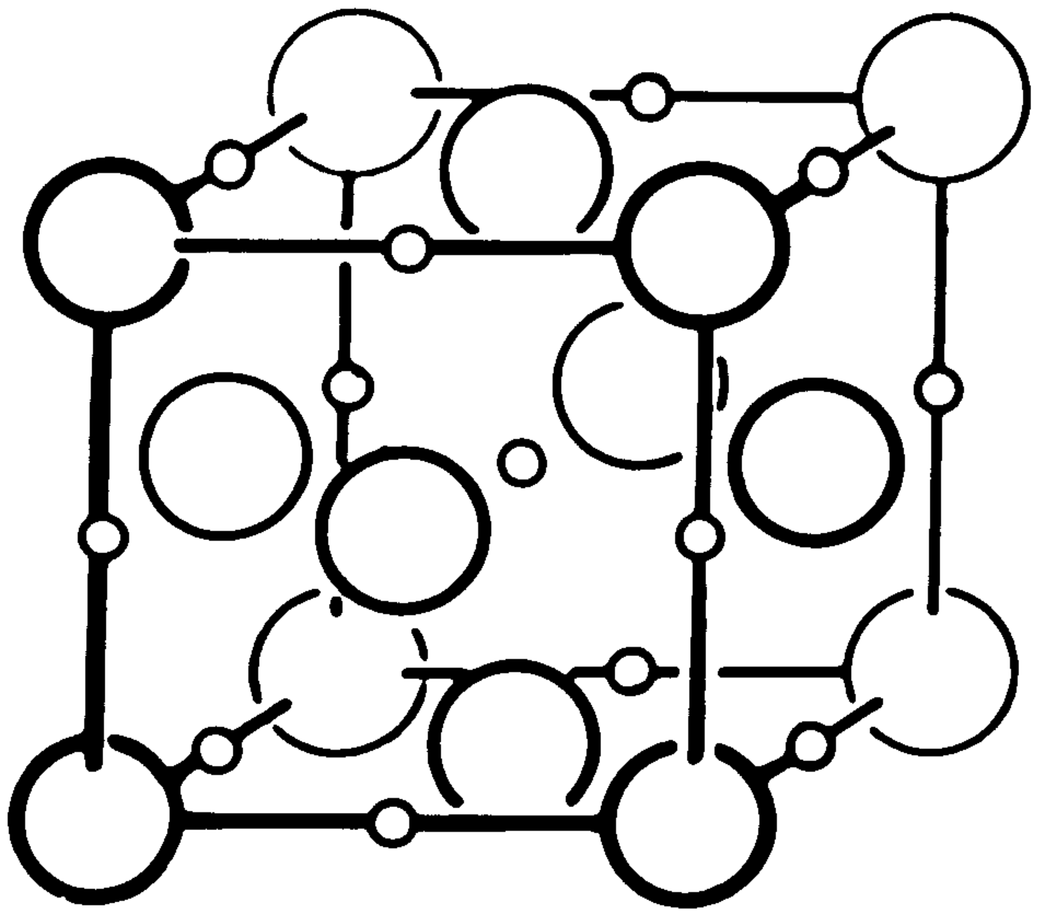

γ′

Fe_4N

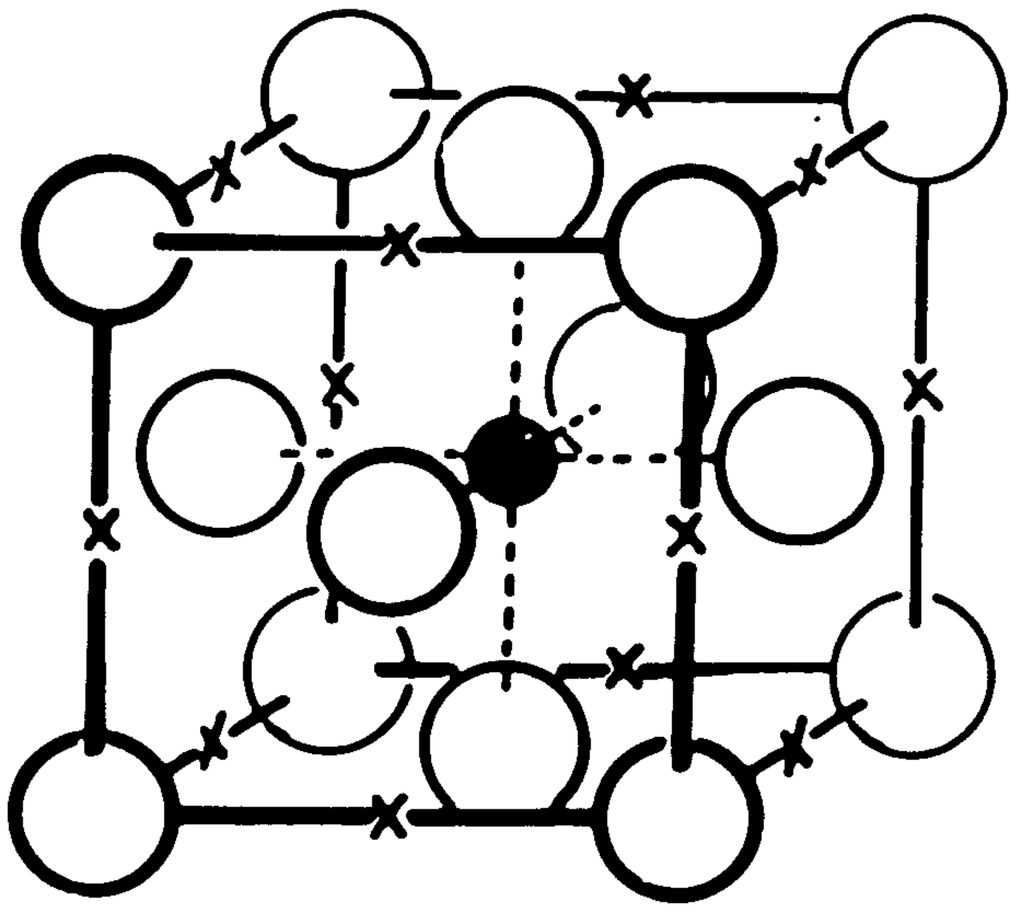

○ Fe atoms

× unoccupied interstices

o octahedral interstices 1 in 10 randomly filled

● N atom

Body centred tetragonal nitrogen-martensite (α') is isostructural with carbon-martensite and is obtained by quenching nitrogen-austenite. α''- $Fe_{16}N_2$ occurs as an intermediate precipitate during the tempering of nitrogen-martensite or the aging of supersaturated nitrogen-ferrite. The composition ranges and unit cell dimensions of all iron-nitrogen phases are summarised in Table I.1.

I.2 The quench-aging of nitrogen-ferrite

Contrary to what might be expected from the phase diagram, the aging of supersaturated nitrogen-ferrite at low temperatures is not a single stage process. Dijkstra (1949) aged an iron - 0.05 wt.%N alloy at 250°C and established by internal friction and metallographic methods that initially a precipitate designated as "N-phase I" grew as platelets in three perpendicular directions. After forty minutes a new phase ("N-phase II") was precipitated and this increased at the expense of the first phase until after three hours none of the latter remained. This second phase was assumed by Dijkstra to be γ'- Fe_4N. Further internal friction studies by Wert (1949) showed that the rate-controlling step in the precipitation of "N-phase I" was the diffusivity of nitrogen in ferrite.

Using X-ray techniques, Jack & Maxwell (1952) showed that the initial precipitate was α''- $Fe_{16}N_2$; a phase characterized by Jack (1951b) during the tempering of nitrogen-martensite at low temperatures. Jack & Maxwell suggested that α'' was precipitated as thin platelets on $\{100\}_\alpha$ planes with $[00]_{\alpha''}$ normal to the plane of the platelet. This was based on the observation that no more than three orientations of α'' were observed in any one grain in optical micrographs and on the relaxation of the Laue conditions for diffraction from α''- $Fe_{16}N_2$ lattices planes where l is large compared with h and k; this suggests that the plates of precipitate are thin in the c-direction.

Table I.1

Unit-cell dimensions and composition limits of iron-nitrogen phases

phase symbol	crystal structure	composition limits	unit-cell dimensions, Å	wt.%N	references
α	b.c.c.	0 - 0.1wt.%N;	a = 2.866	0	Wriedt & Zwell (1962)
		$Fe-FeN_{0.01}$	a = 2.869	0.1	
γ	f.c.c.	0 - 2.8wt.%N;	a = 3.615	1.5	Paranjpe et. al.(1950)
		$Fe-FeN_{0.12}$	a = 3.654	2.8	
			a = 3.571	0	Jack (1951a)
			a = 3.645	2.4	
γ'	cubic	5.29-5.7wt.%N;	a = 3.791	5.29	Paranjpe et. al.(1950)
		$FeN_{0.23}-FeN_{0.24}$	a = 3.801	5.71	
		5.75-6.10wt%N;	a = 3.787	5.75	Jack (1948)
		$FeN_{0.24}-FeN_{0.26}$	a = 3.795	6.10	
ε	c.p.hexagonal (dimensions for pseudo-cell)	5.70-11.0wt.%N;	a = 2.660; c = 4.344	5.70	Jack (1948)
		$FeN_{0.24}-FeN_{0.49}$	a = 2.764; c = 4.420	11.0	
			a = 2.657; c = 4.380	7.30	Paranjpe et.al.(1950)
			a = 2.770; c = 4.432	11.0	
ζ	orthorhombic (dimensions for pseudo-cell)	11.1-11.3wt.%N;	a = 2.762; b = 4.830;	11.3	Jack (1948)
		$FeN_{0.50}-FeN_{0.51}$	c = 4.416.		
α'	b.c. tetragonal	as γ-austenite	a = 2.851; c = 3.071	2.30	Jack (1951a)
α"	tetragonal	3.1wt.%N	a = 5.72 ; c = 6.29	3.1	Jack (1951b)
		$FeN_{0.13}$			

The α''- $Fe_{16}N_2$ crystal structure is shown in Figure I.4 and consists of eight body-centred cubic ferrite cells distorted by the presence of nitrogen. The nitrogen atoms occupy two of the sixteen interstices whose tetrad axes are all parallel with one of the cube directions, i.e. the c-edge. The resulting cell is tetragonal and can be considered as an anisotropic distortion of the ferrite structure with an expansion ($\sim$11%) in the c-direction and a slight contraction ($\sim$0.3%) in the two a-directions. This phase could then be expected to precipitate as thin platelets on $\{100\}_\alpha$ planes with $[001]_\alpha$ normal to the plane of each precipitate.

It seems possible for γ'- Fe_4N to be nucleated directly from α''- $Fe_{16}N_2$ since the latter can be considered as an array of distorted face-centred cubic cells with the octahedral interstices at $(\frac{1}{2},\frac{1}{2},\frac{1}{2})$ occupied in alternate cells. However, there is no metallographic evidence that γ' is nucleated from α''.

The orientation relationship proposed by Jack & Maxwell was confirmed by Booker, Norbury & Sutton (1957), Keh & Wreidt (1962), Hale & M^{c}Lean (1963) and Roberts (1970). Hrivnak (1961) states that up to 300^{o}C ε- Fe_3N is the first phase to precipitate on aging supersaturated nitrogen-ferrite but this has not been substantiated by later investigations.

The orientation relationship between γ-Fe_4N and α- iron was shown by Mehl, Barrett & Jerabek (1934) and by Booker, Norbury & Sutton (1957) to be:

$$(\,112\,)_{\gamma'} /\!/ (\,210\,)_\alpha \quad ; \qquad [110]_{\gamma'} /\!/ [001]_\alpha .$$

Growth of γ' plates is such that $(112)_{\gamma'}$ is parallel to the plate surface.

I.3 The chromium-nitrogen system

This system has been studied extensively over the past 150 years (see Hansen, 1958) and with few exceptions these investigations

Fig. I. 4

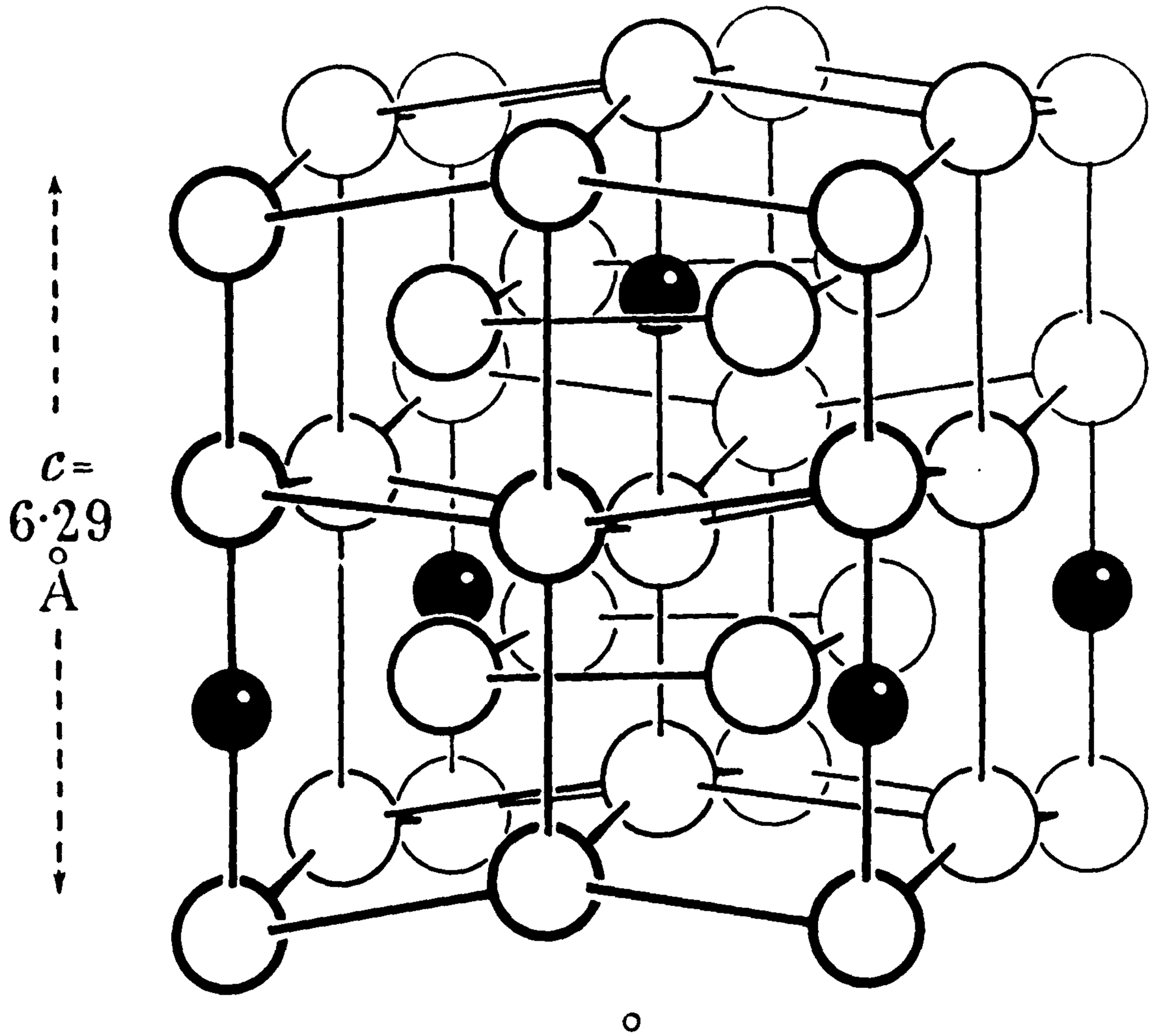

have indicated the existence of only two nitrides of chromium, Cr_2N and CrN. Adcock (1926) proposed the phase diagram shown in Figure I.5. Subsequent X-ray work by Blix (1929) showed that Cr_2N has close-packed hexagonal metal-atom arrangement with unit cell dimensions:

$a' = 2.747$; $c' = 4.439$; $c/a = 1.616$Å (at N-poor boundary)
$a' = 2.770$; $c' = 4.474$; $c/a = 1.615$Å (at N-rich boundary).

Later investigation by Eriksson (1934) showed a superlattice due to the ordering of the nitrogen atoms and a range of composition for Cr_2N from 9.3 to 11.9wt.%N with unit cell dimensions:

$a = 4.750$; $c = 4.429$; $c/a = 0.933$Å at 9.3wt.%N
$a = 4.796$; $c = 4.470$; $c/a = 0.932$Å at 11.9wt.%N.

This larger unit cell with the superlattice has three times the volume of the pseudo-cell proposed by Blix with

$$a' = \sqrt{3}.\ a \qquad \text{and} \qquad c' = c$$

where a'and c'are the dimensions of the superlattice cell.

These observations have been confirmed by Hume-Rothery & Pearson (1949).

CrN is face-centred cubic with a = 4.148 (Blix,1929) or 4.149Å (Schönberg, 1954).

I.4 The iron-chromium system

The equilibrium diagram for the industrially important iron-chromium system is shown in Figure I.6 (after Hansen, 1958) and is based mainly on thermal analysis by Adcock (1931) and X-ray and metallographic investigation by Cook & Jones (1943).

I.5 Precipitation in iron-chromium-nitrogen alloys

Although a great deal of research has been carried out on the solubility of nitrogen in iron-chromium alloys (Adcock, 1926 ; Krivobok, 1935; Franks, 1935; Colbeck & Garner, 1939; [illegible] Corney & Turkdogan, 1955) there are few investigations of the ternary

Fig. I.5.

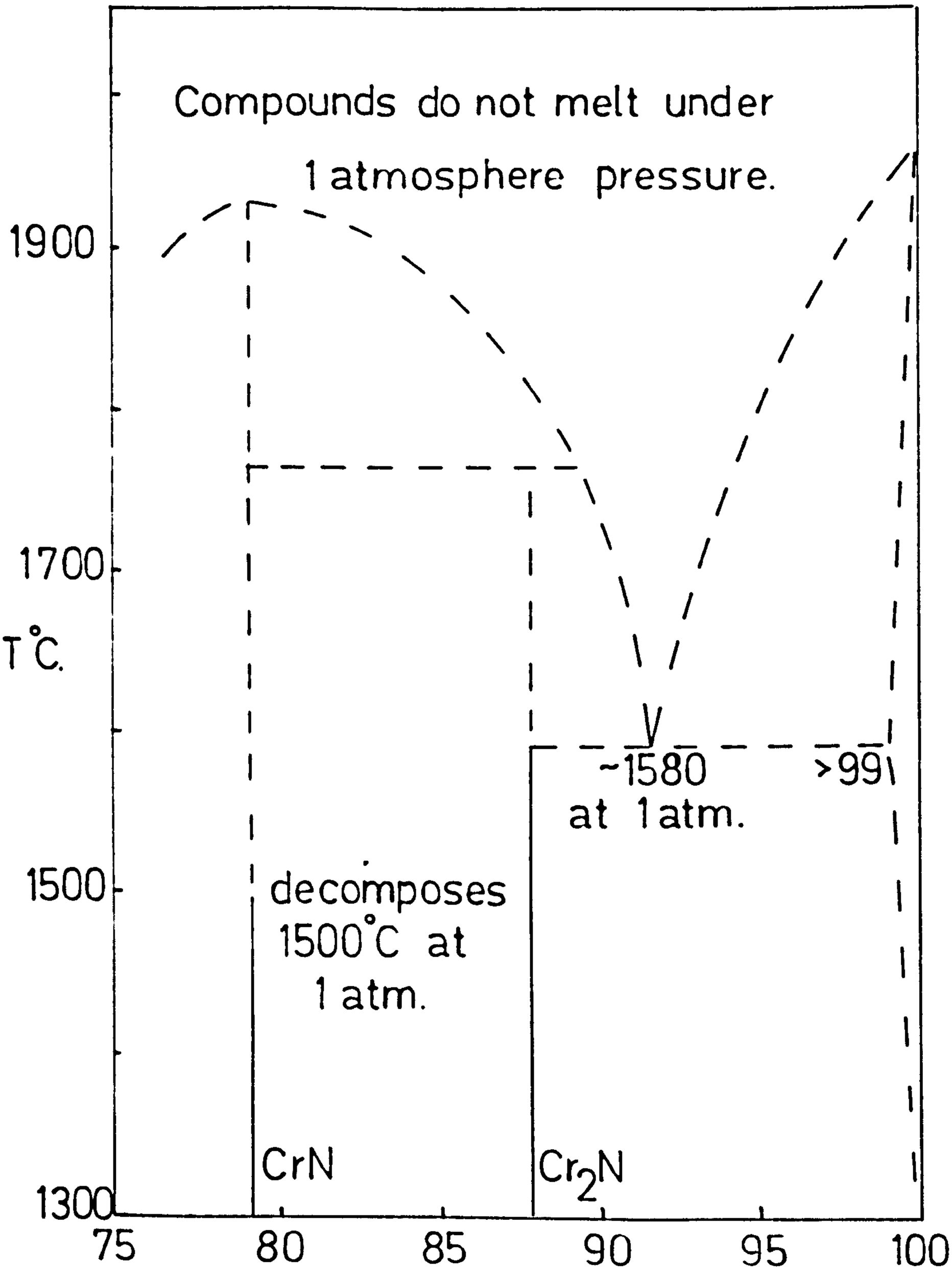

CHROMIUM - NITROGEN PHASE DIAGRAM

(Adcock, 1926.)

Fig. I.6

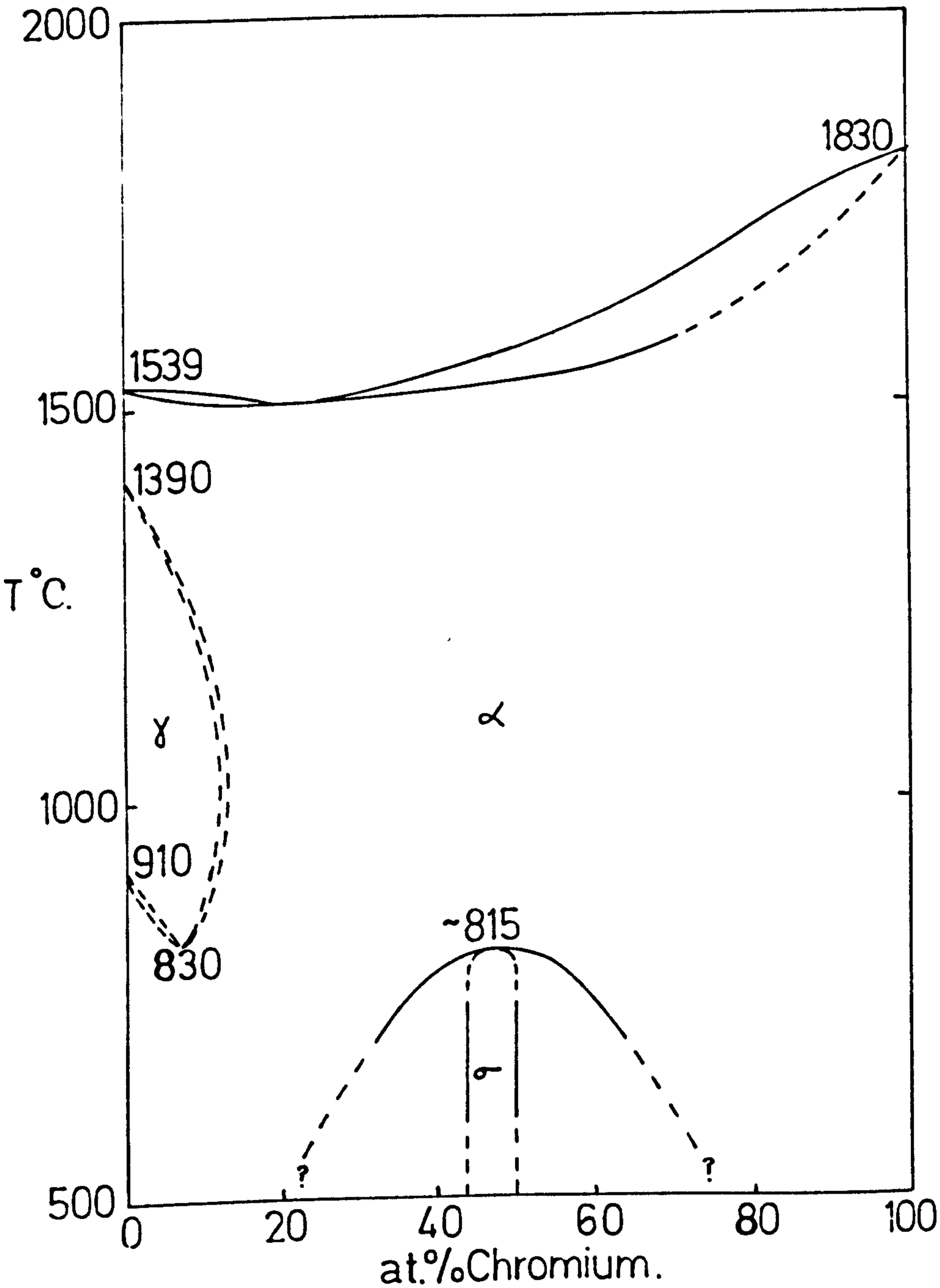

IRON-CHROMIUM PHASE DIAGRAM.

(Hansen, 1958.)

system and little work has been carried out on precipitation of nitrides from these alloys.

Turkdogan & Ignatowicz (1961) studied nitrogen-austenitised iron-chromium steels containing 15 - 30 wt.%Cr and found that Cr_2N was precipitated in the ferrite after quenching from 1200°C; this has been confirmed (Langeborg, 1967).

CrN is precipitated only by quench-aging low chromium alloys (see Imai et. al.,1967); it is the principal nitride formed during the case-hardening of steels by nitriding because chromium is the major alloying element in such steels. The very recent kinetic work of Kindleman & Ansell (1970) on the nitriding of austenitic iron-chromium-niobium-titanium alloys in ammonia shows that the chromium nitride which is formed is CrN.

Chapter II

Experimental Methods

II.1 The preparation of alloy samples

High-purity iron and iron-chromium alloys containing 7.35, 9.9, 14.0, 29.8 and 39.6wt.% chromium were supplied by the British Iron and Steel Research Association. Other pure alloys from the National Physical Laboratory with 1.20, 2.32, 4.12 and 5.58wt.% chromium have also been used. Analyses of all alloys are given in Table II.1.

Pure chromium powder was prepared by crushing chromium flake supplied by Koch Light Ltd.; its analysis is also included in Table II.1.

Samples of the alloys were prepared for investigation by sectioning the as-received hot-rolled bar and then cold rolling to the required thickness. After cleaning, wire of approximately square section or sheet specimens were cut from this rolled strip. Specimens were then abrasively cleaned and degreased before nitriding.

II.2 Nitriding with ammonia-hydrogen gas mixtures

The nitriding potential of an ammonia-hydrogen gas mixture is determined by the ratio of the concentrations of ammonia and hydrogen; Lehrer (1930), Brunhauer, Jefferson, Emmett & Hendricks (1931) and Paranje, Cohen, Bever & Floe (1950). The nitriding reaction is

$$NH_{3(g)} \quad = \quad \underline{N} + \tfrac{3}{2}H_{2(g)} \qquad \ldots\ldots(1)$$

with the equilibrium constant

$$K_1 \quad = \quad a_N \cdot p_{H_2}^{3/2} \Big/ p_{NH_3}$$

where a_N is the activity of nitrogen in the nitride phase and p_{NH_3} and p_{H_2} are the partial pressures of ammonia and hydrogen

Table II.1

Analysis of metals and alloys (wt.%)

Alloy	C	Cr	Si	Mn	S	P	Ni	O	N
38AF3*	0.0028	1.20	0.003	0.005	0.0048	0.0001	0.006	0.002	0.0008
38AF2*	0.0038	2.32	0.003	-	0.0045	-	-	0.0024	0.0014
37AF3*	0.0042	4.12	0.003	-	0.0039	-	-	0.001	0.0032
37AF2*	0.003	5.58	0.014	-	0.0042	0.001	0.005	0.0015	0.0022
Bisra Fe	0.004	0.01	0.005	0.01	0.0018	0.0007	0.01	0.002	0.003
K1007[x]	0.01	7.35	-	-	-	-	-	-	-
K1008[x]	0.01	9.9	-	-	-	-	-	-	-
K1010[x]	0.01	14.0	-	-	-	-	-	-	-
K1183[x]	0.006	29.8	-	-	-	-	-	-	-
K1184[x]	0.005	39.6	-	-	-	-	-	-	-
Cr	—	99.99	-	-	-	-	-	-	-

* N.P.L. Reference numbers.

x B.I.S.R.A. Cast numbers.

respectively. The activity of nitrogen is therefore proportional to $p_{NH_3}/p_{H_2}^{3/2}$.

In the iron-nitrogen system at 620°C the successive phases formed with increasing nitrogen content are α- solid solution, γ- solid solution and γ'- Fe_4N. When an iron specimen is exposed to an ammonia-hydrogen mixture of sufficient nitrogen potential to form Fe_4N then the activity of the combined nitrogen will vary in the following way. It will increase from zero in the α pure metal to a value of $a_N^{\alpha\text{-max}}$ in the saturated nitrogen ferrite (i.e. at the limit of the terminal solid solution). The α- phase is then in equilibrium with the γ- phase of composition γ^{min} such that the nitrogen activity $a_N^{\gamma\text{-min}}$ is equal to $a_N^{\alpha\text{-max}}$. As the total nitrogen content increases, the α- phase will disappear. When no α remains, the activity of nitrogen in γ increases and the composition of γ changes. Enentually, the solubility limit in γ is reached and at this point $a_N^{\gamma\text{-max}}$ is equal to $a_N^{\gamma'\text{-min}}$. The γ'- phase then forms at the expense of the γ- phase and finally the activity of nitrogen in the γ' increases to the value in equilibrium with the nitriding gas.

In any single nitride phase the nitrogen activity will vary regularly with composition and therefore, since a_N is proportional to $p_{NH_3}/p_{H_2}^{3/2}$, a gas mixture of given composition is in equilibrium with a nitride of fixed nitrogen content. Theoretically, it is possible to prepare a nitride or iron-nitrogen solid solution of any composition by precise control of the ammonia-hydrogen gas ratio. In practice there are two complicating reactions:

(a) the "cracking" of ammonia,

$$NH_{3(g)} \rightleftharpoons \tfrac{1}{2}N_{2(g)} + \tfrac{3}{2}H_{2(g)} \qquad \ldots.(3)$$

where the equilibrium mixture contains only a few per cent of ammonia at normal nitriding temperatures and,

(b) the thermal decomposition of the nitride

$$\underline{N} \rightleftharpoons \tfrac{1}{2}N_{2(g)} \qquad \ldots.(4)$$

which for iron nitrides is virtually non-reversible at one atmosphere pressure.

If the catalytic effect of the metal sample and the reaction tube upon the cracking of ammonia is constant, then the degree to which the gas approaches its equilibrium $NH_3:H_2:N_2$ mixture is determined by the gas flow. The flow rate must therefore be controlled as well as the gas composition if the required nitrogen potential is to be maintained and if the nitriding rate is to exceed the rate of decomposition of the required nitride. Clearly, the nitriding action of ammonia on metals can be very complex since it depends upon the balance of three reactions which are affected by temperature, by the gas composition, by the catalytic effect of the surfaces to which the gas is exposed, by gas flow rates, by the decomposition pressures of the solid phases and by previous treatment and impurities in the metal itself. As a guide to the nitrogen potentials and to the ammonia hydrogen ratios required to produce given quantities of nitrogen in solution in iron, the diagrams compiled by Lehrer (1930) and shown in Figure II.1 were used.

II.3 Nitrogen-hydrogen nitriding

The nitrogen potential of a nitrogen-hydrogen mixture is determined by the partial pressure of nitrogen. The nitriding reaction is

$$\tfrac{1}{2}N_{2(g)} \rightleftharpoons \underline{N} \qquad \ldots.(5)$$

for which the equilibrium constant is

$$K_2 = a_N / p_{N_2}^{\frac{1}{2}} . \qquad \ldots.(6)$$

Applying Henry's Law, which is obeyed over the whole range of nitrogen solubility in α- iron, equation (6) can be written:

$$K_3 = \text{wt.}\%N / p_{N_2}^{\frac{1}{2}} \qquad \ldots.(7)$$

Similarly, the equilibrium constant for the ammonia nitriding reaction, equation (2), can be written:

Fig. II.1

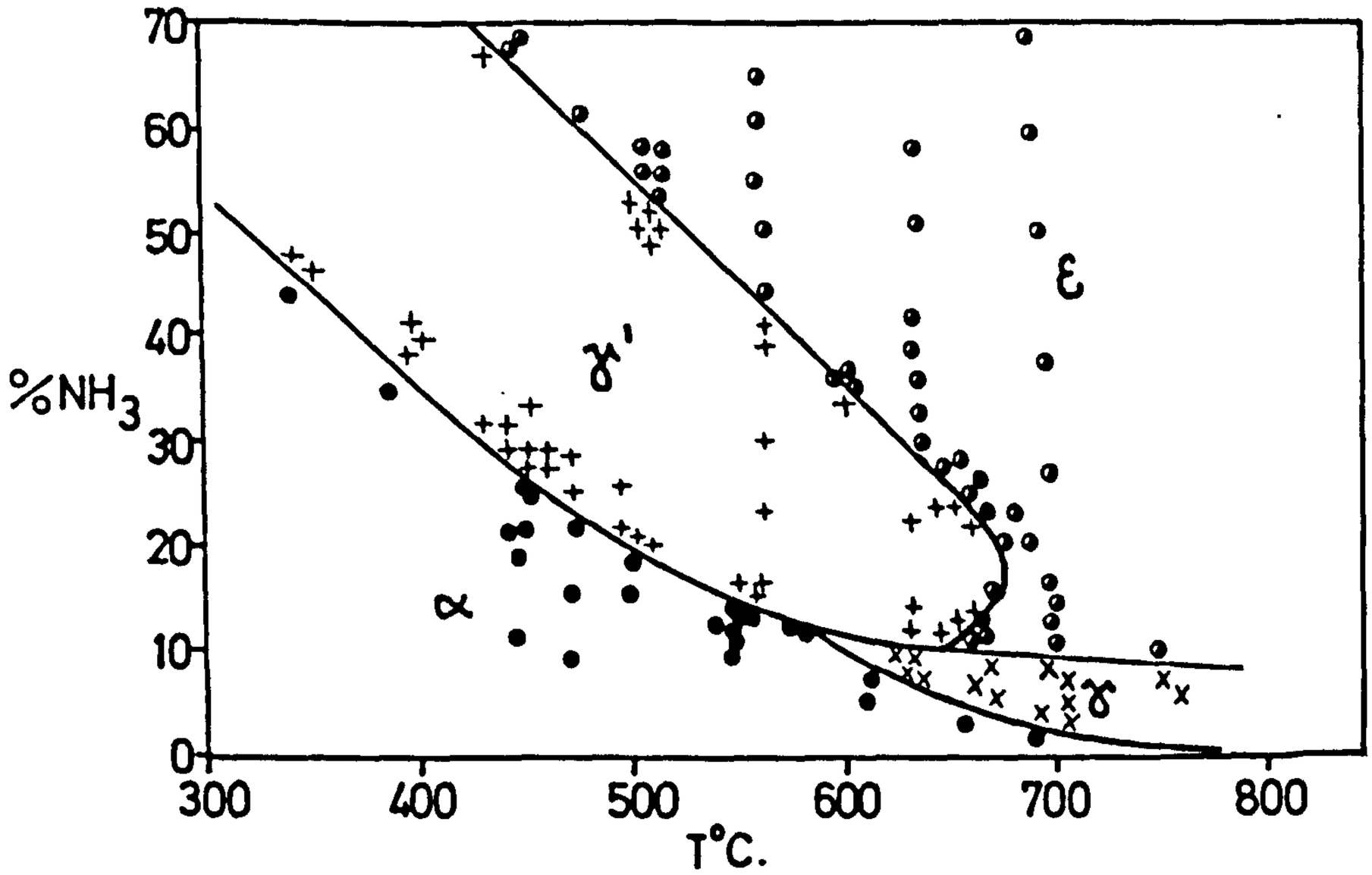

EQUILIBRIUM BETWEEN NH_3-H_2 MIXTURES[1ATM.] AND SOLID PHASES OF THE IRON-NITROGEN SYSTEM [AFTER LEHRER (1930)].

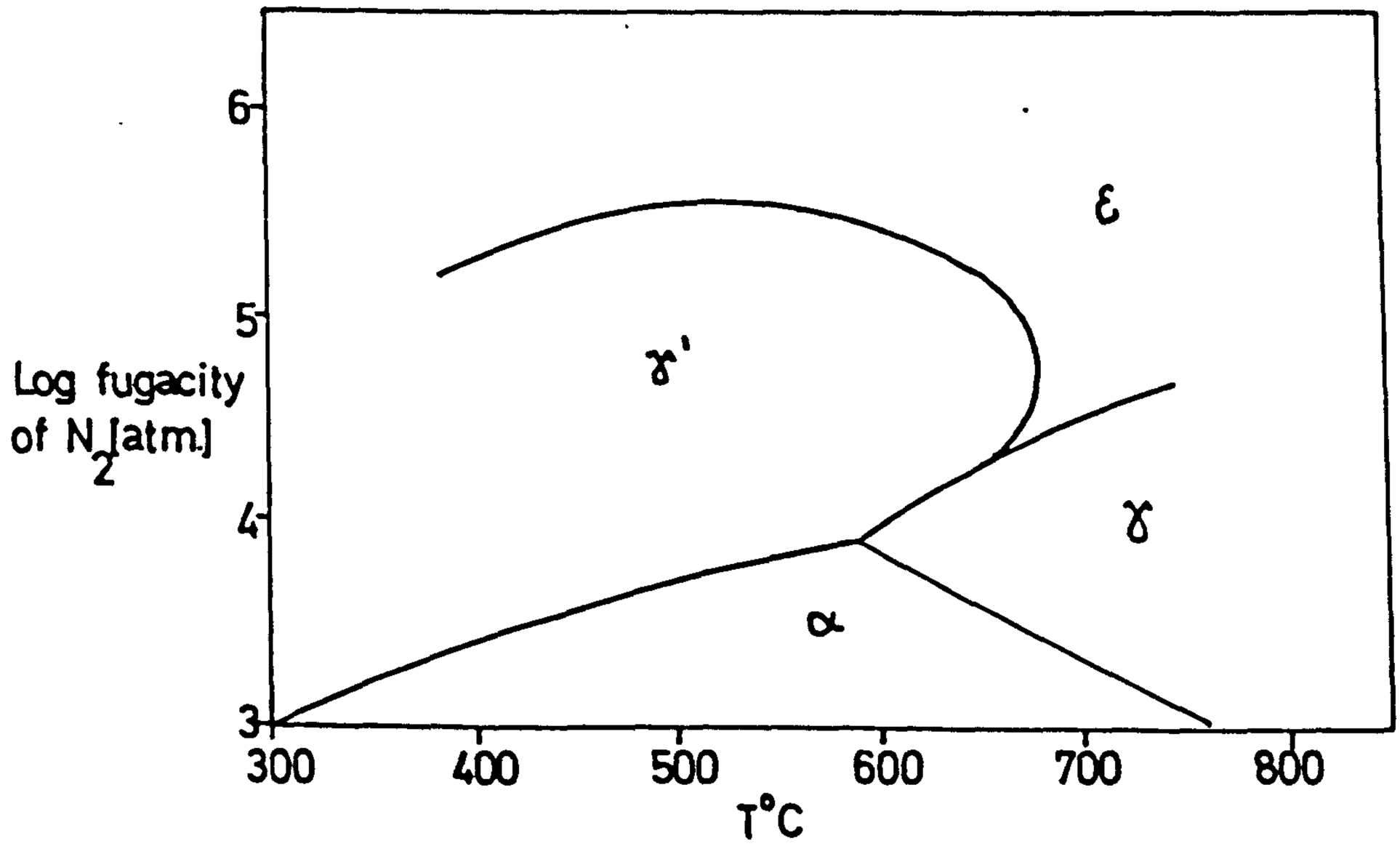

FUGACITY-TEMPERATURE DIAGRAM FOR THE IRON-NITROGEN SYSTEM USING DATA FROM THE PREVIOUS FIGURE.

$$K_4 = \text{wt.}\%N \cdot p_{H_2}^{3/2} / p_{NH_3} \quad \ldots.(8)$$

The range of nitrogen potential of a nitrogen-hydrogen mixture is obviously limited. For example, a piece of iron equilibrated at 600°C in one atmosphere of nitrogen will contain 9.1×10^{-4} wt.%N. At the same temperature in 10%NH_3:H_2 the same piece of iron contains 0.1wt.%N after equilibration and the nitriding potential of such a mixture equals that of nearly ten thousand atmospheres of molecular nitrogen.

The hydrogen in the nitrogen-hydrogen mixture acts as a diluent by reducing the nitrogen partial pressure. Although other gases (e.g. argon) could be used, hydrogen is desirable because commercial nitrogen contains appreciable quantities of oxygen which oxidises the metallic alloying element (internal oxidation) if the latter is less noble than iron. Furthermore, the rate of nitriding can be affected by surface contamination by oxygen. Small concentrations of hydrogen in the nitrogen reduces the oxygen potential of the gas and so eliminates these undesirable effects without any appreciable reduction in nitriding potential.

II.4 Apparatus

The nitriding apparatus is shown in Figure II.2 and II.3. Commercial hydrogen, nitrogen and ammonia were purified by standard methods (see Figure II.4); the activated copper was pre-reduced in hydrogen for several days at 140°C and maintained at 100°C during use. Gas flows were measured by calibrated capillary flow meters (see Figure II.5). Two types of furnace were used, one having a horizontal and the other a vertical alumina reaction tube. The furnace temperature was controlled to $\pm 3C^{o}$ by standard controllers using a Pt-Pt:Rh thermocouple near the furnace resistance winding and the specimen temperature was measured by a chromel:alumel thermocouple in a sheath within the reaction tube directly alongside the specimen. The pressure in the system was maintained slightly

Fig. II.2

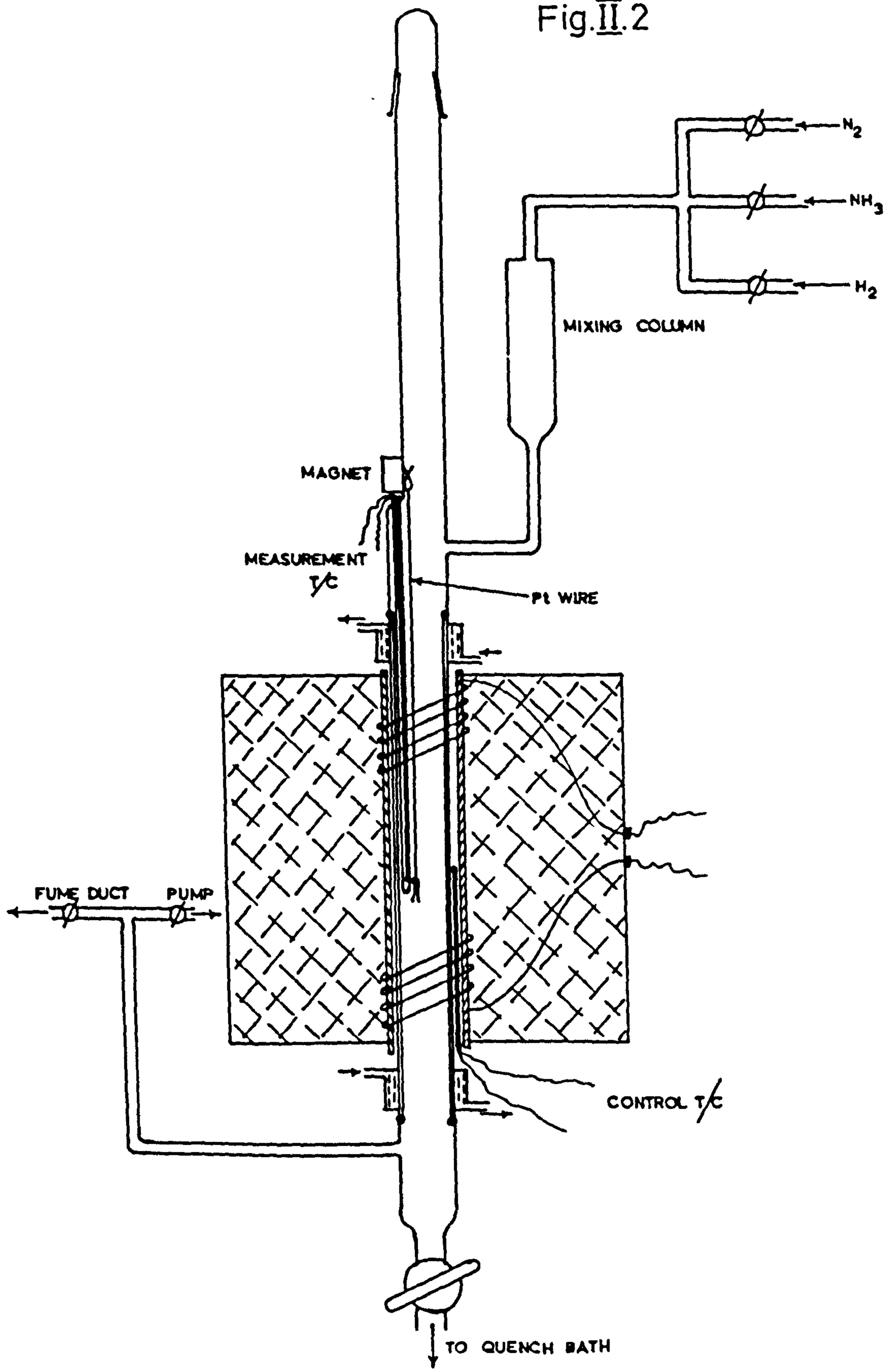

THE VERTICAL NH_3-H_2 AND N_2-H_2 EQUILIBRATION APPARATUS.

Fig.II.3

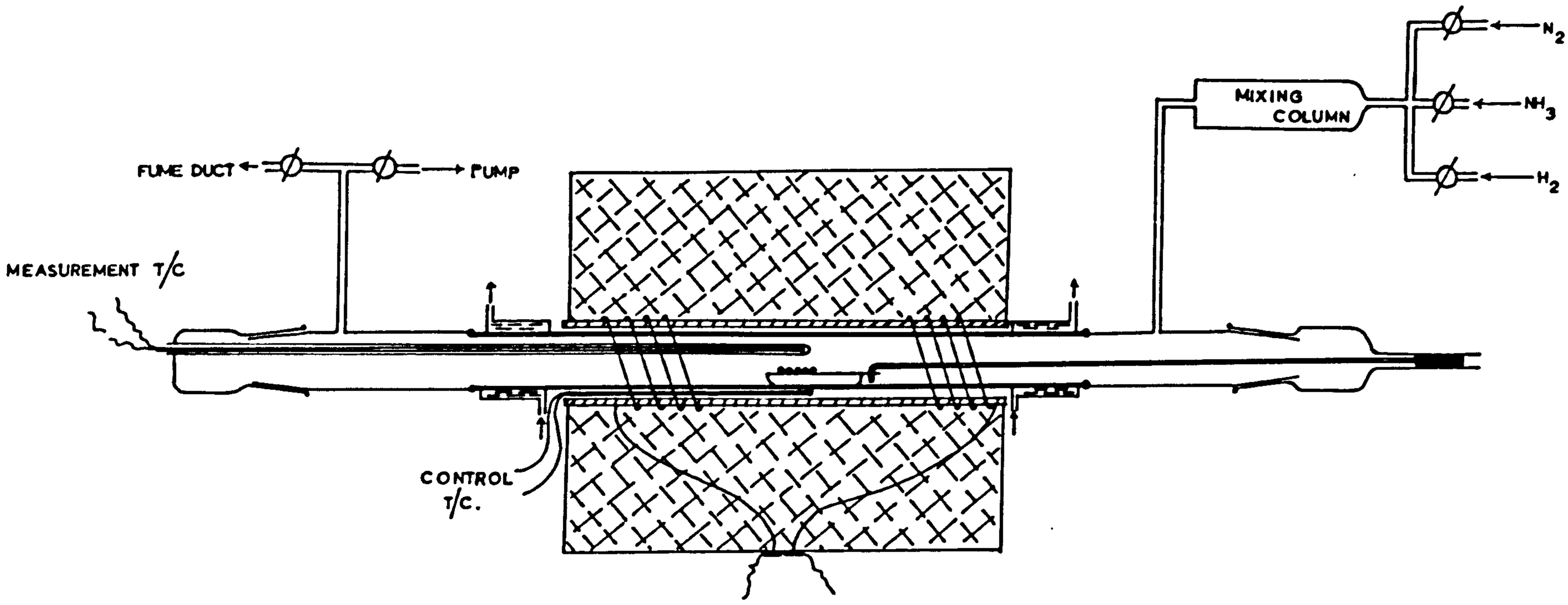

THE AMMONIA–HYDROGEN EQUILIBRATION APPARATUS [HORIZONTAL FURNACE].

Fig. II.4.

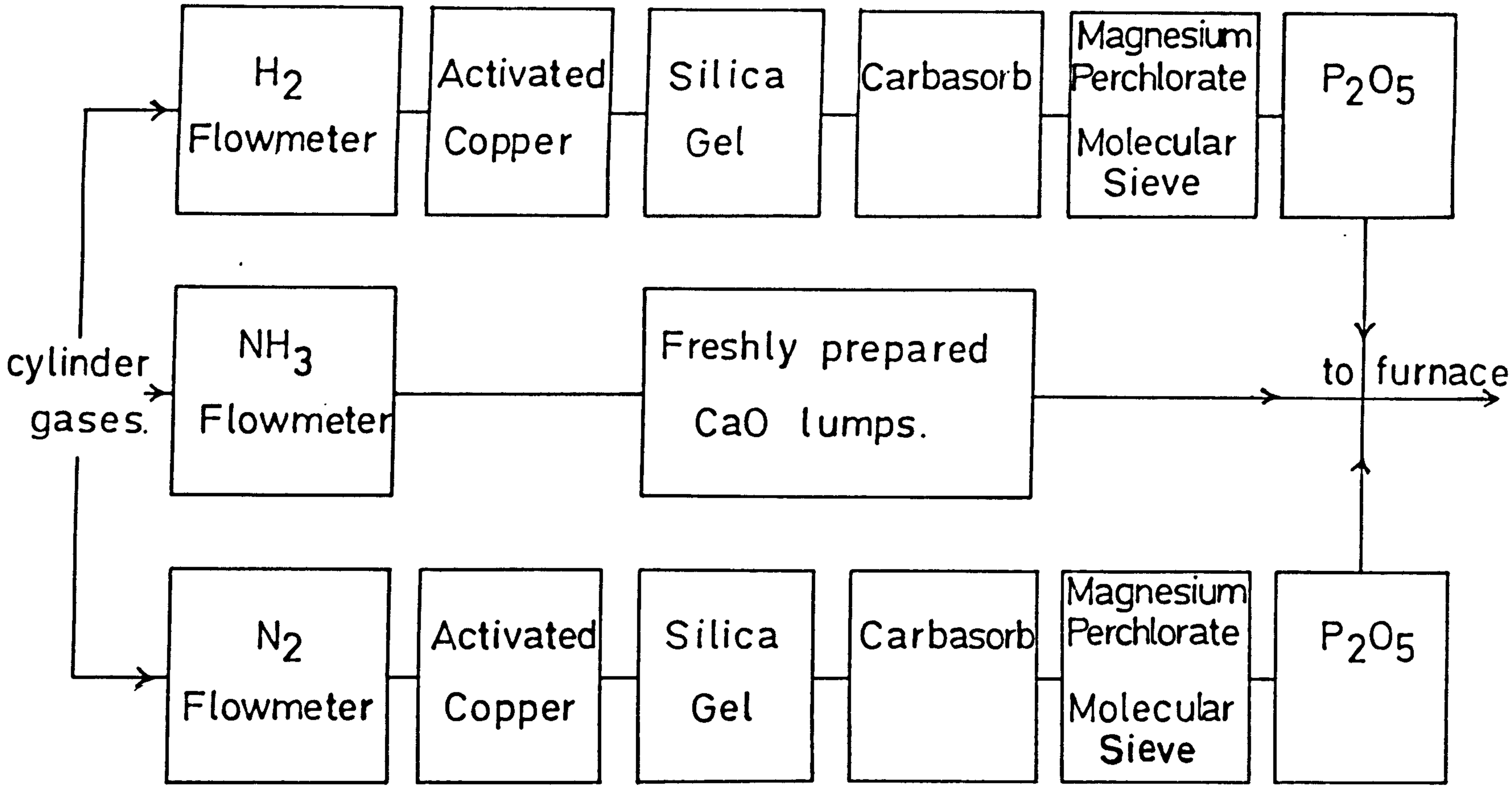

GAS FLOW SYSTEM FOR NH_3-H_2 AND N_2-H_2 EQUILIBRATION.

Fig. II.5

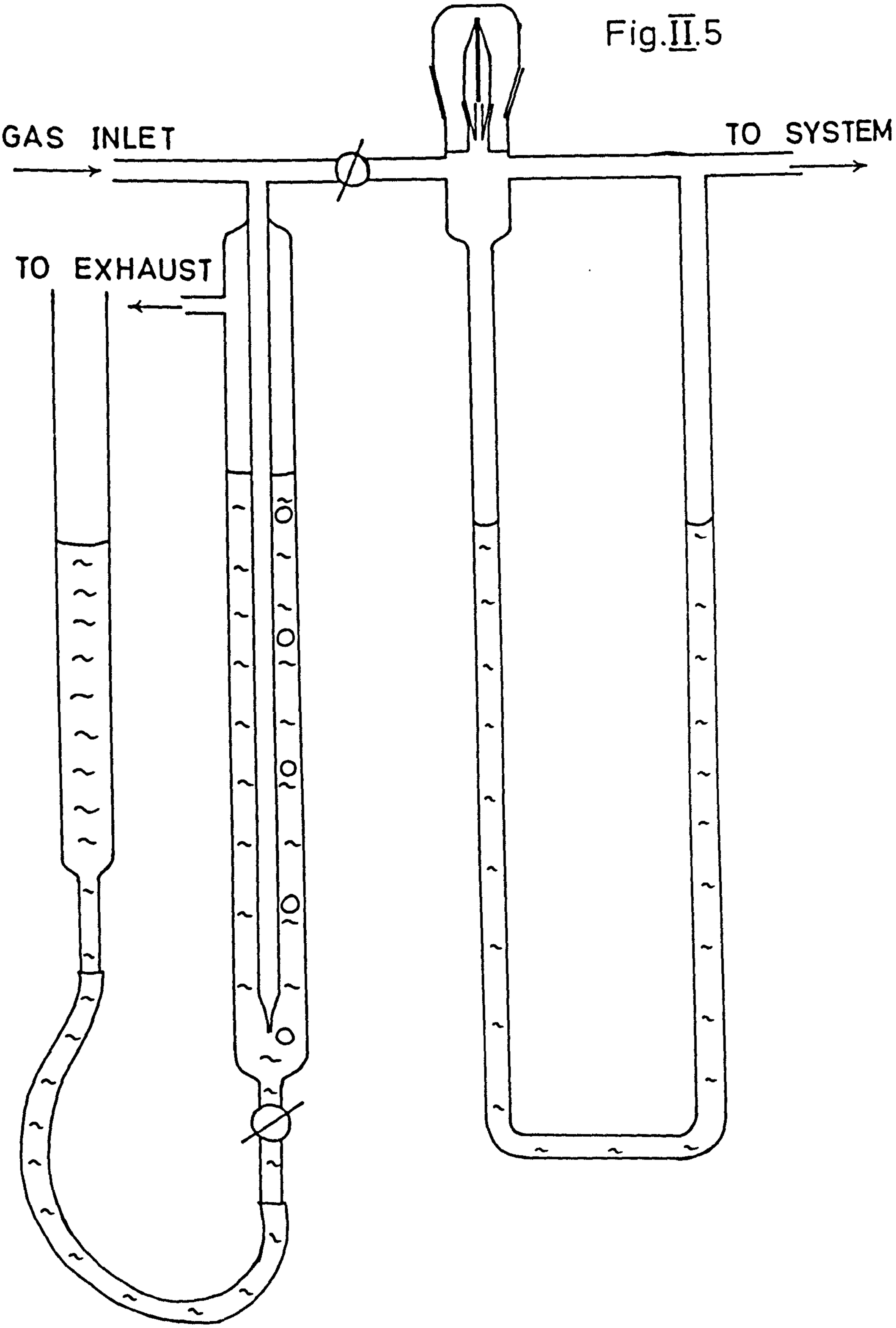

A CAPILLARY FLOWMETER [SCHEMATIC].

above atmospheric by 1 - 2cm. head of oil in an exit bubbler. Capillary flow meters were calibrated by a bubble displacement method. Total flow rates of the order of twelve litres per hour were found to give no detectable ammonia cracking below 650°C. Above this temperature, faster flow rates were necessary and in experiments with pure ammonia a flow of approximately 30 litres per hour was required to maintain the maximum nitrogen potential.

Procedures adopted in the nitriding experiments were:

(a) Horizontal furnace

After cleaning, the strip or wire specimens were laid across an alumina boat which, connected to a silica rod, was placed in the cold end of the reaction tube. The system was then sealed, evacuated and filled with nitrogen. The required ammonia:hydrogen or nitrogen: hydrogen gas mixture was then admitted, flushing out the nitrogen, and allowed to flow usually for half an hour to ensure stable nitriding conditions. The alumina boat and specimens were then moved into the heated reaction zone using a magnet. After nitriding, the boat was withdrawn quickly to a position under the water cooling coils, cooled, and then removed from the apparatus after the nitriding gases had been flushed out with nitrogen. With such small specimens, even this crude quench is sufficient to give martensites under the appropriate nitrogen concentrations. The procedure for powder specimens was similar.

All specimens were weighed before and after nitriding.

(b) Vertical furnace

Specimens were suspended by a platinum wire in the cold upper extension of the furnace. After proceeding as for the horizontal furnace, the specimens were lowered into the hot zone by a magnet acting on a soft iron wire loop attached to the upper end of the platinum wire. After reaction, the wires were raised into the cold zone at the top of the furnace. If a fast quench was required the specimens could be released and dropped into an oil bath which was opened to the system immediately after quenching. After purging

with nitrogen the specimens and the platinum wire were removed from the quench bath.

II.5 Pressure nitriding

For nitriding with high-purity moecular nitrogen, specimens were weighed and sealed into a thick-walled evacuated silica tube (see Figure II.6) with a calculated amount of ε or $\zeta - Fe_2N$ (~11wt.%N) previously prepared by passing ammonia at high flow rates over 100 mesh iron powder at 450°C. When the silica tube is heated above 650°C the ε or $\zeta - Fe_2N$ decomposes completely. The pressure of nitrogen is limited by the strength of the silica tubes and in the present work about forty atmospheres was the maximum. The sealed capsule was heated at the required temperature in a vertical furnace and quenched by allowing it to fall into a water bath. Powder specimens for pressure nitriding were contained in a small open silica container within the thick-walled silica tube.

II.6 X-ray methods

X-ray diffraction patterns of the nitrided materials were obtained with monochromatic X-radiation reflected from a lithium fluoride single crystal. Monochromatic radiation was used to reduce the background intensity during the long exposures that were often necessary to bring up the weak diffraction patterns of precipitated phases. The diffraction patterns were recorded photographically using a 9 and 19cm. diameter cameras. For less critical work vanadium-filtered CrKα radiation was used.

II.7 Metallographic examination

To ensure that the time to reach equilibrium during nitriding was conveniently short, wires of square cross section were cut from strips 0.5mm. thick and although this is suitable for X-ray examination, metallography and photomicrography are difficult with such specimens.

Fig. II. 6

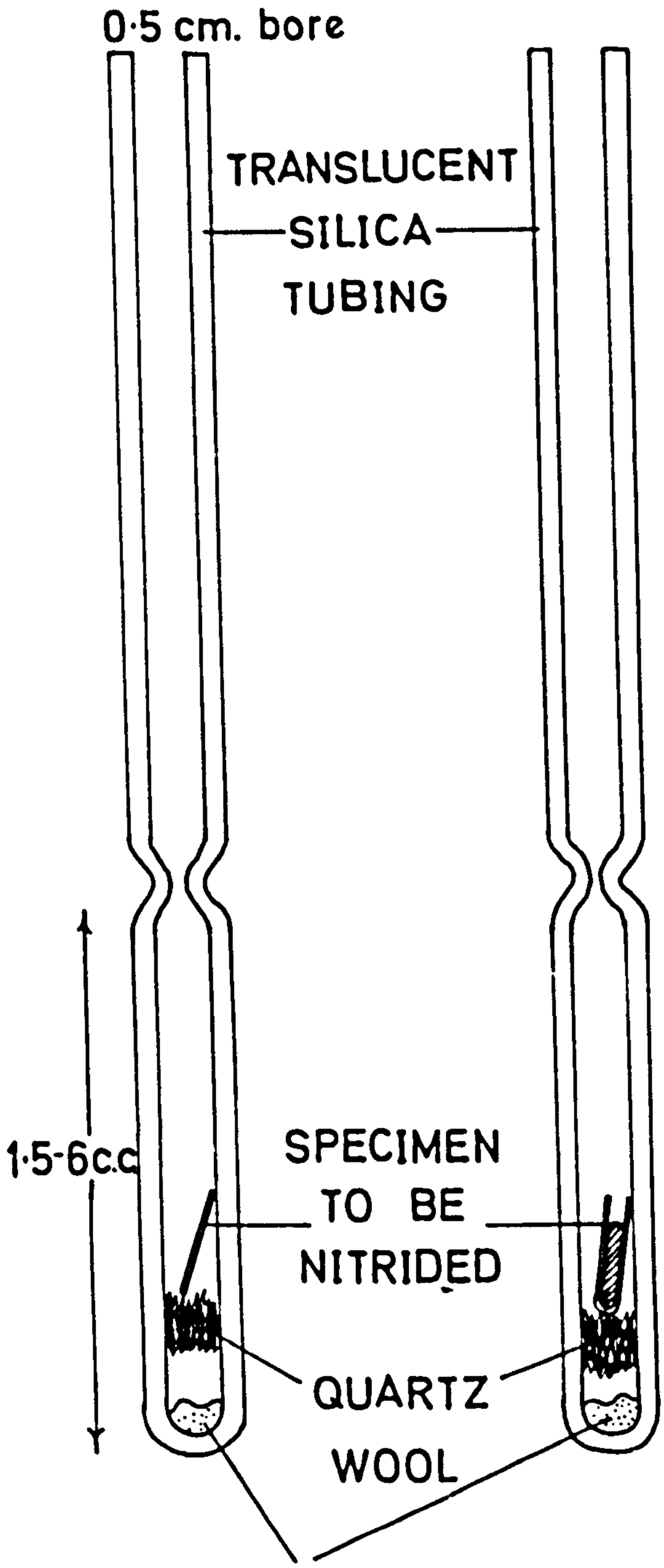

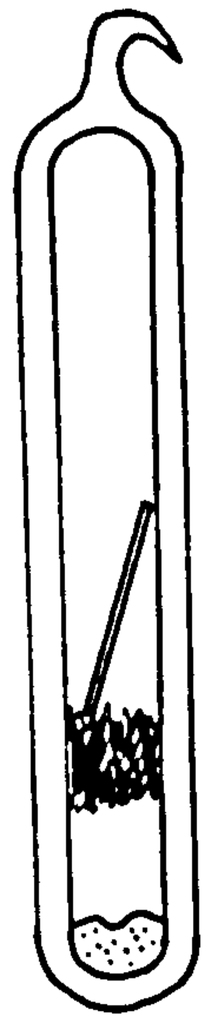

c)

a) Wires b) Powders

METHOD OF SEALING SPECIMENS IN PRESSURE NITRIDING EXPERIMENTS

The specimens were mounted vertically in cold mounting compound in a 2cm. diameter mould or in bakelite under pressure-curing at 125°C. Several specimens were usually mounted together. After reduction on an abrasive wheel the specimens were polished with successively 8, 3, 1 and $\frac{1}{4}\mu$ diamond. 2%"nital" or 10%"chloral" reagents were found to be suitable etchants and the optical microscopy and photomicrography were carried out using a Reichart projection microscope.

II.8 Hardness measurements

Hardness measurements were made using a standard microhardness tester fitted to the Reichart microscope. Where hardness profiles were observed, readings were carried out using a 50gm. load at 50 - 100μ intervals across the specimen.

II.9 Preparation of specimens for electron microscopy

The methods for preparing specimens for electron microscopic examination are summarised in Table II.2.

II.10 Electron microscopes

A J.E.M. 6A electron microscope was used for the examination of extraction replicas and for work at low magnifications. The more critical high-resolution microscopy was carried out on an A.E.I. E.M.6G which is equiped with limited stage tilting facilities ($\pm 5^{o}$) and electromagnetic beam tilts for dark-field operation.

II.11 Chemical analysis

Nitrogen analysis was carried out using a standard micro--Kjeldahl apparatus with colorimetric determination of the ammonia ion concentration using Nessler's reagent; ammonia chloride solution was used as a standard.

The ammonia:hydrogen ratio of the gas mixture passing through the nitriding furnace was checked by chemical analysis. In this, the

Table II.2

Specimen preparation for electron microscopy

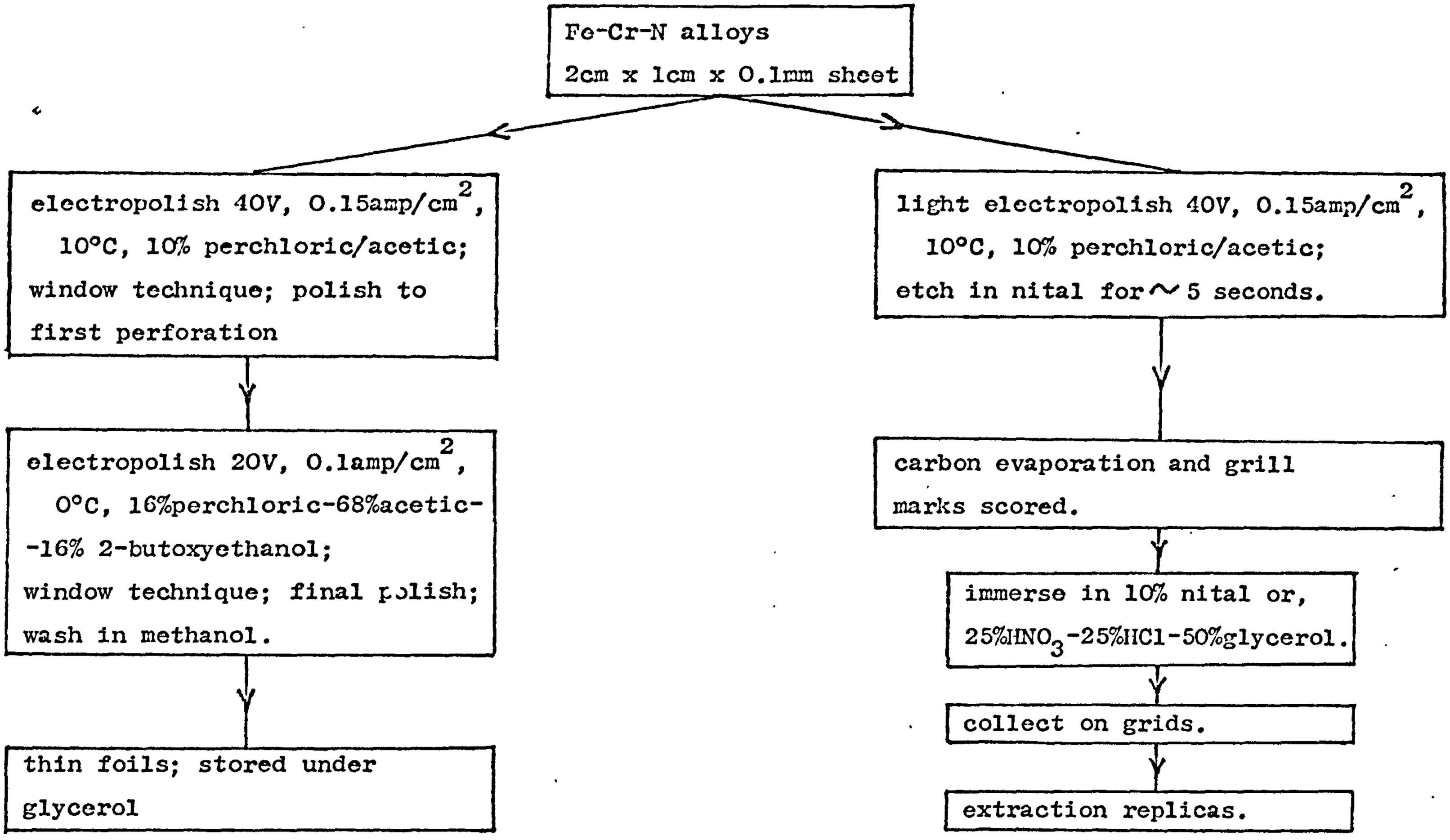

exit gases were passed through a bulb of known volume for a sufficient time to obtain a representative sample. The bulb was then sealed off and the contents flushed out with nitrogen, via a diffuser, into 4% boric acid solution. The resultant solution was titrated with 0.01N hydrochloric acid using a methyl red/methylene blue indicator. The gas composition before as well as after passing through the nitriding furnace was determined in this way by diverting the gas flow through a furnace "by-pass".

Chapter III

The scope of the present investigation

Previous work at Newcastle by Pipkin (1967) and Spiers (1969) on the precipitation of nitrogen from iron alloys containing respectively manganese and molybdenum and by Roberts (1970) on precipitation in Fe-N, Fe-Nb-N and Fe-Si-N alloys showed that characterization of precipitates under a wide range of equilibrium and pseudo-equilibrium conditions was possible by using gas equilibration methods coupled with sensitive X-ray diffraction techniques. A similar approach was adopted in the present investigation of nitride precipitation from iron-chromium alloys.

In iron-chromium-nitrogen alloys it is shown (see Chapter IV) that only CrN and Cr_2N are precipitated in the range 500 - 1,000°C. The particular nitride observed depends upon the chromium activity in the alloy.

In Chapter V the quench-aging of iron-chromium-nitrogen alloys at temperatures where substitutional solutes have negligible diffusivities shows that chromium, because it reduces the activity coefficient of nitrogen in iron, has a marked effect upon the rate and the dispersion of iron nitride precipitation.

Chapters VI and VII describe investigations of the kinetics and morphology, respectively, of homogeneous precipitation in Fe-Cr-N alloys. This complements previous work on the Fe-Mo-N and Fe-Nb-N systems where substitutional-interstitial Guinier-Preston zone formation was recognised for the first time. In the present work homogeneous precipitation requires a high supersaturation of nitrogen, as in G.P. zone formation, but no evidence for clusters or precipitates other than the equilibrium phase is obtained. Reason for this are suggested.

Finally, some observations on the manganese-carbon system and the characterization of a new carbide, $Mn_{22}C_6$, are described in an Appendix.

Chapter IV

Precipitation in iron-chromium-nitrogen alloys

IV.1 Introduction

Precipitation from steels is usually studied by quench aging, but the rapid decrease of the driving force for precipitation which is characteristic of quench aging can be avoided by employing "constant activity aging". This method, which for nitrogen precipitation is carried out in ammonia-hydrogen gas mixtures, produces quantities of precipitate sufficiently large for identification by X-ray diffraction. Figure IV.1 (after Darken, 1958) shows the relative rates of diffusion for substitutional and interstitial atoms in ferrite. It is clear that at all temperatures nitrogen diffuses much more rapidly than chromium. For small sections of low alloy specimens, nitrogen diffuses into the material and equilibrates quickly with the nitriding gas before extensive diffusion of the substitutional alloying element occurs. By maintaining a constant nitrogen potential at the specimen surface, any nitrogen which is precipitated from solid solution as nitride is replenished from the gas atmosphere and further precipitation occurs. If necessary, the aging can be continued until relatively large quantities of precipitate are formed.

Before nitriding, all the iron-chromium alloy wires were annealed for 18 hours in purified hydrogen at 850°C. This pre-treatment removes dissolved oxygen and allows recrystallisation so that specimens are more amenable to metallographic examination.

IV.2 The chromium-nitrogen system

This system is well established (see Chapter I) and so only a few confirmatory runs have been carried out. The observations are shown in Table IV.1 and Figure IV.2.

Chromium powder was prepared by grinding electrolytic chromium

Fig. VI. 1

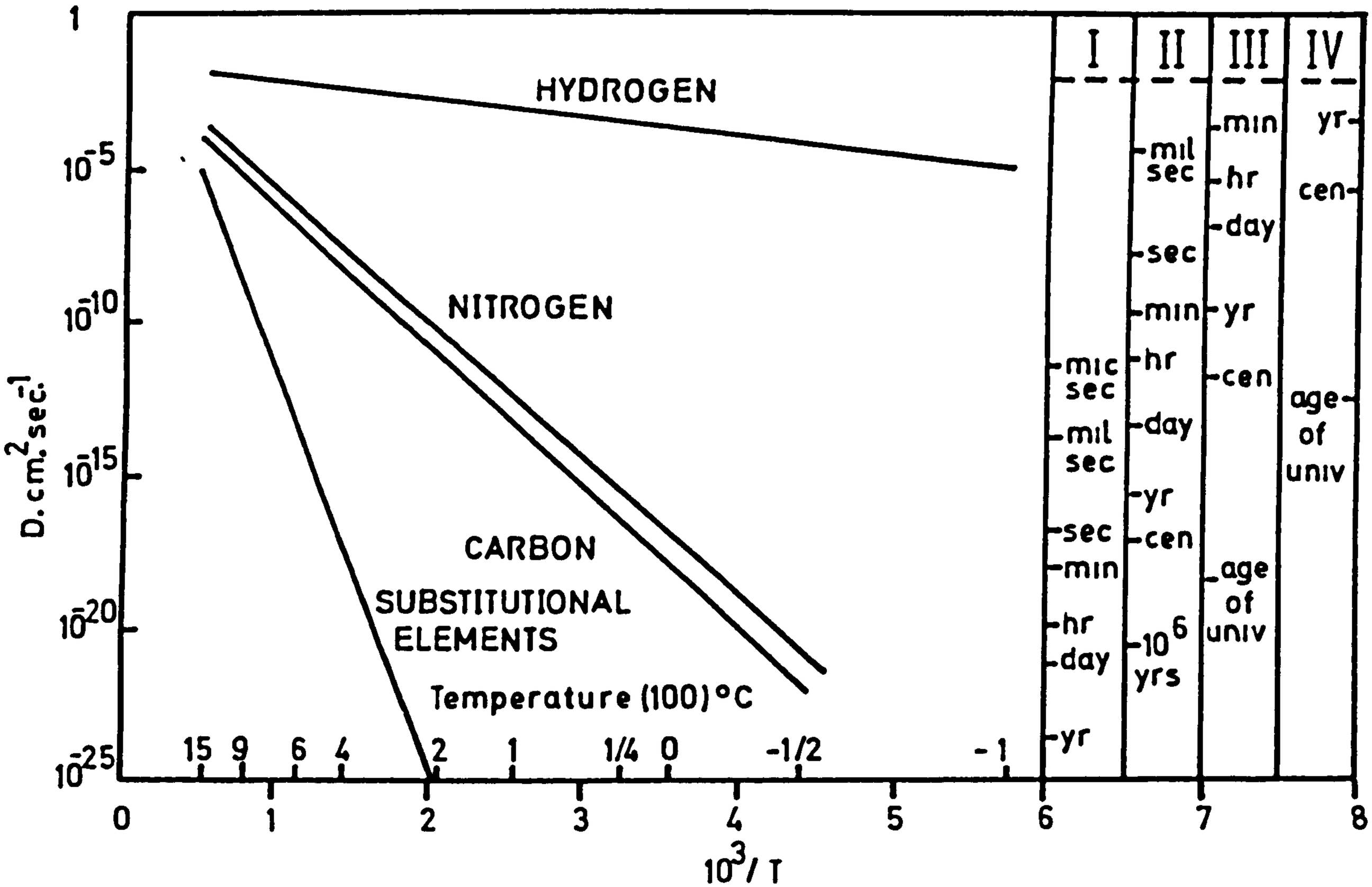

DIFFUSIVITY AND TIME OF MIGRATION IN FERRITE

I. Hop time II. Time for 50% migration to G B radius 10^{-3} cm.

III. IV. Time for slab thickness 2mm / 2m

[From. Darken, L.S. (1958), N.P.L. Symposium, No.9.]

Table IV.1

The nitriding of chromium

run	starting material	nitriding technique	temp. °C	time hrs.	phases formed		
					α-Cr	CrN	Cr_2N
Cr5	powder	pressure nitriding 35 atm.	1000	75		x	x
Cr4	powder	$95NH_3 : 5H_2$	900	48		x	

Fig. IV.2.

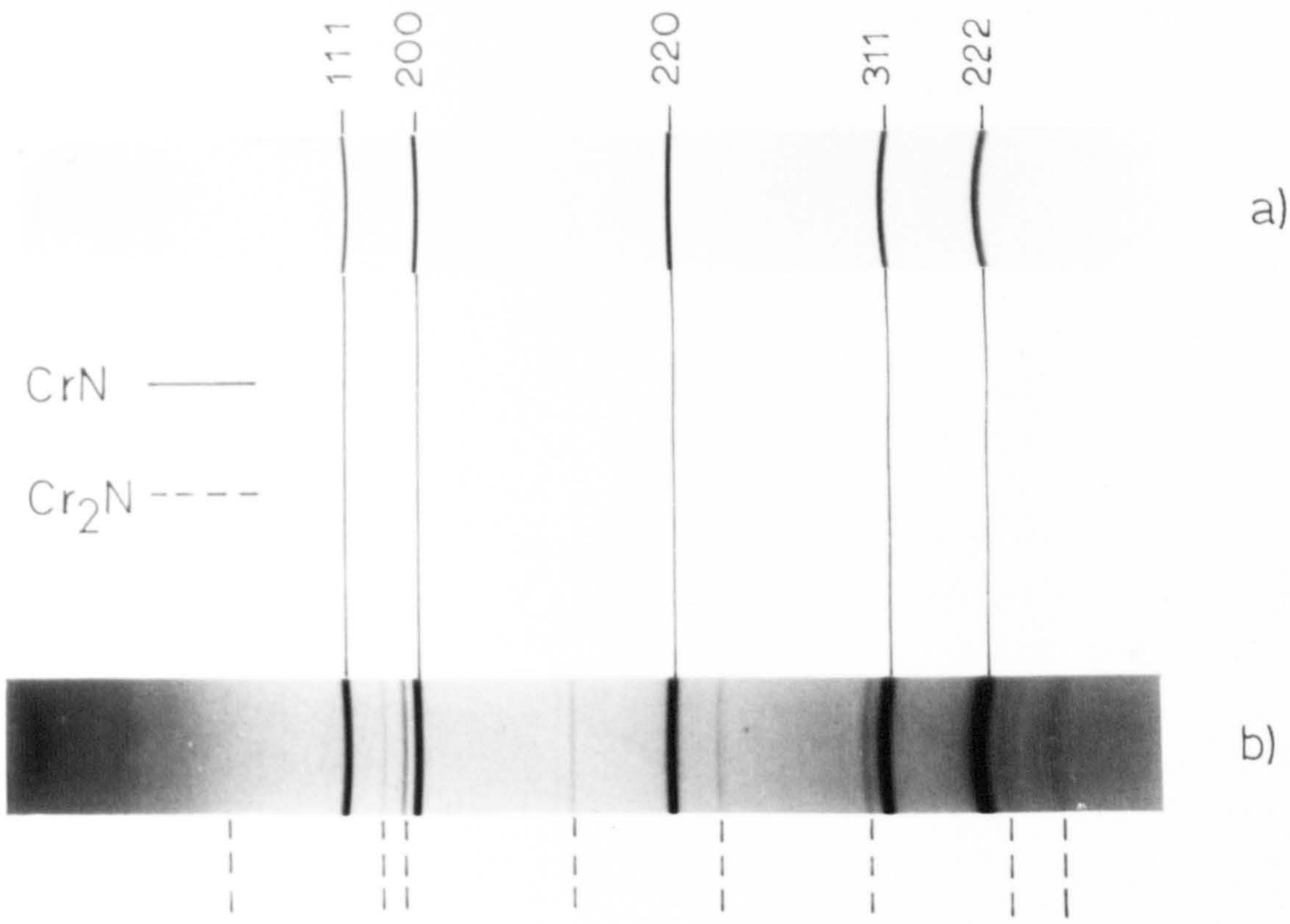

a) Nitrided in ammonia at 900°C.

b) Pressure nitrided at 1000°C.

X-RAY PHOTOGRAPHS OF NITRIDED CHROMIUM POWDER.

flake. Ammonia passed over this at 900°C gave total conversion to CrN. Similar results were obtained by pressure-nitriding chromium powder, but the CrN product contained a trace of Cr_2N due to insufficient nitrogen in the sealed tube for complete conversion. The X-ray data for the two phases are given in Tables IV.2 and IV.3.

These results are consistent with thermodynamic data published by Sano (1937) and Seybolt & Oriani (1956). The critical nitrogen pressures for formation of CrN and Cr_2N at 575°C are shown in Figure IV.3; at all temperatures below 1,000°C, using the nitriding techniques described in Chapter II, pure chromium will form CrN.

IV.3 Precipitation in Fe-Cr-N alloys

A summary of the observations of precipitation in Fe-Cr-N alloys is given in Tables IV.4, IV.5 and IV.6.

Previous work by Pipkin (1967) and Spiers (1969) clearly demonstrates the effect of varying the concentration of a substitutional alloying element on the sequence of precipitated phases when iron alloys are aged. Similar effects are observed in iron-chromium--nitrogen alloys.

In ammonia-hydrogen mixtures (see Table IV.4) the nitride precipitated in alloys of different chromium content is always CrN. This is illustrated in Figure IV.4 where the amount of CrN increases as the concentration of chromium increases.

On "constant activity aging" in nitrogen-hydrogen mixtures the results listed in Table IV.5 were obtained.

At 865°C, alloys with high chromium contents precipitated both CrN and Cr_2N but with lower concentrations only CrN is formed. At 1028°C precipitation is observed only in the high chromium alloys where Cr_2N is formed (see Figure IV.5) while the lower alloys transform to homogeneous nitrogen austenite.

Table IV,2

X-ray data for CrN

CrKα radiation a = 4,150 Å

intensity	hkl	$\sin^2\theta$ obs.	$\sin^2\theta$ calc.
m	111	0,2285	0,2289
s	200	0,3038	0,3052
s	220	0,6128	0,6104
s	311	0,8412	0,8393
s	222	0,9145	0,9156

Table IV.3

X-ray data for Cr_2N

CrKα radiation a = 4.469; c = 4.790 Å

intensity	hkl	$\sin^2\theta$ obs.	$\sin^2\theta$ calc.
w	101	0.1400	0.1418
w	110	0.2285	0.2283
m	002	0.2628	0.2628
s	111	0.2936	0.2940
vw	201	0.3690	0.3681
s	112	0.4907	0.4913
-	211	-	0.5948
s	300	0.6864	0.6849
vs	113	0.8197	0.8198
-	203	-	0.8941
vw	220	0.9145	0.9132
-	302	-	0.9492
m	221	0.9787	0.9802

Fig. IV. 3.

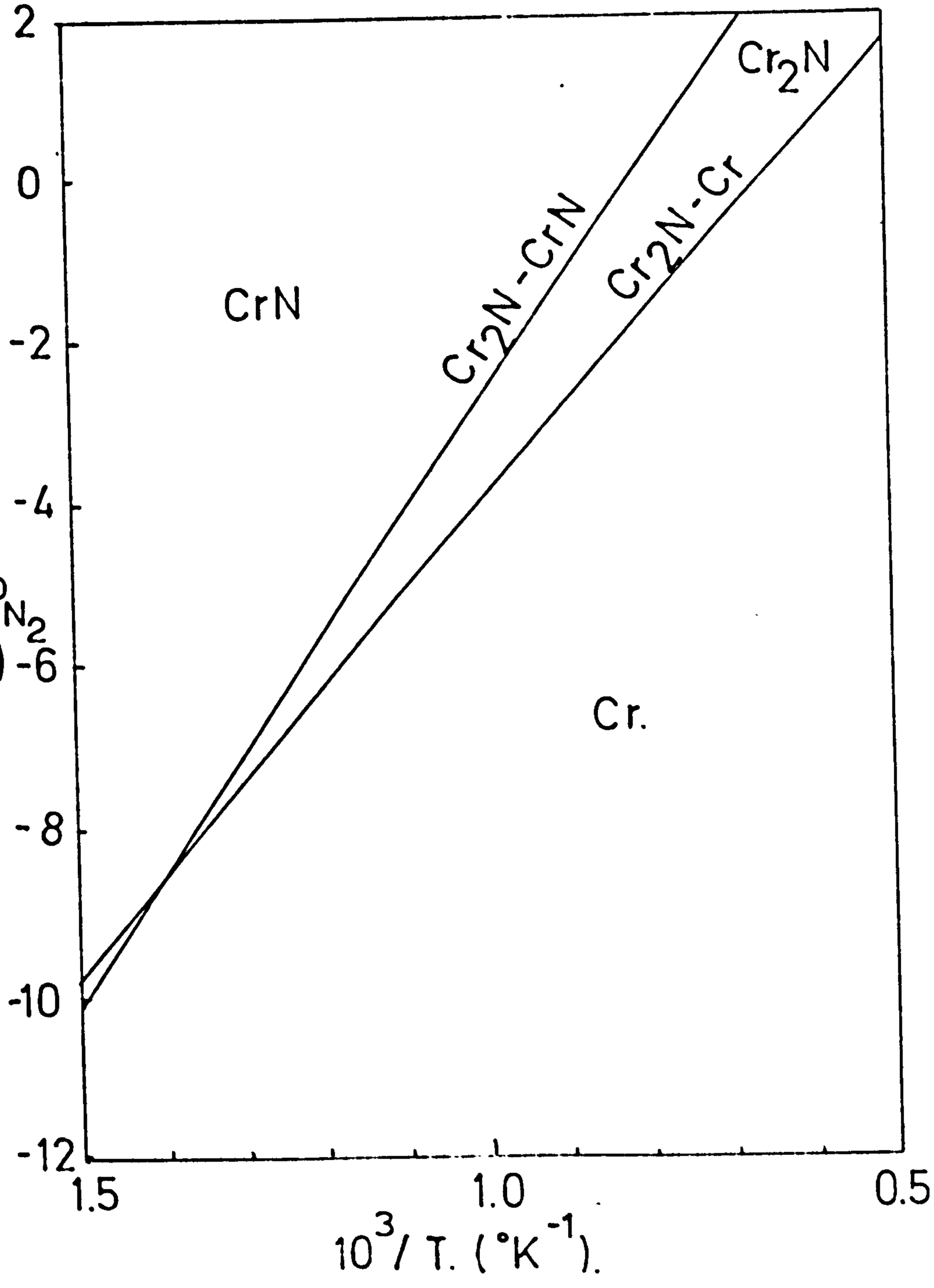

CRITICÄL NITROGEN PRESSURES FOR FORMATION OF CHROMIUM NITRIDES.

(from Servi and Forgeng, 1959.)

Table IV.4

Nitriding iron-chromium alloys with ammonia-hydrogen mixtures

run	chromium	$NH_3:H_2$	temp.	time	phases formed					
CF	%		°C.	hrs.	α-Fe-Cr	γ-Fe-Cr	CrN	Cr_2N	Fe_4N	α'-martensite
1	5.6	7:93	590	24	x		x			
2	4.1	7:93	590	24	x		x			
3	2.3	7:93	590	24	x					
4	5.6	8.92	650	80	x	x	x			
5	4.1	8.92	650	80	x	x	x			
6	5.6	15:85	650	96	x	x	x		x	
7	4.1	15:85	650	96	x	x	x		x	
8	2.3	15:85	650	96	x	x	x		x	
9	5.6	8:92	665	96	x	x	x			x
10	4.1	8:92	665	96	x	x	x			x
11	2.3	8:92	665	96	x	x	x			x
12	1.2	8:92	665	96	x	x	x			x
13	5.6	6:94	736	96	x	x	x		(x)	
14	4.1	6:94	736	96	x	x	x		(x)	
15	2.3	6:94	736	96	x	x	x		(x)	

Table IV.4

Nitriding iron-chromium alloys with ammonia-hydrogen mixtures (continued)

run CF	chromium %	$NH_3:H_2$	temp. °C.	time hrs.	phases formed α-Fe-Cr	γ-Fe-Cr	CrN	Cr_2N	Fe_4N	α'-martensite
16	1.2	6:94	736	96	x	x	x		(x)	
17	0	11:89	580	73	x					
18	5.6	11:89	580	73	x		x			
19	9.9	11:89	580	73	x		x			
20	14.0	11:89	580	73	x		x			
21	29.8	11:89	580	73	x		x			
22	39.6	11:89	580	73	x		x			
23	0	"100:0"	895	24	x					
24	5.6	"100:0"	895	24	x		x			
25	9.9	"100:0"	895	24	x		x			
26	14.0	"100:0"	895	24	x		x			
27	29.8	"100:0"	895	24	x		x			
28	5.6	6:94	709	2	x					
29	14.0	6:94	709	2	x		x			

(x) precipitated during cooling

Table IV.5

Nitriding iron-chromium with nitrogen-hydrogen mixtures

run Fe-Cr	chromium %	N_2:H_2	temp. °C.	time hrs.	phases formed α-Fe-Cr	CrN	Cr_2N
1	9.90	42:58	865	48	x	x	
2	14.0	42:58	865	48	x	x	
3	29.8	42:58	865	48	x	x	x
4	5.6	59:41	865	67.5	x	x	
5	9.9	59:41	865	67.5	x	x	
6	14.0	59:41	865	67.5	x	x	
7	29.8	59:41	865	67.5	x	x	x
8	39.6	59:41	865	67.5	x	x	x
9	5.6	80:20	865	40	x	x	
10	9.9	80:20	865	40	x	x	
11	14.0	80:20	865	40	x	x	
12	29.8	80:20	865	40	x	x	x
13	39.6	80:20	865	40	x	x	x
14	0	25:75	1028	14	x		
15	5.6	25:75	1028	14	x		
16	9.9	25:75	1028	14	x		
17	14.0	25:75	1028	14	x		
18	29.8	25:75	1028	14	x		x
19	39.6	25:75	1028	14	x		x

Table IV.6

Nitriding iron-chromium alloys by pressure nitriding in molecular nitrogen

run FeCr	chromium %	atm.	temp. °C	time hrs.	phases formed -Fe-Cr	CrN	Cr_2N
1	4.1	40	700	120	x	x	
2	4.1	10	700	120	x	x	
3	5.6	30	950	24	x	x	
4	9.9	30	950	24	x	x	
5	14.0	30	950	24	x	x	
6	29.8	30	950	24	x	x	x
7	39.6	30	950	24	x	x	x

Fig. IV. 4.

wt%Cr

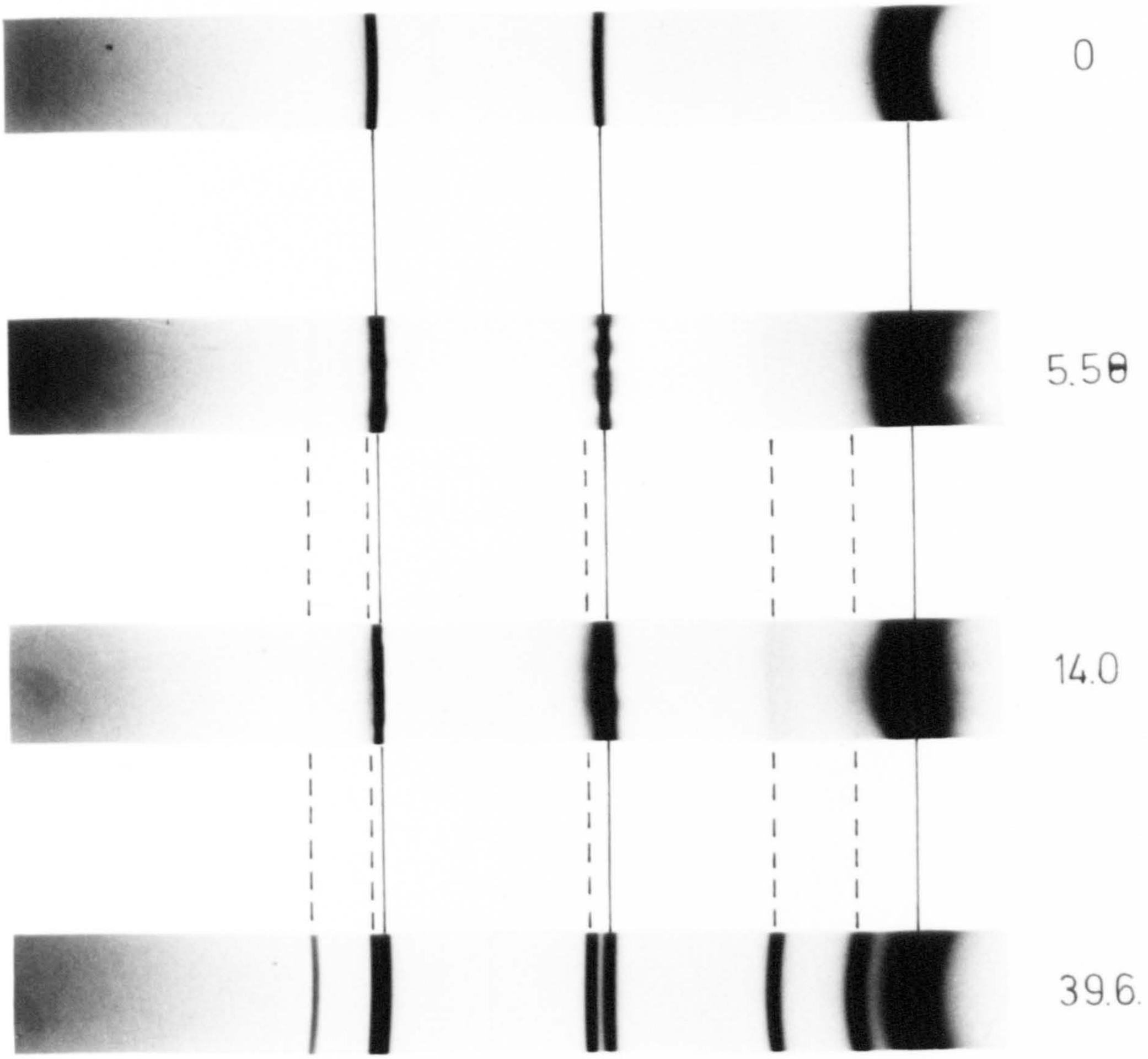

PRECIPITATION IN ALLOYS NITRIDED IN

11% NH_3-H_2 AT 580°C. FOR 73h.

Fig. IV.5.

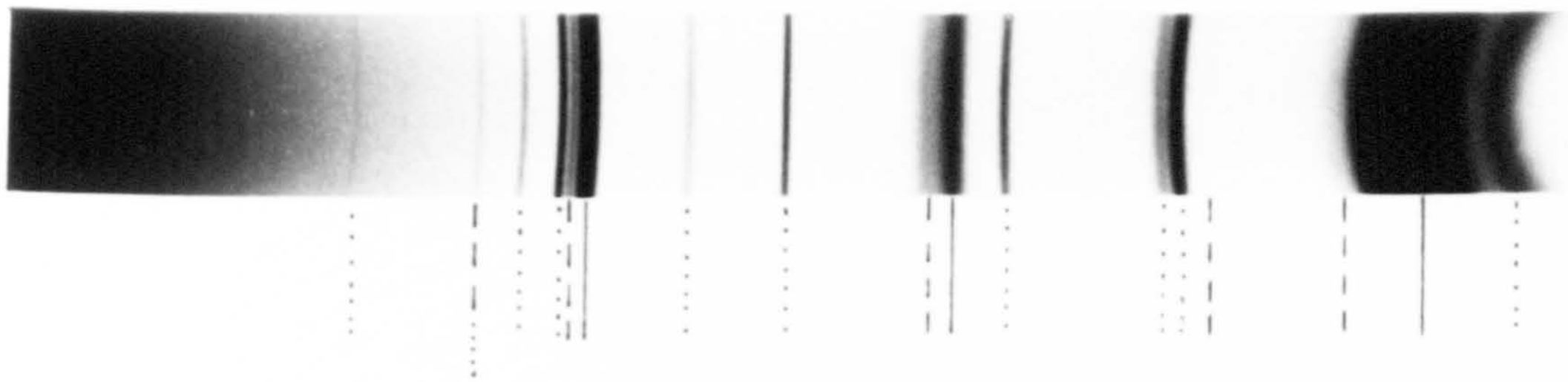

PRECIPITATION IN 29.8wt.% Cr-Fe ALLOY

NITRIDED IN NITROGEN-HYDROGEN MIXTURE

AT 1028°C.

The results of pressure nitriding shown in Table IV.6 are similar to those obtained with nitrogen-hydrogen mixtures. Alloys with less than 14%Cr precipitated CrN and the 29.8 and 39.6%Cr alloys formed Cr_2N.

All nitriding results clearly show that the particular nitride precipitated from Fe-Cr-N alloys at 500 - 1,000°C and low nitrogen activities depends on the chromium concentration. With less than about 20wt.% chromium CrN is the stable phase; with higher than this critical content, Cr_2N is always formed at high temperatures and CrN at lower ones. The experimental observations are consistent with the phase relationships given by Turkdugan and shown in Figure IV.6. At 865°C in alloys containing less than 15% chromium and low nitrogen potentials an austenite solid solution is formed but with higher nitrogen potentials more nitrogen is taken up by the alloy until the solubility limit of CrN is exceeded and so this phase is precipitated (see runs 1, 2, 4, 5, 6, 9, 10 and 11). Alloys with higher chromium contents than 20wt.% initially precipitate Cr_2N but, as the chromium activity in solution decreases, this nitride becomes unstable with respect to CrN; see runs 3, 7, 8, 12 and 13.

The reaction taking place in ammonia-hydrogen mixtures may be written as:

$$CrN + \tfrac{3}{2}H_2 = Cr + NH_3 \qquad ....(9)$$

At 575°C the equilibrium constant (K) for this reaction, derived from data compiled by Pearson & Ende (1953), is 6.90×10^{-6}. It is then possible to compute the ammonia-hydrogen ratios in equilibrium with CrN at any chromium activity from

$$K = \frac{a_{Cr} \cdot p_{NH_3}}{a_{CrN} \cdot p_{H_2}^{3/2}} = 6.90 \times 10^{-6} \qquad ....(10)$$

if a_{CrN} is taken as unity.

When CrN is formed in an alloy at 575°C with $p_{NH_3}/p_{H_2}^{3/2} = 0.005$, i.e. in about $0.5NH_3$:$99.5H_2$ gas mixture, the concentration of chromium remaining in solid solution is approximately 0.14wt.%. It can therefore be concluded that in all the experiments carried out in

Fig. IV. 6.

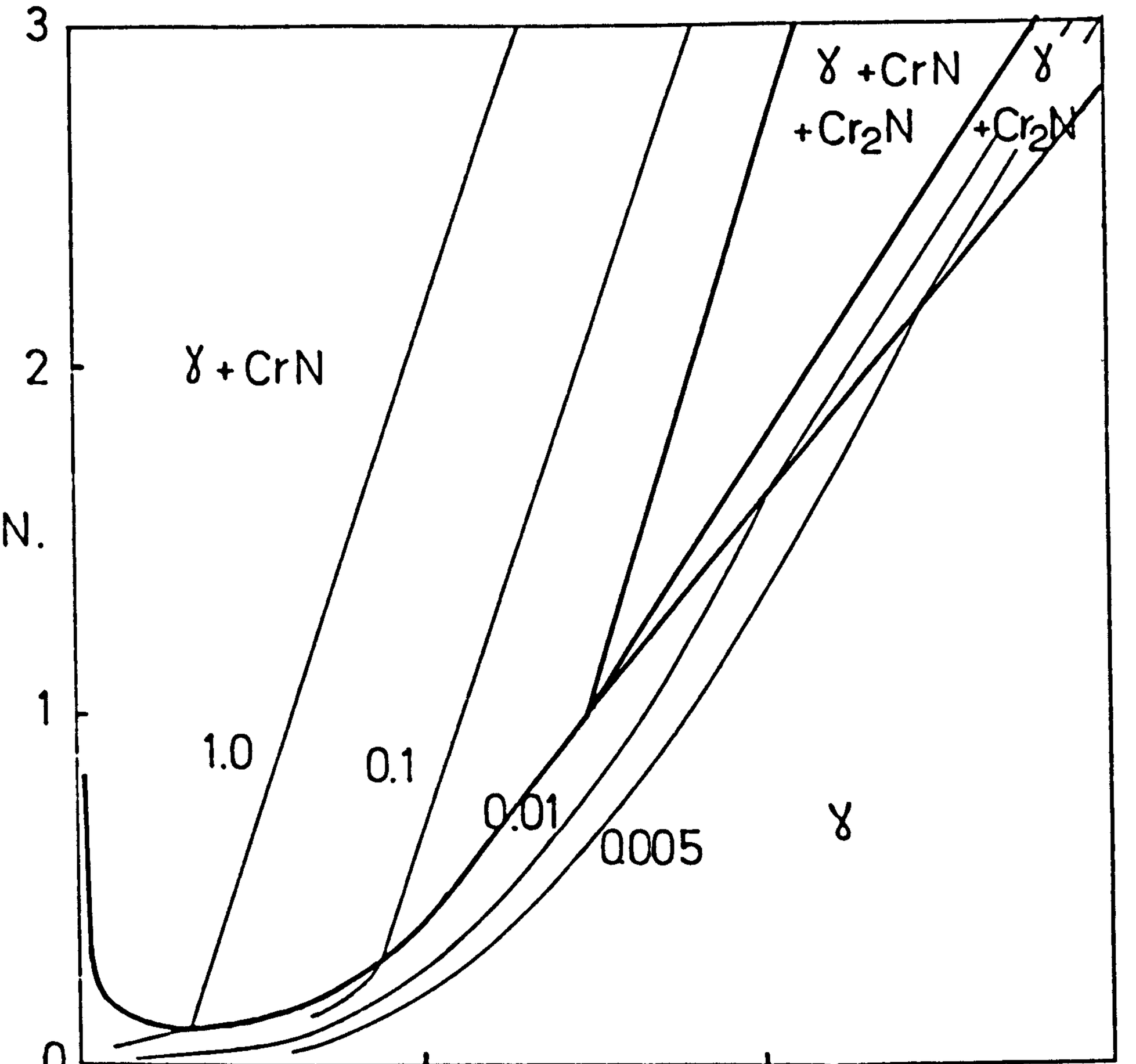

— lines of constant nitrogen pressure.

THE IRON-CHROMIUM-NITROGEN SYSTEM AT 800°C.

(from the data of Turkdugan, 1964.)

the present work, effectively all the chromium in the alloy is precipitated as nitride at the ammonia concentrations used. This is also indicated by the comparison of observed and calculated weight gains shown in Figure IV.7. After nitriding, the alloy consists of iron-nitrogen solid solution, a trace of chromium, and CrN. Increasing the nitrogen potential merely increases the nitrogen in solid solution in a manner similar to that in the Fe-N binary system, and with still higher nitrogen potentials the usual iron-nitrogen phases are formed. The X-ray photographs from runs 6, 7 and 8, reproduced in Figure IV.8 show the phases to be expected on this basis.

The results indicate that at low nitrogen potentials a critical chromium concentration exists at which Cr_2N becomes unstable with respect to CrN. This observation should, of course, be explicable in terms of the thermodynamic properties of the ternary system.

As a first approximation it is assumed that in ternary Fe-Cr-N alloys there is only a chromium-nitrogen interaction with no interaction between chromium and iron. On this assumption, the nitrides formed are binary chromium nitrides containing negligible iron. The free energies of formation of the chromium nitrides are given in Table IV.7 and assume that ΔH and ΔS are independant of temperature. Since chromium nitrides are more stable than γ'- Fe_4N they are much less soluble in iron than the latter.

The integral molar free energies of formation per gram atom of the nitrides at 575°C and 865°C are plotted in Figure IV.9 where each nitride is assumed for simplicity to be stoichiometric with a negligible range of homogeneity so that each free energy-composition is represented by a vertical straight line. The ordinates at nitrogen atom fraction of zero and unity represent the chemical potentials ($\Delta\mu$) of chromium and nitrogen, respectively, in solid solution in ferrite and tangents to the integral molar free energy curves cut these ordinates at points respesenting the chemical potentials of the two component elements in equilibrium with the appropriate nitride. The chemical potentials are related to the activities of the elements

Fig. IV. 7.

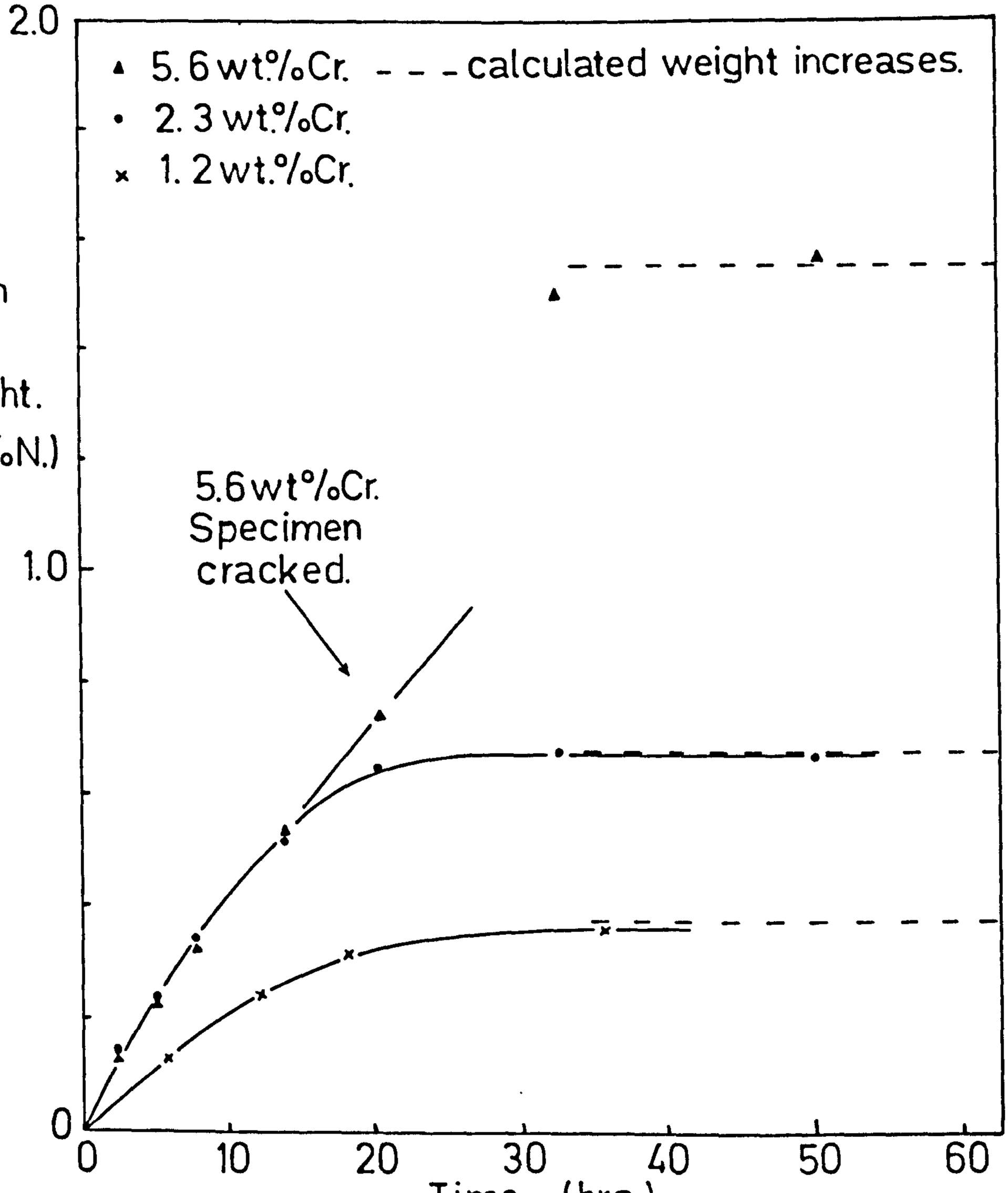

WEIGHT GAIN - TIME CURVES FOR CONSTANT ACTIVITY

AGED IRON-CHROMIUM ALLOYS IN 10%NH_3-H_2 AT 575°C.

Fig. IV.8.

wt%Cr.

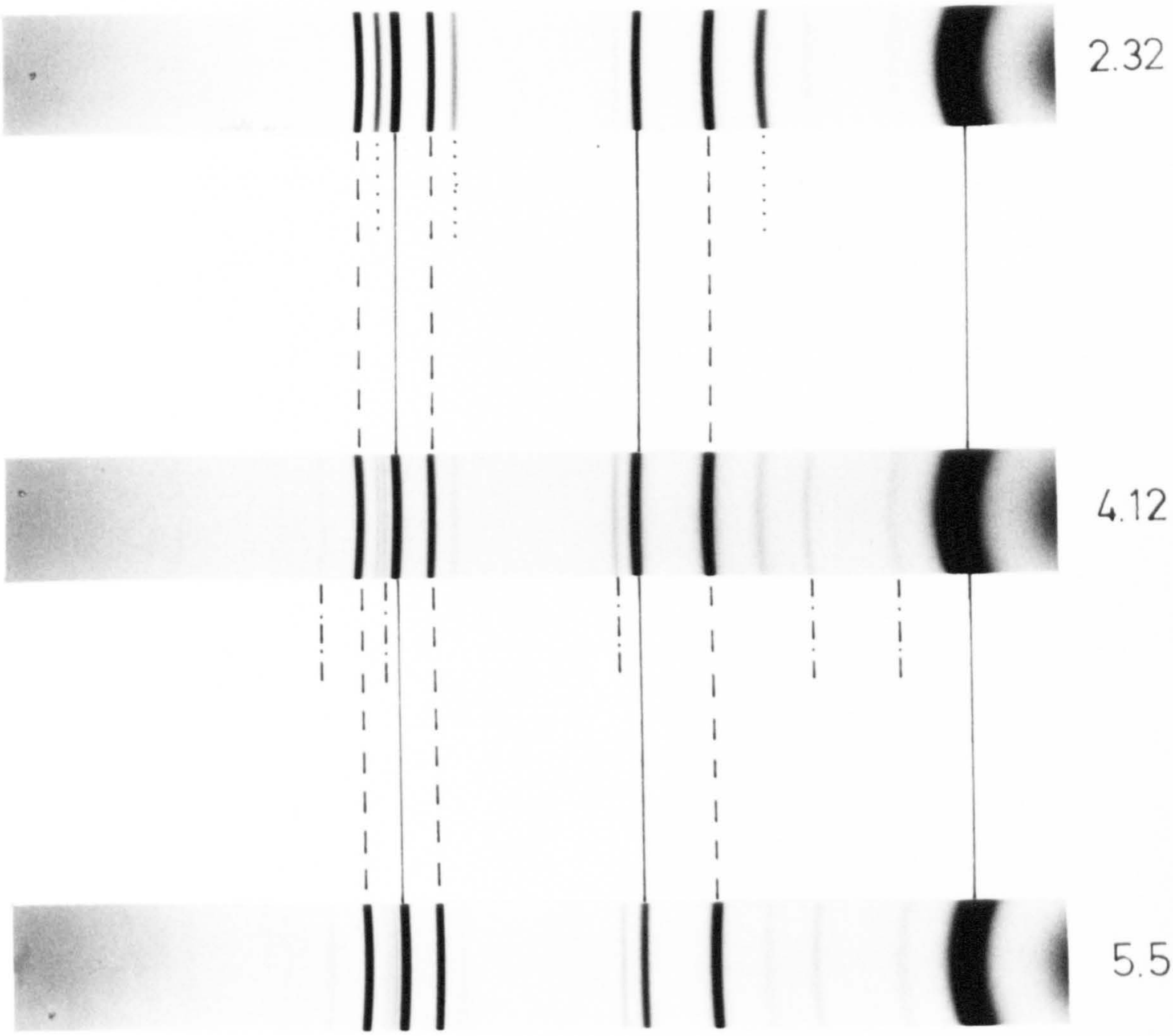

α-Fe. —— γ-Fe. .....

CrN -.-.- γ'-Fe_4N ----

X-RAY PHOTOGRAPHS OF ALLOYS NITRIDED IN

15%NH_3-H_2 AT 650°C FOR 73h.

Table IV.7

Thermodynamic data for iron and chromium nitrides

(from Kubachewski & Evans, 1958)

nitride	H°_{298}(k.cal.)	S°_{298}(cal./deg.)
$2Cr + \frac{1}{2}N_2 \longrightarrow Cr_2N$	-25.2 + 3.0	16.2 + 2.0
$Cr + \frac{1}{2}N_2 \longrightarrow CrN$	-28.2 + 2.5	20.6 + 1.2
$4Fe + \frac{1}{2}N_2 \longrightarrow Fe_4N$	- 2.6 + 2.0	37.3

Fig. IV. 9.

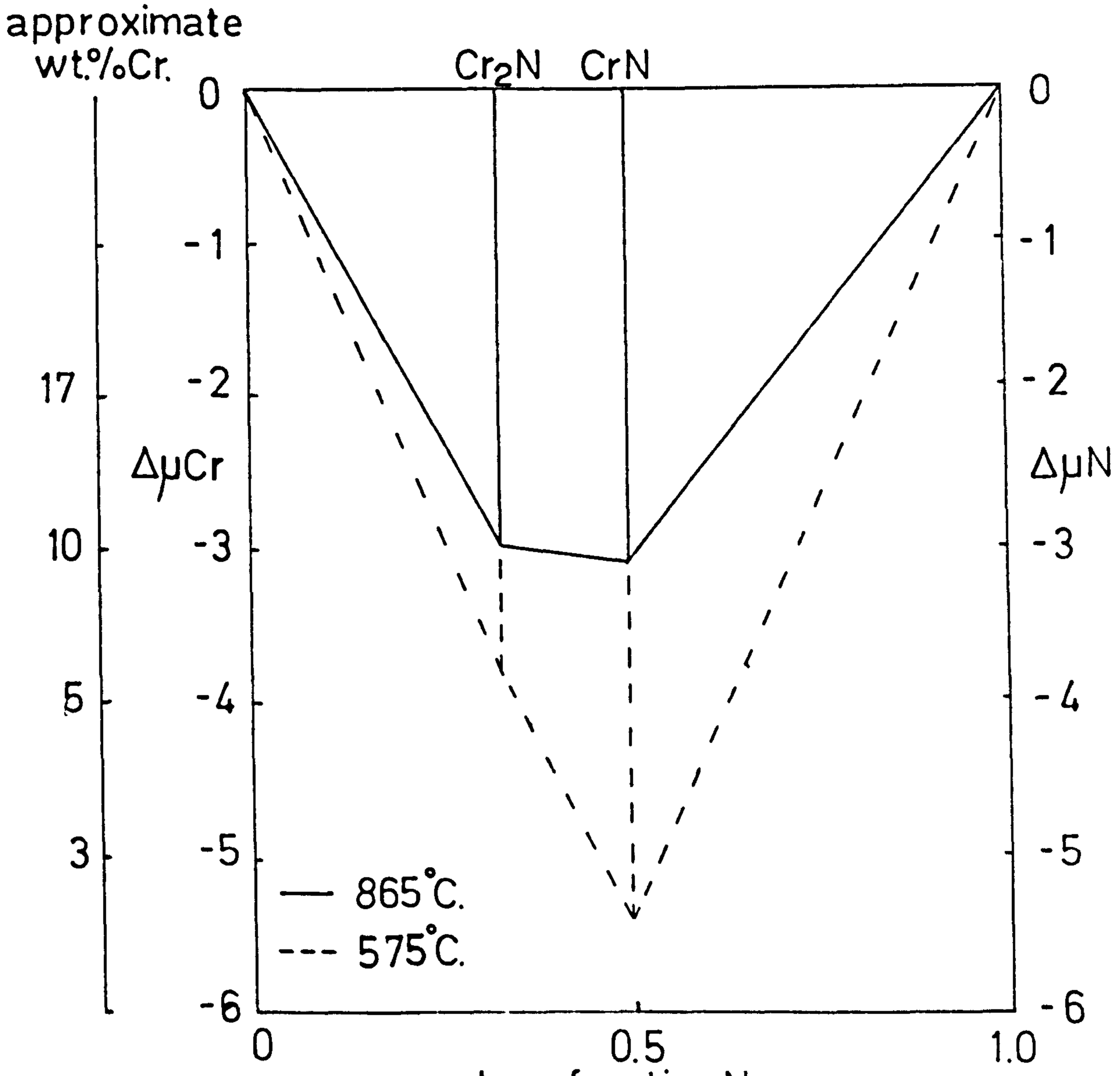

FREE ENERGY - COMPOSITION DIAGRAM FOR

THE CHROMIUM - NITROGEN SYSTEM

in solution by:

$$\Delta\mu_{Cr} = RT \ln a_{Cr} \quad \ldots.(11)$$

and $$\Delta\mu_{N} = RT \ln a_{N}. \quad \ldots.(12)$$

As the concentration of nitrogen in solution is of the order of 0.1wt.%N ideal solution behaviour is assumed and so

$$\Delta\mu_{N} = RT \ln [N] \quad \ldots.(13)$$

where [N] represents the concentration of nitrogen in solution. With activity data for iron-chromium alloys taken from Jeannin et. al. (1963) the solubility of nitrogen and chromium in equilibrium with each nitride precipitated from a given chromium ferrite can be determined.

Figure IV.9 shows that the nitride formed is dependant upon both the chromium and nitrogen contents of the ferrite during aging. However, errors of ± 1 - 2k.cal. in the available thermodynamic data, suggest that only a semi-quantitative discussion is appropriate.

At 575°C it can be predicted that CrN is more stable than Cr_2N and is always the nitride precipitated in the iron-chromium alloys used in the present investigation. At 865°C, "constant activity aging" of alloys with chromium contents lower than 17wt.% will precipitate CrN if the nitrogen activity is sufficiently high. The chromium content in solution will decrease to that in equilibrium with CrN and the gas mixture i.e. approximately 4wt.%Cr at 865°C with 80% nitrogen:20% hydrogen.

With concentrations of chromium greater than about 17wt.%, Cr_2N is stable and this phase precipitates on aging until the chromium content in ferritic solid solution falls to 17wt.% at which stage CrN is nucleated and grows at the expense of the primary precipitate. On completion of the process only CrN remains. The chromium content thus governs the nature of the primary precipitated phase but the extent to which the process proceeds is determined by time for a given applied nitrogen potential. In "constant activity aging" only

a single nitride is present at final equilibrium and so in runs 3, 7, 8, 12 and 13 CrN is growing at the expense of the Cr_2N. However, a mixture of two nitrides can remain in equilibrium in quench aged alloys since the dissolved nitrogen potential varies continuously during the precipitation process. A mixed nitride is obtained in alloys which, when reaching the Cr_2N - CrN transition point, have only sufficient supersaturated nitrogen to convert part of the lower nitride to the higher nitride.

IV.4 Conclusions

(a) The following seven phases are observed in Fe - Cr- N alloys:

α - ferrite, γ - austenite, γ'- Fe_4N, α''- $Fe_{16}N_2$
α' - martensite, CrN and Cr_2N.

No ternary phase is formed.

(b) The phase precipitated from a given alloy is dependant on both the nitrogen and chromium concentrations in accordance with the known thermodynamic data for the system.

Chapter V

Low temperature aging of Fe-Cr-N alloys

V.1 Introduction

No previous work has been published on the aging of Fe-Cr-N alloys at low temperatures. However, it is possible to predict the behaviour of these alloys from similar work on Fe-Mn-N alloys by Pipkin (1967), on Fe-Mo-N alloys by Spiers (1969) and on Fe-Si-N alloys by Roberts (1970). The results of these investigations are interpreted in terms of the effect of the substitutional alloying element on the activity coefficient of nitrogen in ferrite and the corresponding change in the critical nucleus size for formation of iron nitrides.

It is believed that Fe-Cr-N alloys behave in a similar manner during low temperature aging.

V.2 Experimental

The work of Spiers (1970) indicated that a homogeneous Fe-Mo-N alloy could be prepared by nitriding iron-molybdenum alloys, containing up to 5wt.%Mo, in a $16NH_3:84H_2$ gas mixture at $460^{o}C$ for approximately twenty hours. Longer times, higher temperatures or higher nitrogen potentials than these lead to precipitation of molybdenum nitrides.

Iron-chromium alloys were therefore nitrided for 13 hours in $19NH_3:81H_2$ at $465^{o}C$ (equivalent to 0.027wt.%N in pure iron) after which X-ray and metallographic examination showed no precipitation of chromium nitride. After aging at $125^{o}C$ and $250^{o}C$ in small evacuated silica capsules, specimens were water quenched.

Interstitial nitrogen interacts with dislocations and vacancies in addition to substitutional atoms. Cold working, for example, changes the effective activity coefficient of nitrogen (Darken & Wriedt, 1965) and hence the kinetics and morphology of nitride

precipitation. These factors were eliminated in the present work by hydrogen annealing prior to nitriding and by careful handling of the specimens.

V.3 Results of the low temperature aging of Fe-Cr-N alloys

The aging behaviour of four alloys, containing 0, 1.2, 2.3 and 5.6wt.% chromium, was initially studied at 250°C. Photomicrographs of quench-aged iron and iron-chromium alloys nitrided to the same nitrogen activity are shown in Figures V.1 - 3. The well known two stage precipitation process at 250°C (Dijkstra, 1949; Jack & Maxwell, 1952) in which the initial α''- $Fe_{16}N_2$ transforms completely to γ'- Fe_4N after about three hours is not observed because the alloys were nitrided to a nitrogen activity below that in equilibrium with $Fe_{16}N_2$ at 250°C. At this temperature the nitrogen activity in pure ferrite in equilibrium with $Fe_{16}N_2$ is equivalent to 0.03wt.%N in solution whereas, the nitrogen activity in the above alloys is equivalent to only 0.028wt.%N in pure iron.

In the pure iron and 1.20wt.%Cr alloy, γ'- Fe_4N was observed as characteristic small V's or needles of precipitate after five hours aging but no precipitate was observed after 1.5 hours. Figures V.1 and 2 show that the γ'- Fe_4N precipitates are bigger in 1.20wt.%Cr alloy and the precipitation is slower than in pure iron; the higher chromium alloys contain no observable precipitates. Subsequent hardness measurements shown in Table V.1 indicate that even at 465°C some chromium diffusion and hence chromium nitride formation occur because the higher chromium alloys had hardness values much higher than could be explained by solid solution hardening.

By nitriding for shorter times and at lower temperatures an attempt was made to observe precipitation in all the alloys but iron nitrides were never observed on aging 2.3 and 5.6wt.%Cr alloys.

Aging at 125°C for 51hours (see Figure V.3) produces $Fe_{16}N_2$ in the pure iron and 1.20wt.%Cr alloy. Once again the precipitates

Fig.V.1.

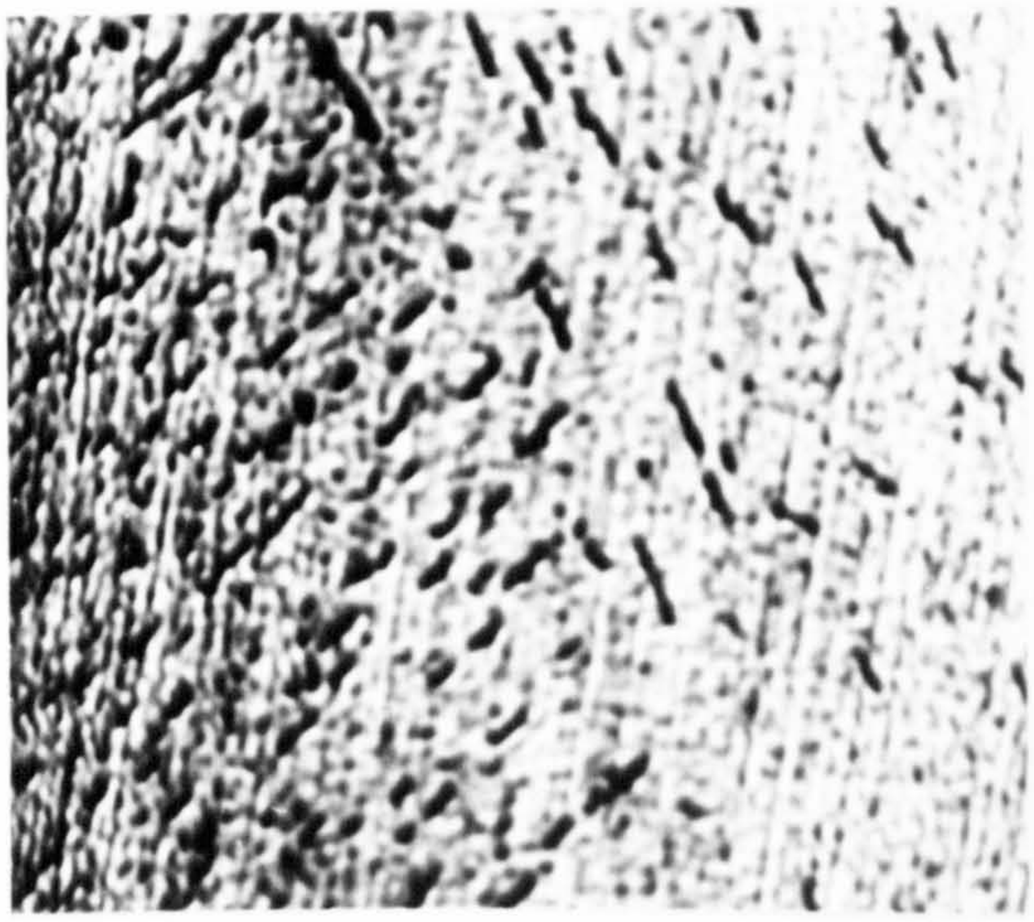

PURE IRON X 600.

1.2%Cr-Fe. X 600.

2.3%Cr-Fe. X 600.

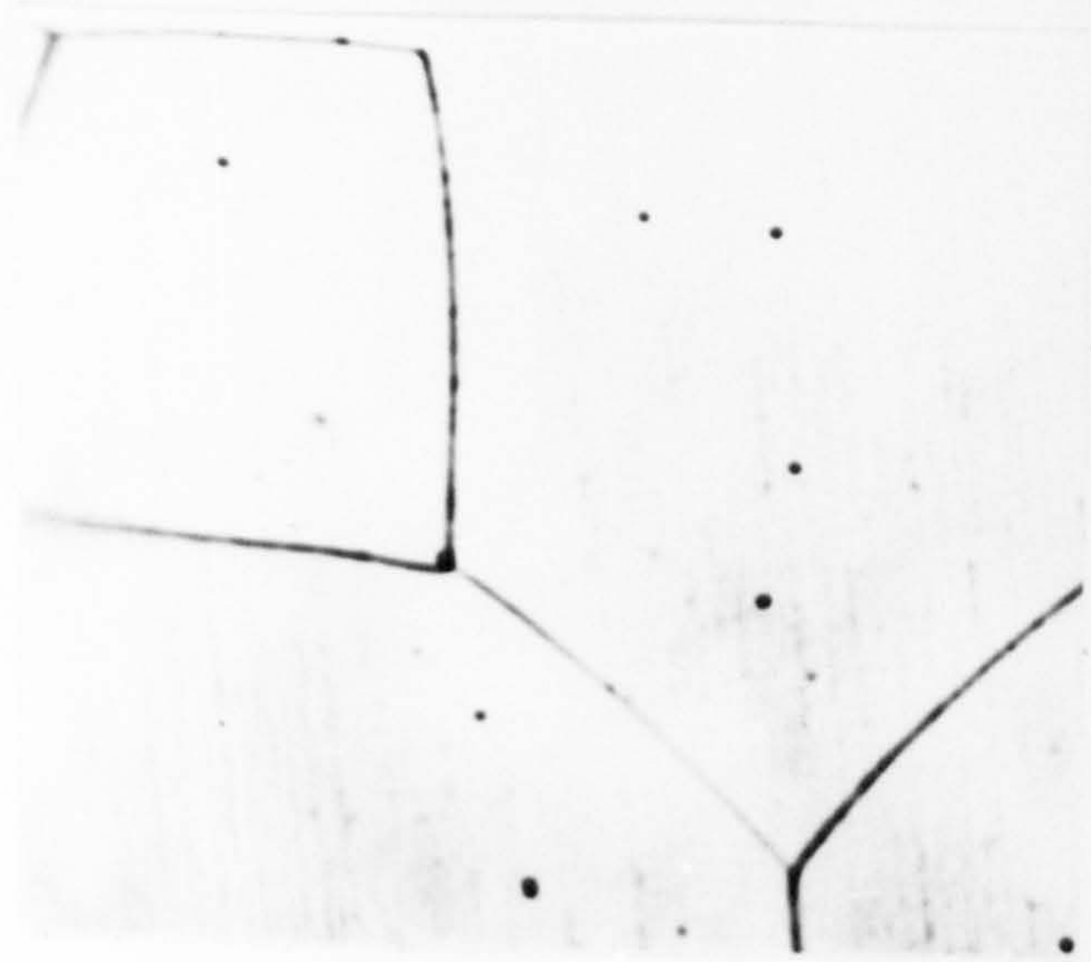

5.6%Cr-Fe. X 600.

PHOTOMICROGRAPHS OF IRON-CHROMIUM ALLOYS.

(Nitrided 465°C. 19%NH_3-H_2. 13h. Aged. 250°C. 5h.)

(Fe_4N Precipitated.)

Fig.V.2.

PURE IRON X 600.

1.2%Cr-Fe. X600.

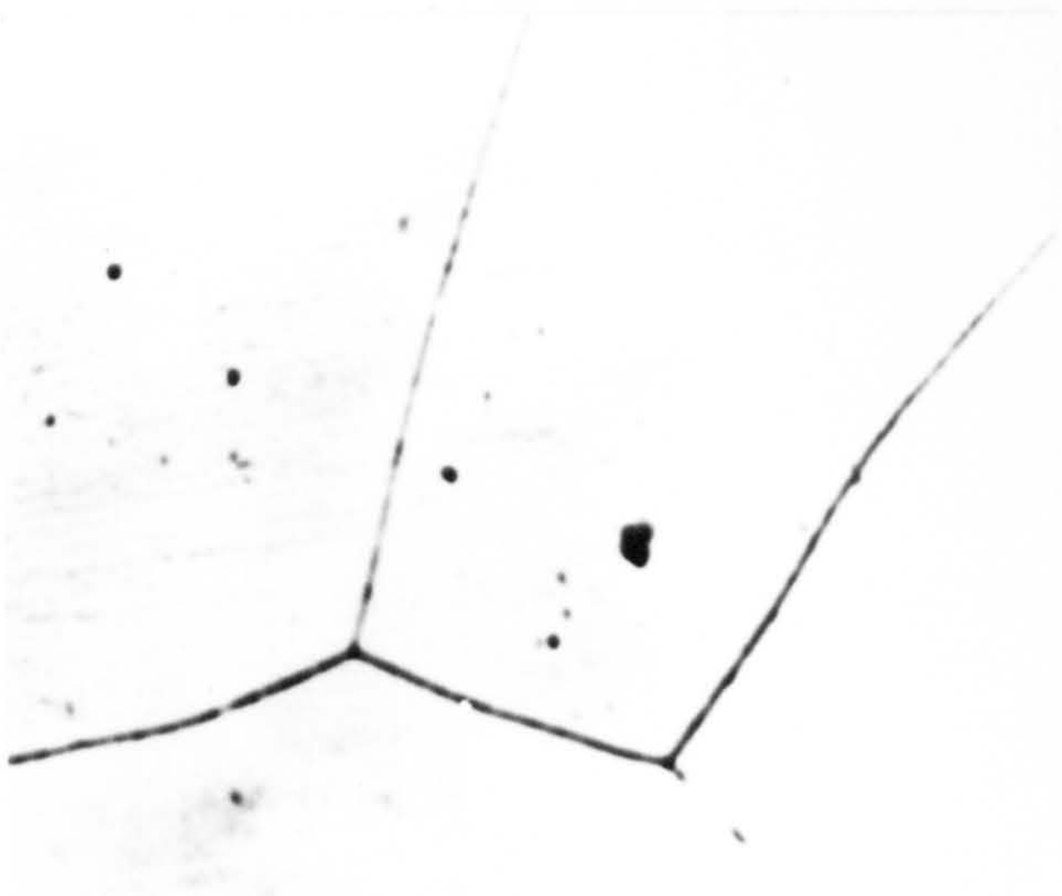

2.3%Cr-Fe. X600.

5.6%Cr-Fe. X600.

PHOTOMICROGRAPHS OF IRON-CHROMIUM ALLOYS

(Nitrided 465°C. 19%NH_3-H_2 13h. Aged 250°C. 17h.)

(Fe_4N Precipitated.)

Fig. V.3.

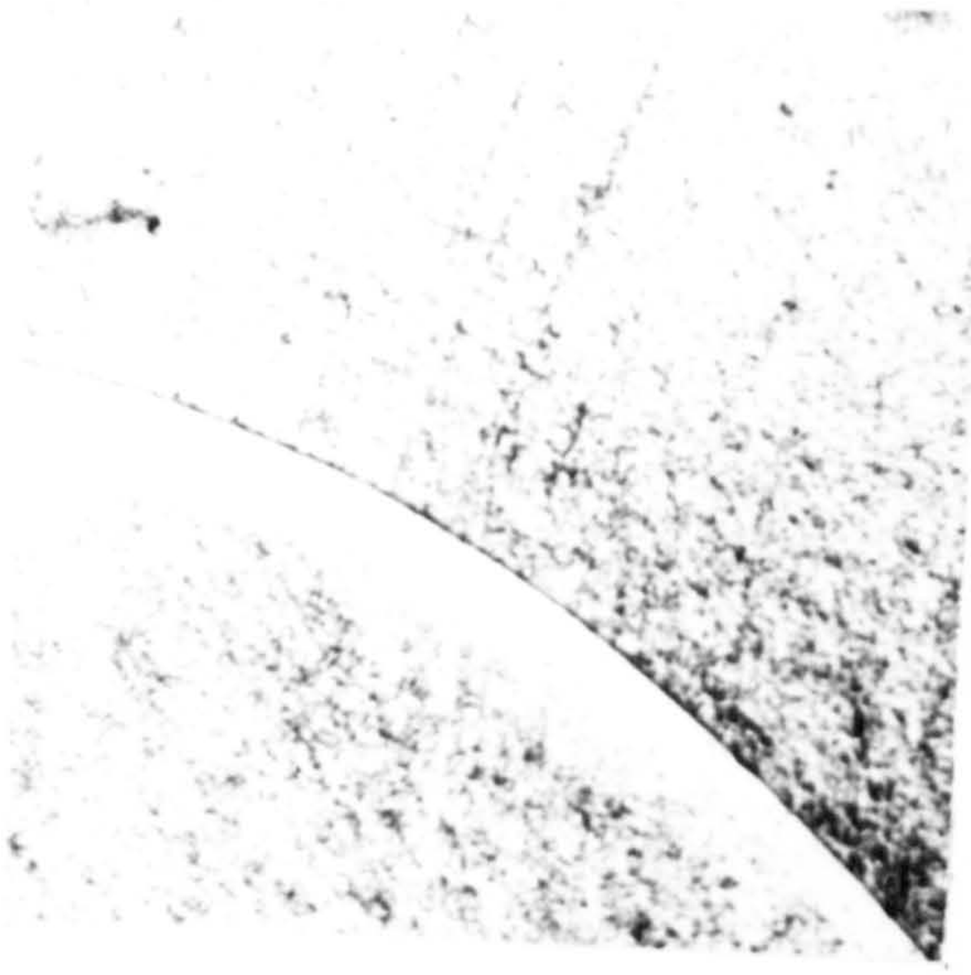

PURE IRON X 1000.

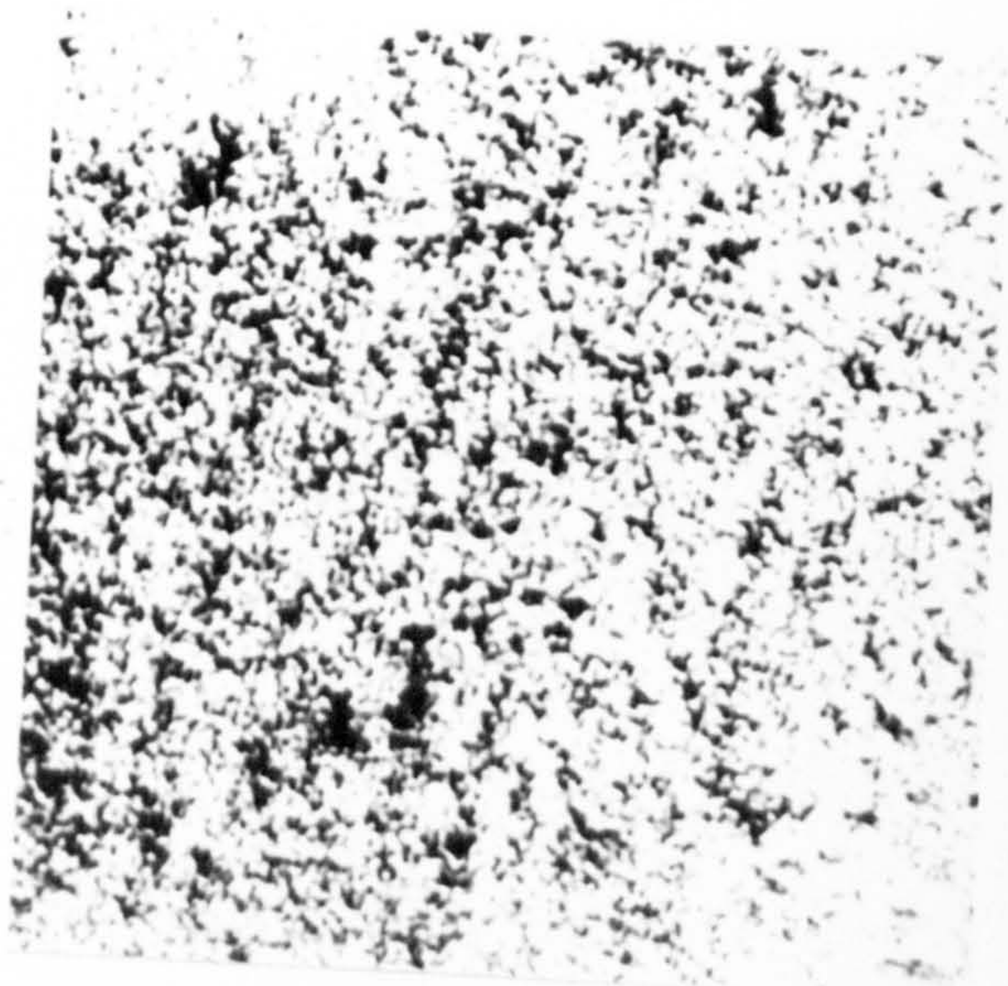

1.2% Cr-Fe. X 1000.

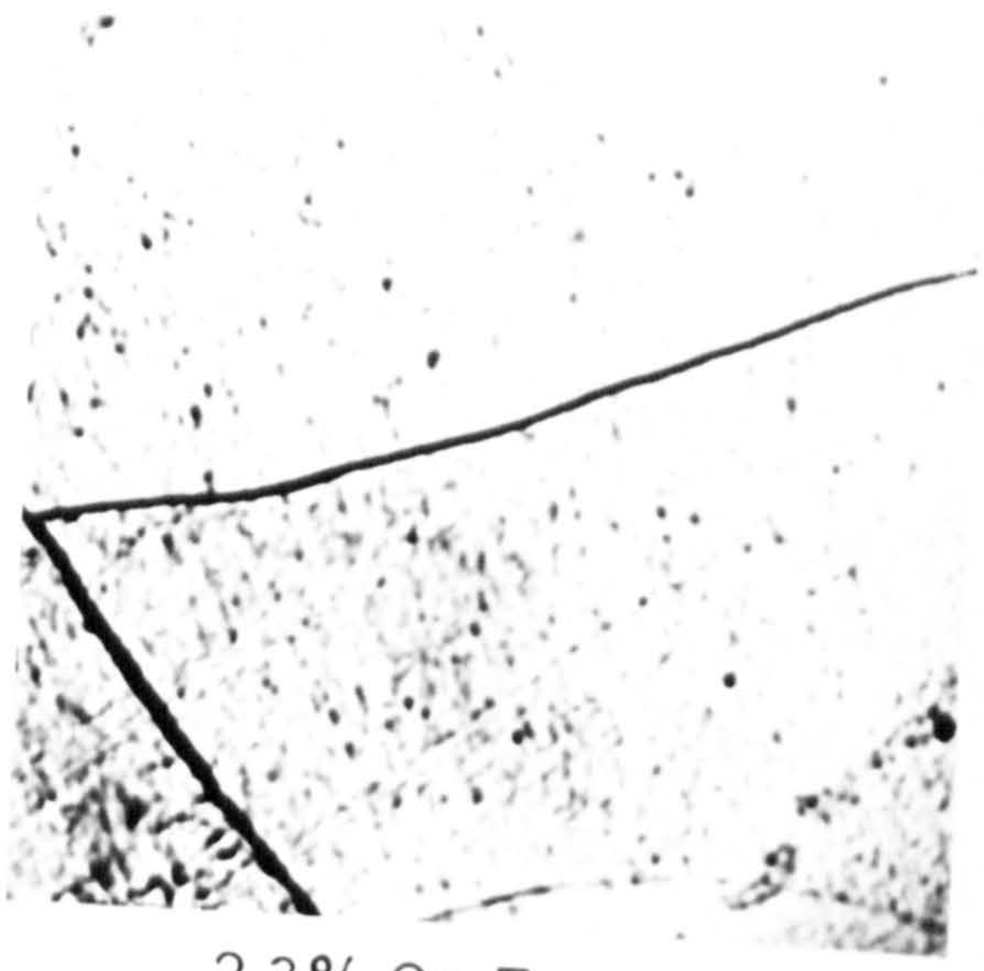

2.3% Cr-Fe. X 1000.

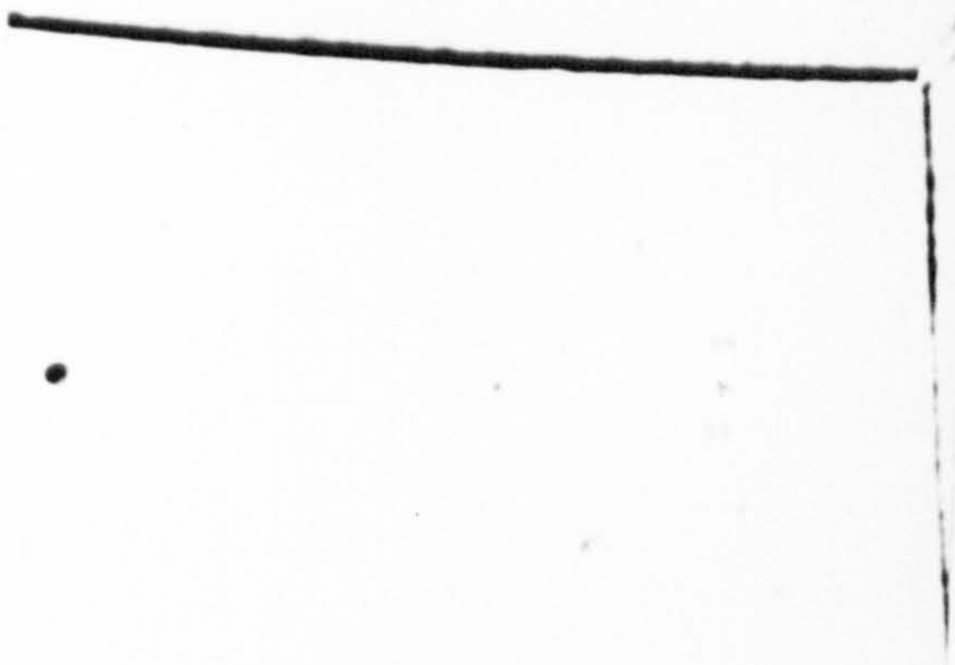

5.6% Cr-Fe. X 1000.

PHOTOMICROGRAPHS OF IRON-CHROMIUM ALLOYS.

(Nitrided 465°C. 19% NH_3-H_2. 13h. Aged 125°C. 51h.)

($Fe_{16}N_2$ Precipitated.)

Table V.1

Microhardness values for alloys "constant activity aged" at 465°C

wt.%Cr	H_M (kg/mm^2)	H_M (kg/mm^2) (as annealed)
0	140	90
1.2	150	100
2.3	330	120
5.6	410	150

are larger in the chromium alloy than in the pure iron.

V.4 Discussion

The effects of alloying elements (x) on the activity coefficient of nitrogen in liquid iron $(f_N^x)^{\ast}$ are shown in Figure V.4; the relative effects are expected to be much more pronounced in solid iron as the departure from ideality increases with decreasing temperature.

Metallographic examination of aged alloys demonstrates that the size of γ'- Fe_4N and α''- $Fe_{16}N_2$ precipitates increase as the chromium content increases and the quantity of precipitate increases with chromium content.

During nitriding, for a given nitrogen activity $p_{NH_3}/p_{H_2}^{3/2}$ in the nitriding gas, the nitrogen concentration in solid solution varies according to whether the activity coefficient is decreased or increased since:

$$K \cdot p_{NH_3}/p_{H_2}^{3/2} = a_N = f_N^{Cr} \cdot [wt.\%N] \qquad \ldots.(14)$$

where K is the equilibrium constant.

For a substitutional solute which decreases f_N^x the total amount of nitrogen precipitated must increase. Since chromium decreases the activity coefficient of nitrogen then the increase in the quantity of precipitate is explained but not the variation in precipitate size.

The latter observation is explained by nucleation theory which gives the critical radius (r^*) for nucleation of a spherical particle (Heal & Hardy, 1954) as:

$$r^* = \frac{-2\sigma}{\Delta G_v} \qquad \ldots.(15)$$

where ΔG_v is the free energy change per unit volume;

σ is the surface energy per unit area of the particle-matrix interface;

and where any strain energy contribution is neglected.

(* f_N^x is the activity coefficient of nitrogen in the alloy using the infinitely dilute solution of nitrogen in α-iron as the standard state i.e. $a_N = f_N^x \cdot$ wt.%N, where $f_N^x \rightarrow 1$ as wt.%N $\rightarrow$ 0.)

Fig V.4

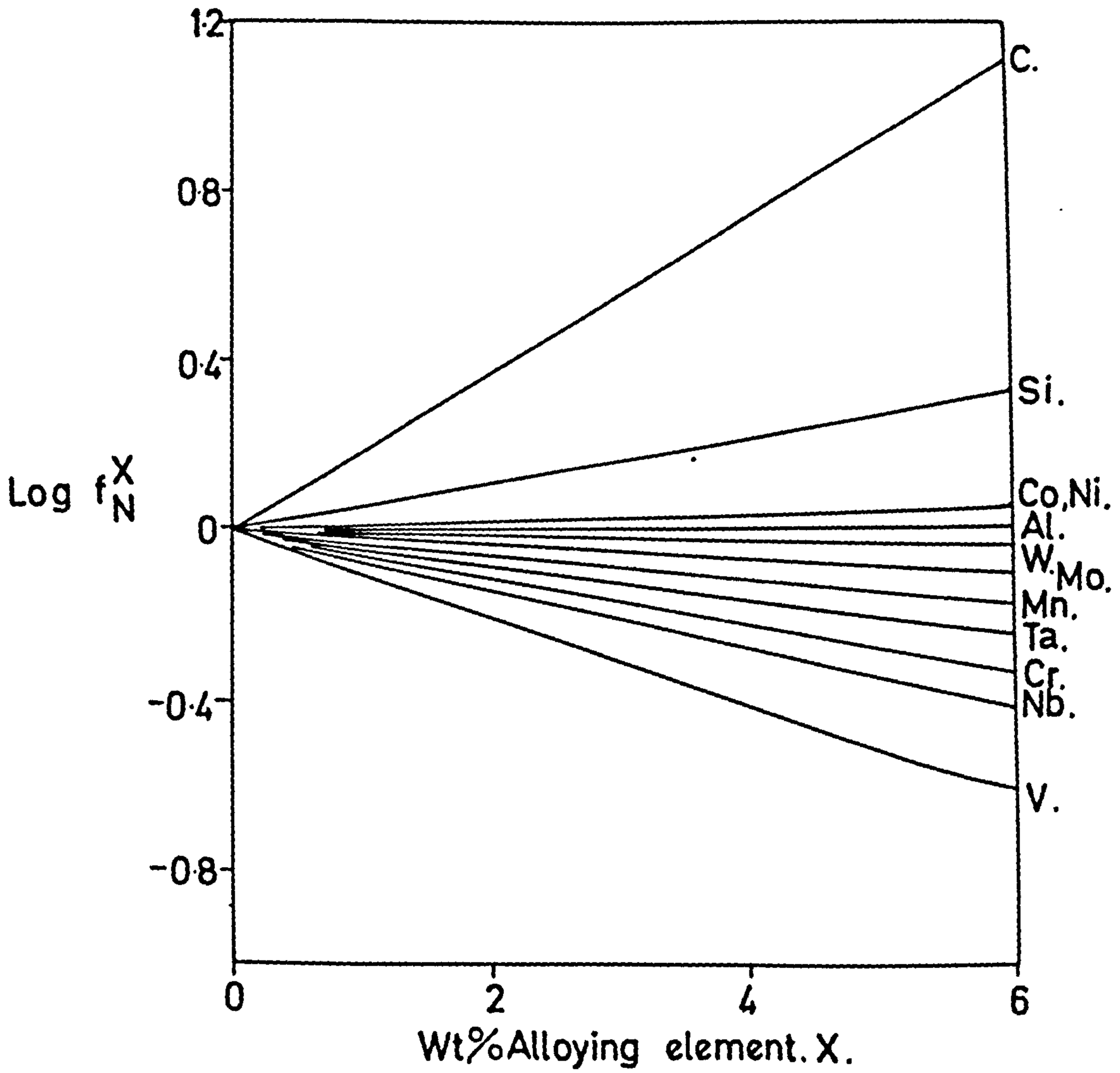

THE EFFECT OF ALLOYING ELEMENTS ON THE ACTIVITY COEFFICIENT OF NITROGEN IN IRON AT 1600°C

[from Schenck et.al.(1958) & Pehlke and Elliott (1960).]

The driving force for precipitation per unit volume is

$$\Delta G_v = \frac{-RT}{\Omega} \cdot \ln \frac{a_1}{a_2} \quad \ldots.(16)$$

where a_1 is the solute activity in the supersaturated solid solution at T^oK ;

a_2 is the activity in equilibrium with the precipitated phase at the same temperature

and Ω is the molar volume of the precipitate.

After nitriding with the same gas mixtures both the pure iron and the iron alloys have the same nitrogen activity. When the temperature is reduced f_N^x changes because the solution deviates further from ideality and hence at the aging temperature the nitrogen activity in the alloy ferrite is altered relative to that in pure iron. Alloying additions which decrease f_N^x cause a further decrease in the activity coefficient with decreasing temperature and so the activity a_1 decreases and, assuming σ is constant, r^* is increased. Conversely, r^* is decreased by alloy additions that increase f_N^x .

This effect of the substitutional alloying element on r^* could explain the absence of precipitation in 2.3 and 5.6wt.%Cr alloys as r^* may be so large that it inhibits homogeneous precipitation of iron nitrides. A more likely explanation is that the amount of nitrogen in solution in these higher chromium alloys is reduced due to the precipitation of CrN at the nitriding temperature and therefore precipitation of iron nitrides does not occur on aging at low temperature. The hardness increases observed with 2.3 and 5.6wt.%Cr alloys also indicate that precipitation of CrN has occurred during nitriding.

Precipitates in quench-aged iron-chromium-nitrogen alloys are larger than those in similarly treated iron-nitrogen alloys. These observations are in complete agreement with the previous work on Fe-Mn-N (Pipkin, 1967) and Fe-Mo-N (Spiers, 1969) where precipitates in the alloy ferrites are coarser because manganese and molybdenum similarly decrease the activity coefficient of nitrogen in iron. The relative sizes of precipitates for alloys with approximately 1wt.% of

substitutional element treated under similar conditions are in agreement with the relative effect of the chromium, manganese and molybdenum on f_N^x (see Figure V.4) i.e. the precipitates in chromium alloys are coarser than those in manganese ferrite and in turn these are larger than in molybdenum ferrite (see Figure V.5).

The work on Fe-Si-N alloys (Roberts, 1970) showed in striking contrast that the opposite effects occur in these alloys because silicon increases the activity coefficient of nitrogen in iron.

V.5 Conclusions

(a) The aging of iron-chromium-nitrogen alloys at low temperatures is explained by the effect of chromium on the activity coefficient of nitrogen in solution in ferrite.

(b) Chromium decreases the activity coefficient of nitrogen in ferrite and the activity coefficient for a given chromium content decreases still further with decreasing temperature.

(c) At a given nitrogen potential, the increased amount of precipitate in the chromium alloy with respect to pure iron is due to the decreased activity coefficient.

(d) The coarsening of γ'- Fe_4N precipitates as the chromium content increases is also a result of the change in activity coefficient of nitrogen in iron and is accounted for in terms of nucleation theory.

Fig. V. 5

PURE IRON X1000 0.58at.%Si-Fe. X1000.

Nitrided 590°C. 9%NH_3-H_2. 24h. Aged 250°C. 24h.

PURE IRON X600 1.17at.%Mo-Fe. X600

Nitrided 460°C. 16%NH_3-H_2. 20h. Aged 250°C. 24h.

PURE IRON X600 1.29at.%Cr-Fe. X600.

Nitrided 465°C. 19%NH_3-H_2 13h. Aged 250°C. 17h.

PHOTOMICROGRAPHS OF AGED Fe-X-N ALLOYS.

Chapter VI

Homogeneous precipitation in iron-chromium-nitrogen alloys

VI.1 Introduction

Spiers (1969) showed that the nitriding of iron-molybdenum alloys below 600°C produced very hard materials associated with non-equilibrium precipitation. Electron microscopy and electron diffraction showed that the precipitation sequence was similar to that observed in face-centred cubic alloys i.e.

G.P. zones ⟶ metastable intermediate ⟶ equilibrium precipitate
precipitate

and demonstrated for the first time the occurrence of Guinier-Preston zones containing both substitutional and interstitial solute atoms. It seemed important to establish whether similar precipitation sequences were a general feature of iron-substitutional element-nitrogen systems. Roberts (1970) showed that pre-precipitation effects occurred in Fe-Nb-N alloys and the present work aimed at investigating the more industrially important Fe-Cr-N system. It seemed of interest

(a) to establish the sequence of homogeneous precipitation stages, if any, in Fe-Cr-N alloys; and

(b) to characterize the phases formed and their orientation relationships with the matrix.

VI.2 The electron microscopy of Fe-Cr-N alloys

Thin foils of the materials obtained by nitriding were examined in the electron microscope under experimental conditions tabulated in Table VI.1.

The micrograph shown in Figure VI.1 is typical of the structure observed on nitriding 1.2wt.%Cr alloy at 575°C. The electron diffraction patterns exhibit marked streaking in $\langle 100 \rangle_\alpha$ directions and dark field photographs taken from the region of maximum intensity in the streak

The treatment of foils and electron microscopic observations

wt.%Cr	$NH_3:H_2$	temperature °C	time (hrs)	CrN mean dics$_o$size, A	observations
1.2	6:94	575	6	200	streaked CrN spots
1.2	6:94	575	18	300	" " "
1.2	10:90	575	48	400	" " "
5.6	6:94	575	12	300	needle-like growths in transformed areas.
5.6	6:94	575	25	300-400	
5.6	6:94	575	120	600-700	
9.9	6:94	575	120	1000	
1.2	15:85	520	21	100	continuous streaking
1.2	15:85	520	126	100	" "
1.2	15:85	520	252	150	" "
1.2	19:81	475	242	100	" "
5.6	19:81	475	242	-	completely transformed to growths.
9.9	19:81	475	242	-	" " " "
9.9	6:94	575	120	1000	replica - CrN laths in grain boundaries.

Fig. VI. 1.

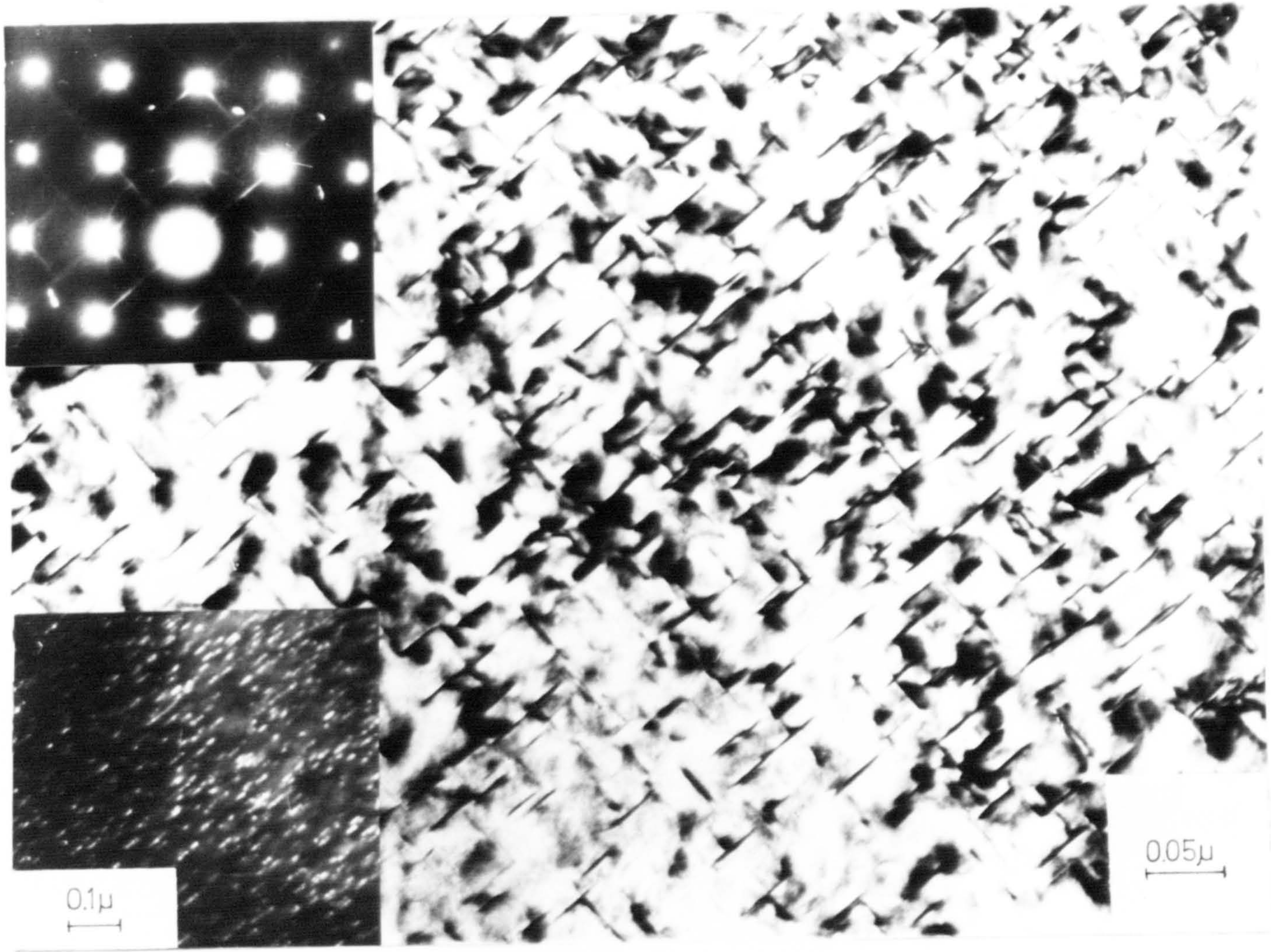

COHERENT PARTICLES OF CrN PRECIPITATED BY CONSTANT ACTIVITY AGEING

IRON - 1.2% CHROMIUM ALLOY.

(Nitrided 575°C. 6% NH_3-H_2 18h.)

shows that the precipitates are responsible for the streaks. Further aging of 1.2wt.%Cr alloys results in growth of the precipitate with a resultant decrease in the diffraction streaking. The diffraction patterns shown in Figure VI.2 from a thin foil of Fe : 5.6wt.%Cr nitrided for 5 days at 575°C in $6NH_3:94H_2$ are identical to those found in 1.2 and 2.3wt.%Cr alloys after the precipitates have grown large enough to give a discrete diffraction pattern. In all these alloys the disc-shaped precipitates on $\{100\}_\alpha$ planes give the same diffraction patterns and these are indexed as arising from face-centred cubic CrN with the Baker-Nutting (1959) orientation relationship:

$$(001)_\alpha \,//\, (001)\ CrN \quad ; \quad [100]_\alpha \,//\, [110]\ CrN \ .$$

The micrographs of Figures VI.3 and 4 are from a carbon extraction replica taken from the surface of nitrided 9.9wt.%Cr alloy. This shows homogeneous precipitation of CrN discs in the ferrite grains together with grain boundary laths of CrN.

At lower temperatures the kinetics of nitriding and rates of precipitate growth are obviously slower. Figure VI.5 illustrates an early stage in the nitriding of 1.2wt.%Cr alloy at 520°C. The disc-shaped precipitates are only 100Å across and the $\langle 100 \rangle$ diffraction pattern is continuously streaked. The $\langle 111 \rangle$ diffraction pattern taken from another grain in the thin foil shows three spikes of intensity around the $\{110\}$ diffraction spots. These rods of intensity in reciprocal space along $\langle 100 \rangle$ matrix directions are clear evidence of the disc-like nature of the particles lying on $\langle 100 \rangle$ matrix planes. This material was subsequently studied in a one million volt electron microscope to determine the nature of these small precipitates and the diffraction pattern shown in Figure VI.6 was obtained. It illustrates the value of high voltage instruments in that the lower wavelength of the electron beam allows the production of a diffraction pattern from smaller precipitates. The discrete diffraction patterns from the three orientations of CrN are clearly discernable superimposed on the (320) matrix pattern.

Fig.VI.2.

Fig. VI. 3.

HOMOGENEOUS PRECIPITATION OF CrN IN IRON-5.6%CHROMIUM ALLOY

(Nitrided 575°C. 6%NH_3-H_2 120h.)

Fig. VI.4.

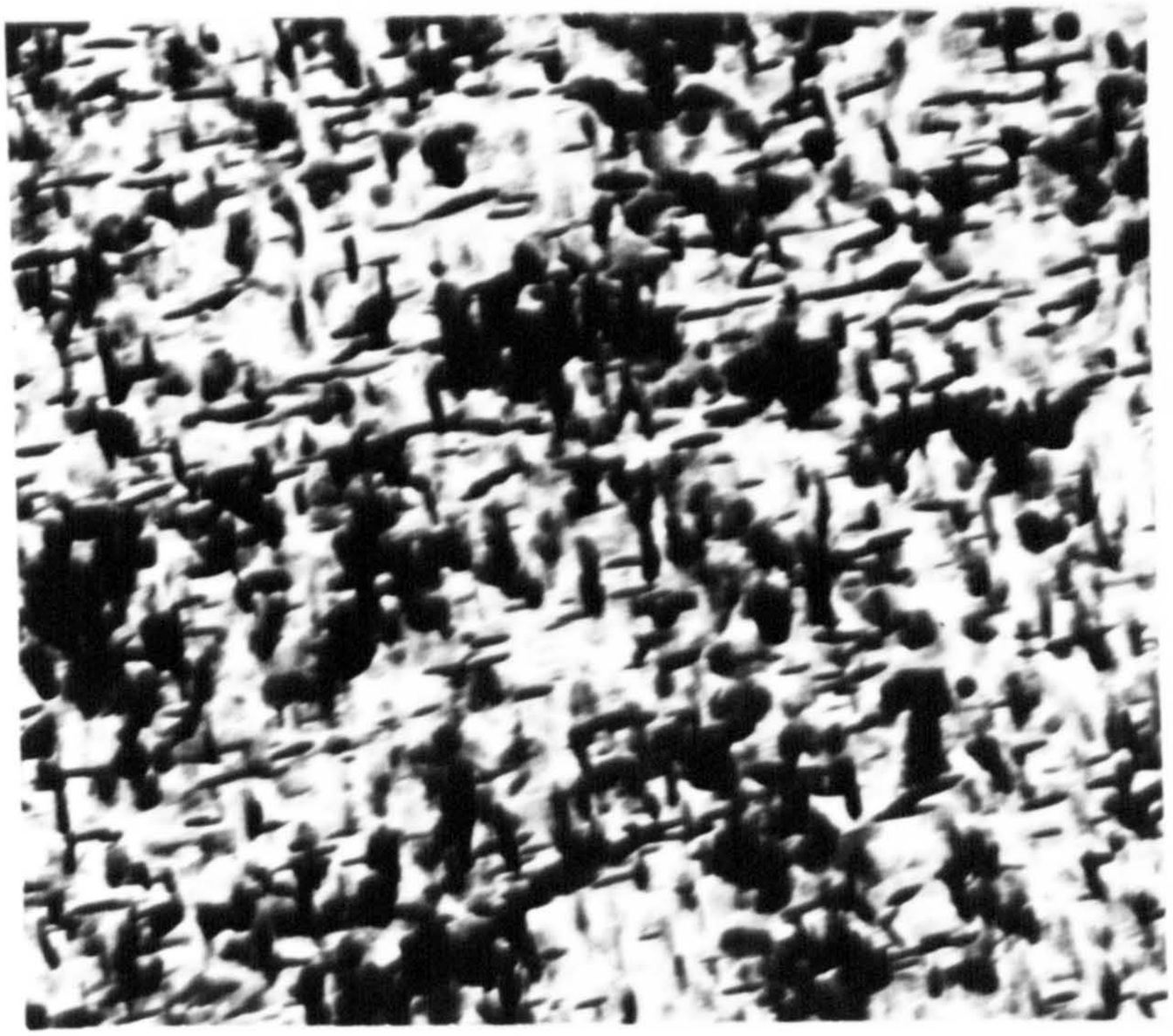

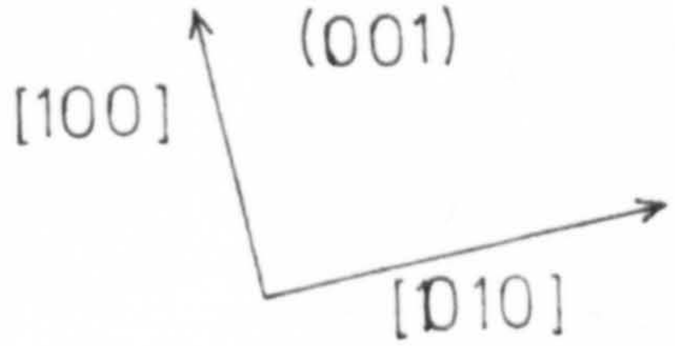

0.2μ.

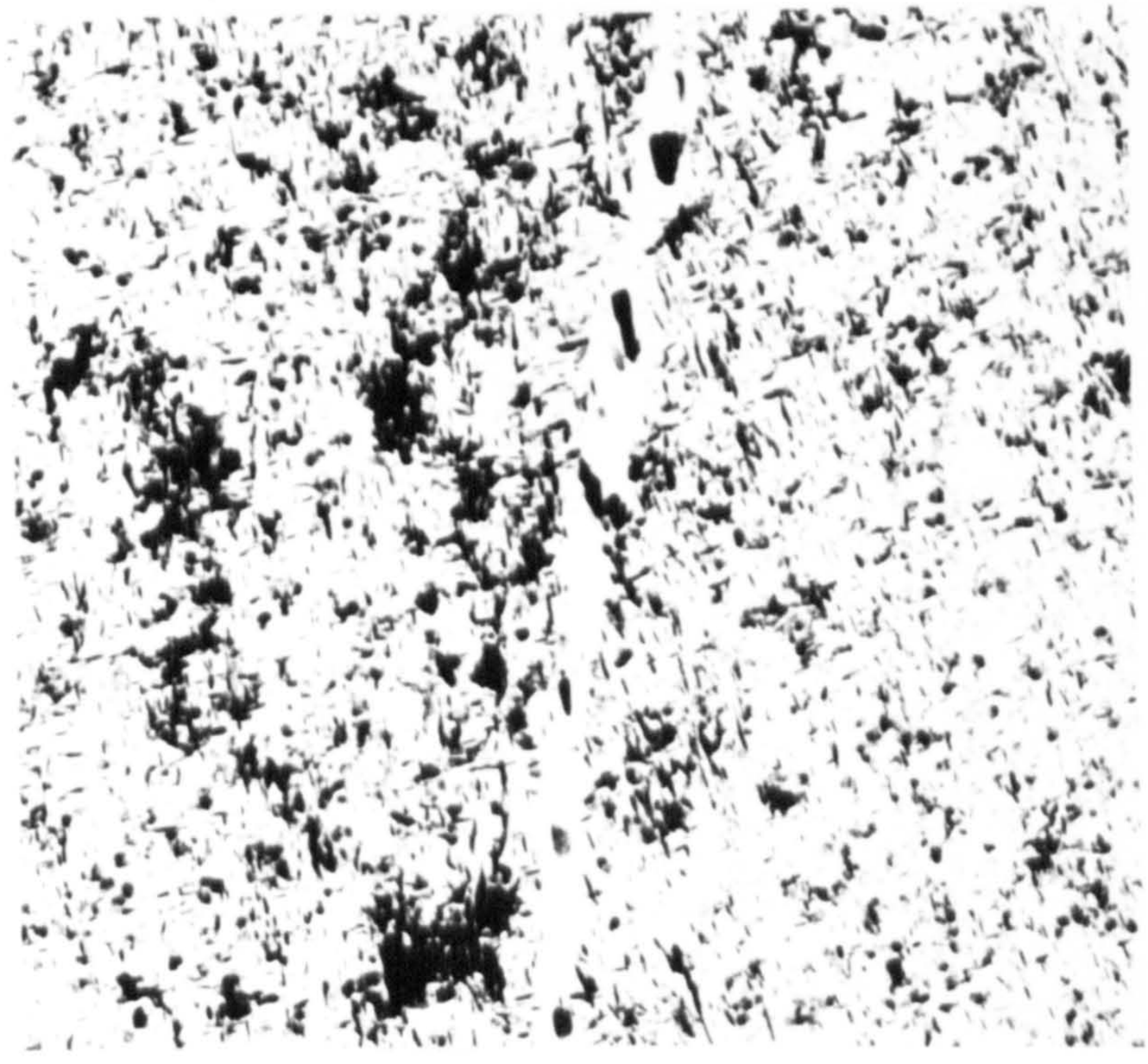

0.5μ.

HOMOGENEOUS AND GRAIN BOUNDARY PRECIPITATION OF CrN IN IRON - 9.9% CHROMIUM ALLOY.

(Nitrided 575°C. 6% NH_3-H_2. 97h. : carbon replica.)

Fig.VI.5.

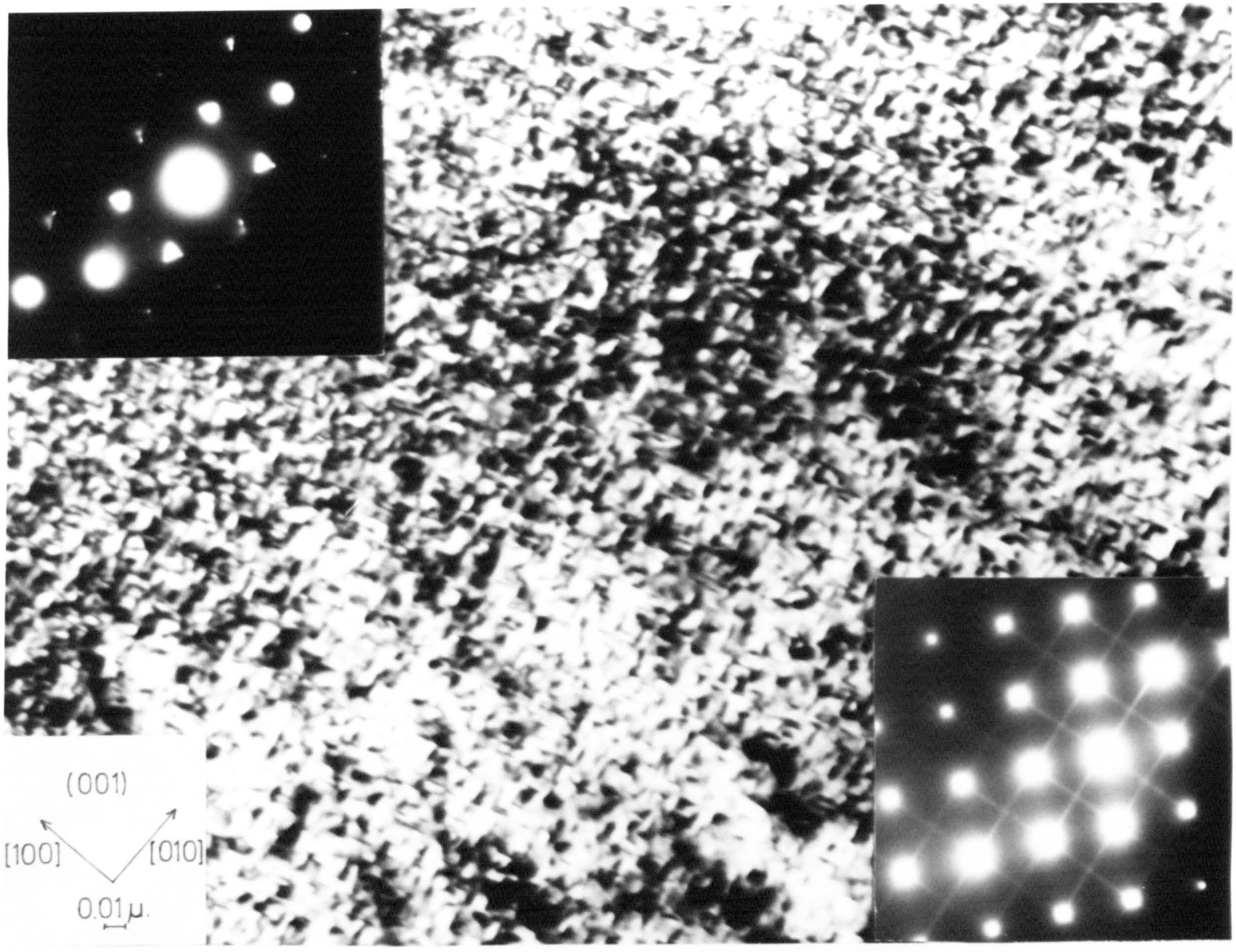

COHERENT PARTICLES OF CrN PRECIPITATED BY CONSTANT ACTIVITY AGEING

IRON - 1.2% CHROMIUM ALLOY.

(Nitrided 520°C. 15% NH_3 - H_2. 21h.)

Fig.VI.6.

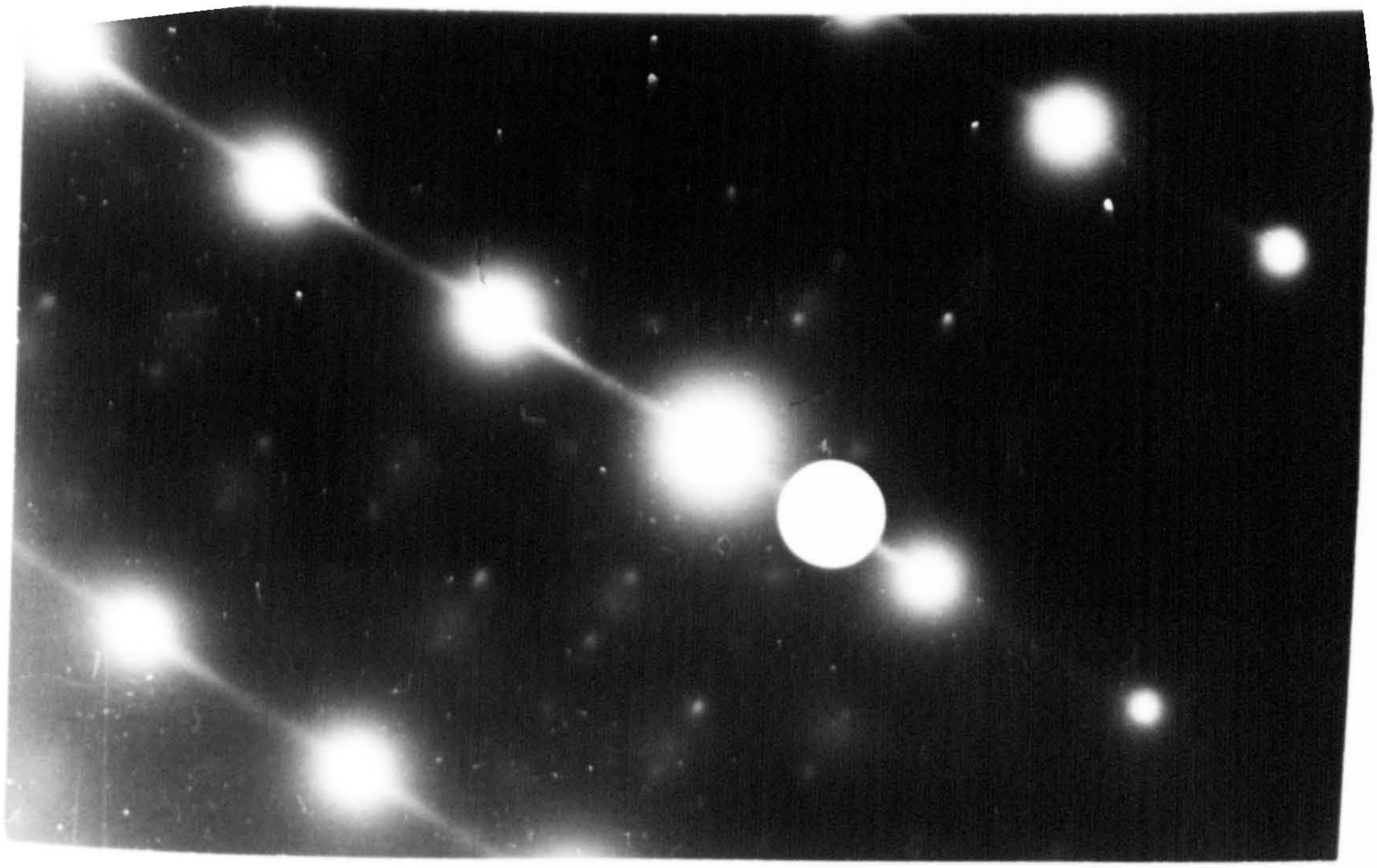

[320]Matrix(M) [111]CrN(A) [112]CrN(B) [510]CrN(C) Zones.
s-streaked CrN spot.

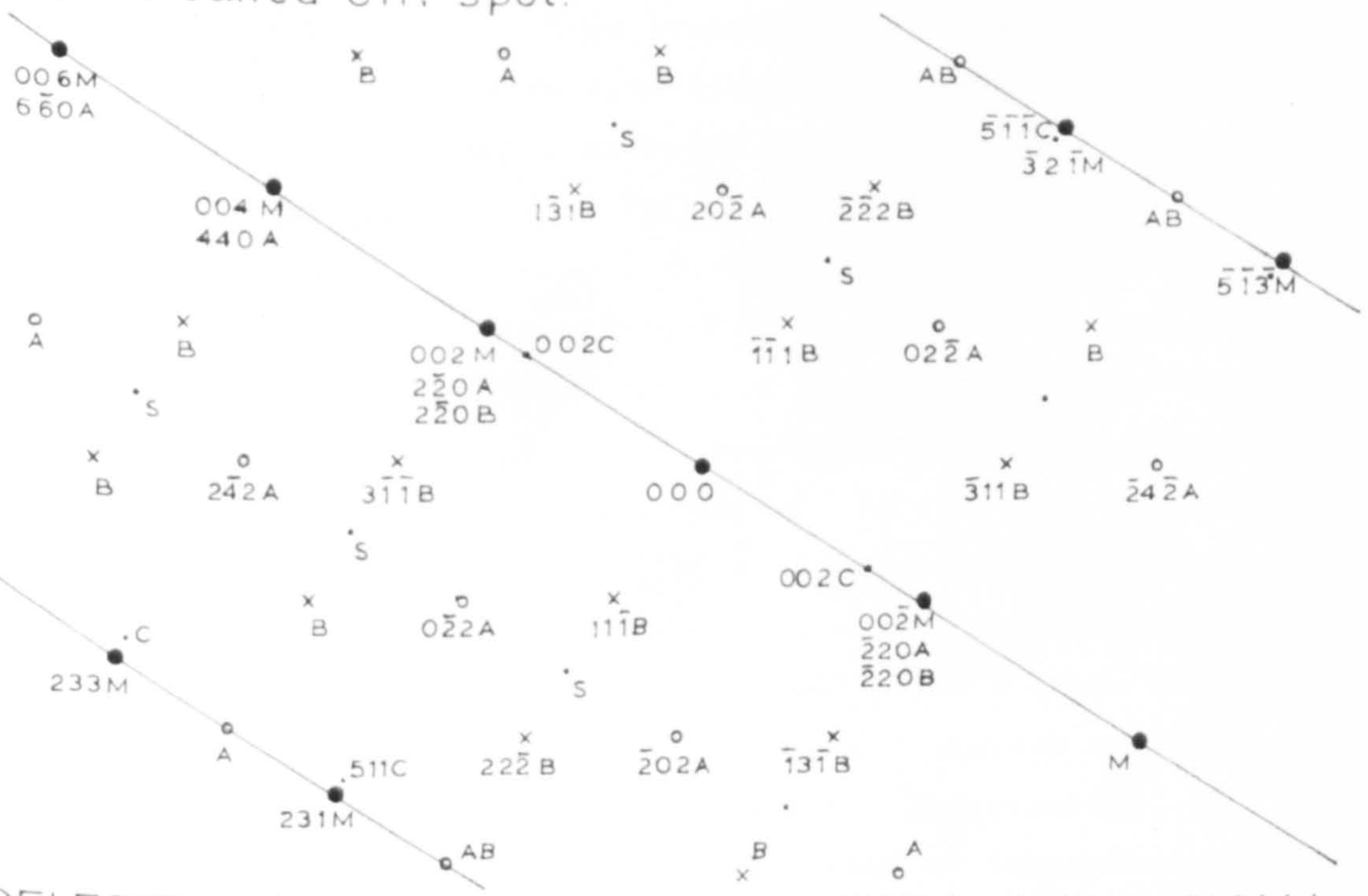

SELECTED AREA DIFFRACTION PATTERN FROM SMALL COHERENT PARTICLES OBSERVED IN 1M.V. ELECTRON MICROSCOPE. (Nitrided 520°C. 15%NH_3-H_2. 21h.)

The weight gain data obtained on nitriding alloys at 475°C for ten days is shown in Table VI.2 and clearly indicates conversion of the chromium to CrN; the latter was further confirmed by X-ray diffraction for the chromium-rich alloys. Examination of the lower 1.2wt.%Cr alloy in the electron microscope showed that homogeneous precipitation, completely analogous to that shown in Figure VI.5, had occurred.

VI.3 The transformation of nitrided iron-chromium alloys on aging

Prolonged nitriding at temperatures below 600°C, of alloys containing more than 5wt.%Cr produces growths from the grain boundaries which increase on continuing the nitriding until the whole of the matrix has transformed. Untransformed areas retain their high hardness until the transformation front has passed, after which the hardness decreases to 600 - 700 V.M.H.

Electron micrographs from transformed regions are shown in Figure VI.7. The precipitates were identified as CrN by X-ray and electron diffraction and their acicular morphology (see Figure VI.8) is identical to that observed by Spiers (1970) in Fe-Mo-N alloys. The work of Grozier et. al. (1963) on the transformation of nitrogen--ferrite to austenite is characterized by similar needle type growths nucleated along grain boundaries and this led to the suggestion that the transformation of Fe-Mo-N alloys during prolonged nitriding is associated with the formation of austenite. In addition, the recent investigations by Berry et. al. (1970) of fibrous alloy-carbide growth during the isothermal transformation of austenitic iron--molybdenum-carbon to Mo_2C and ferrite at 600 - 900°C shows that the decomposition of carbon-austenite produces a similar morphology to that observed in the present investigation. Nevertheless, the formation and growth of fibres in Fe-Cr-N alloys at temperatures as low as 475°C (see Figure VI.9) suggests that austenite formation is not a prerequisite for such transformations. The process is simply the conversion of small homogeneously precipitated CrN, a state with

Table VI.2

Weight changes in nitriding iron-chromium alloys at 475°C

wt.%Cr	average observed weight gain (wt.%N)	calculated * weight gain (wt.%N)	H_M (kg/mm^2)
1.2	0.30	0.33	550
2.3	0.68	0.63	850
5.6	1.46	1.41	660
9.9	2.40	2.31	650

* 0.03wt.%N in solution in ferrite.

Fig.VI.7.

0.1μ

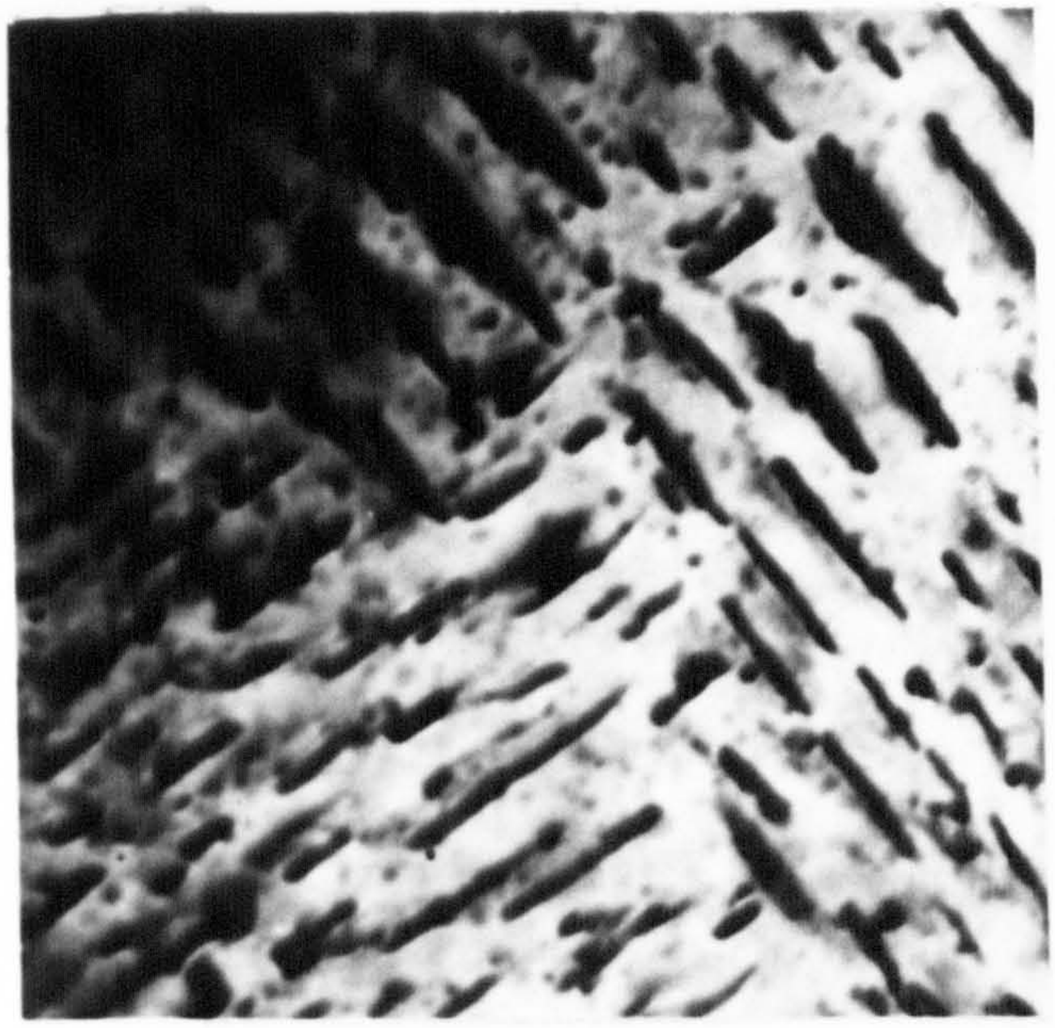

0.1μ

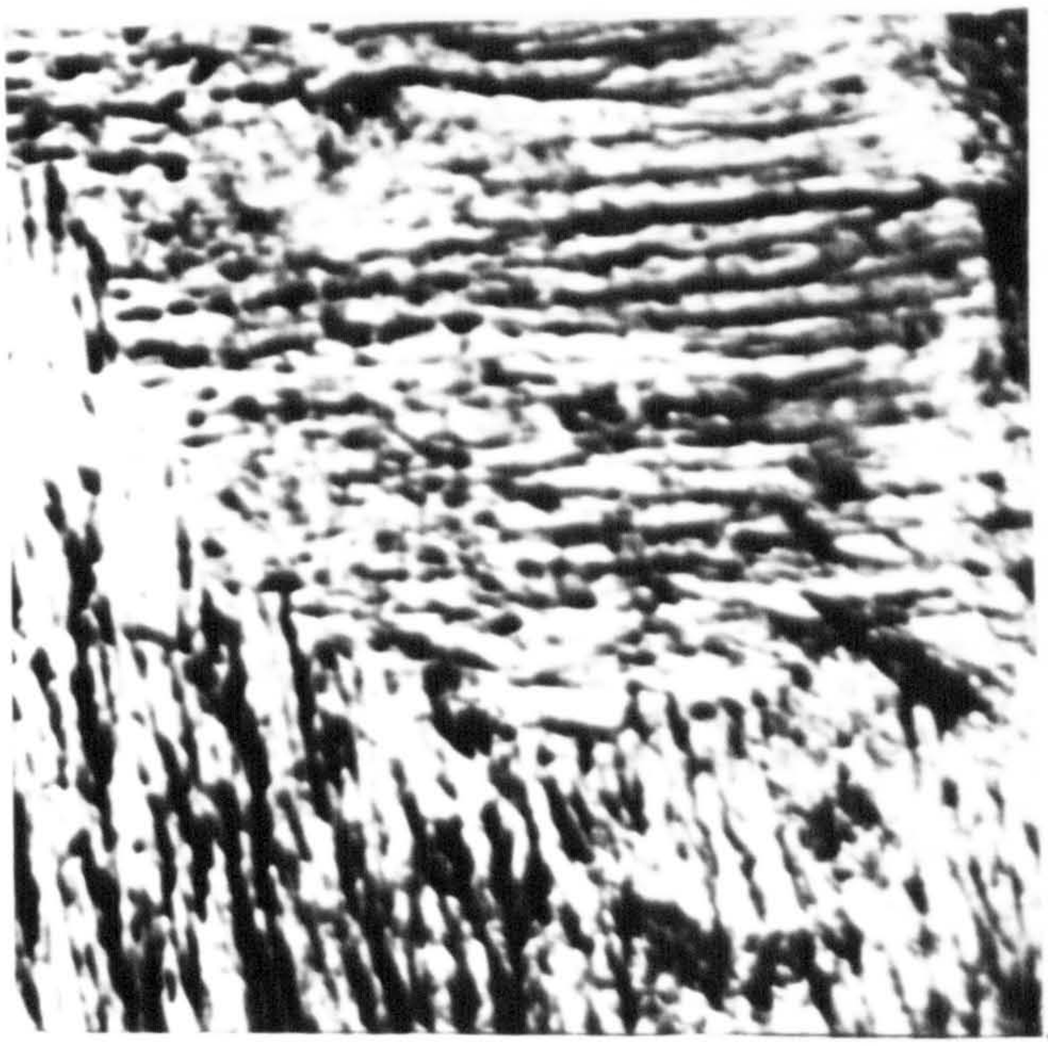

0.1μ

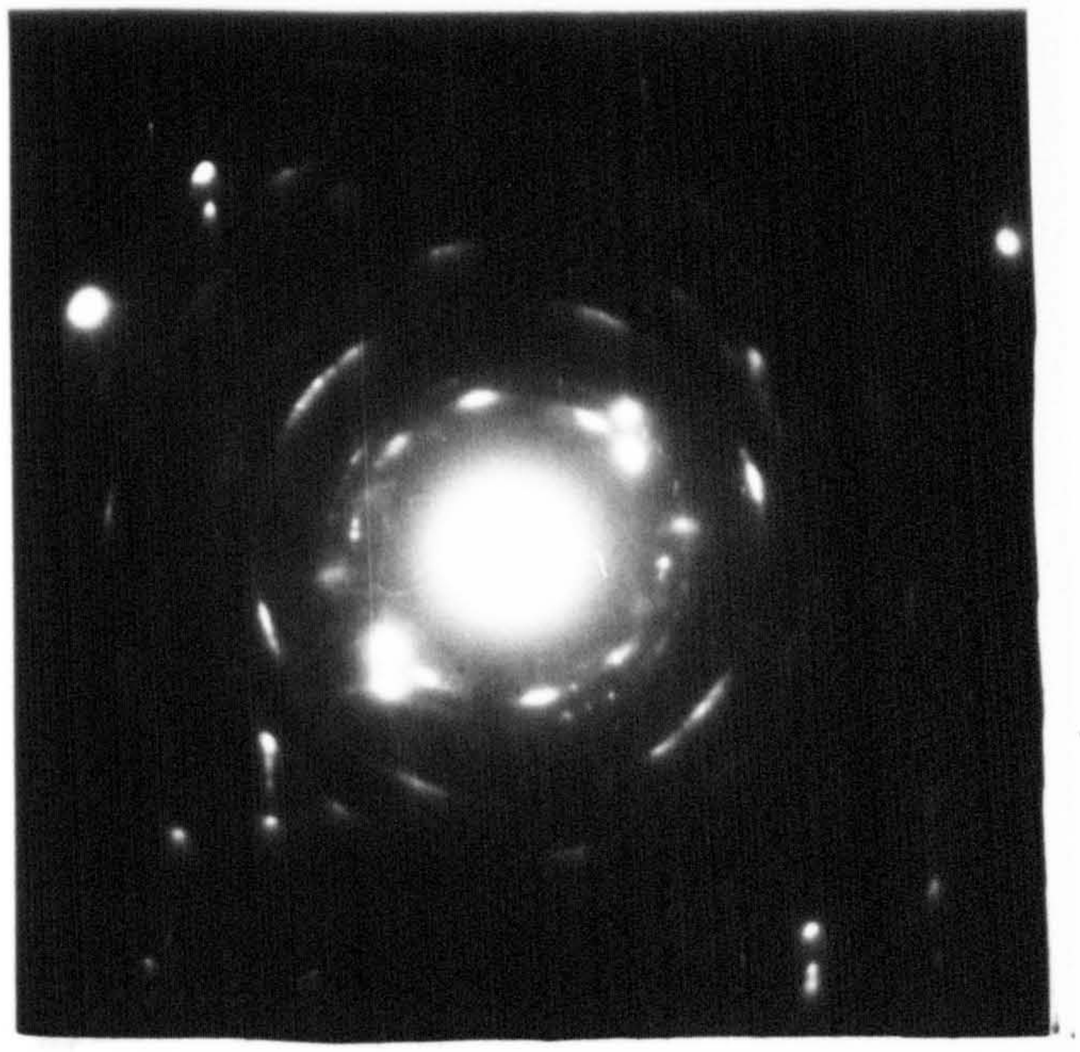

S.A.D. from thin foil.

HETEROGENEOUS PRECIPITATION OF CrN IN IRON - 5.6% CHROMIUM ALLOY.

(Nitrided 575 °C. 6% NH_3-H_2 12h.)

Fig. VI. 8.

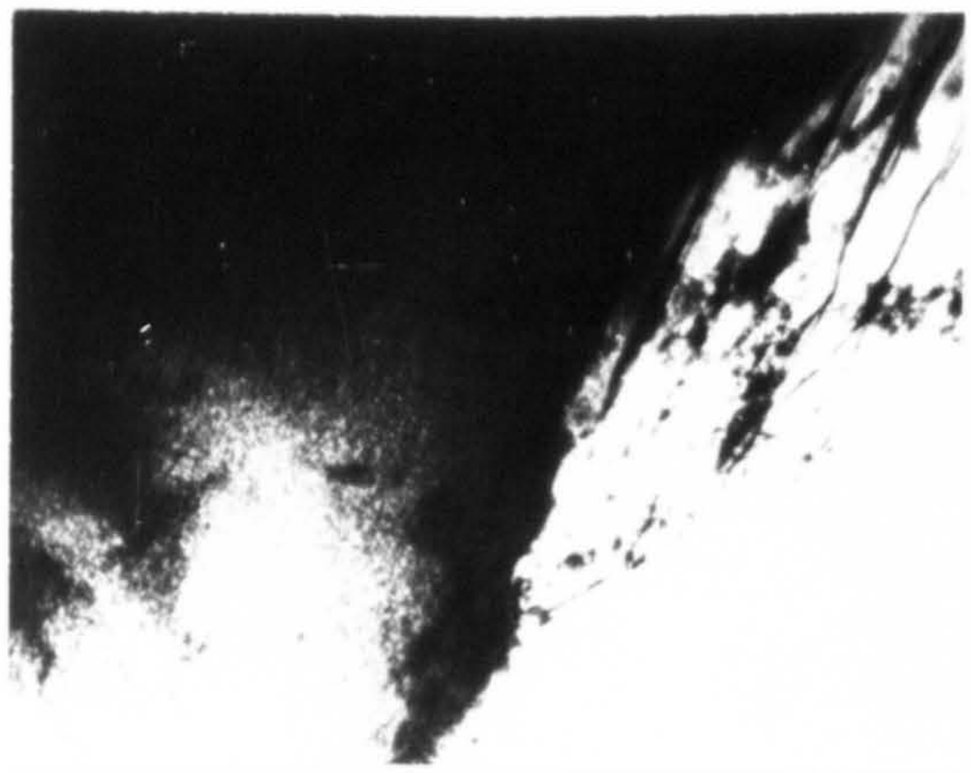

2 days X 8,000

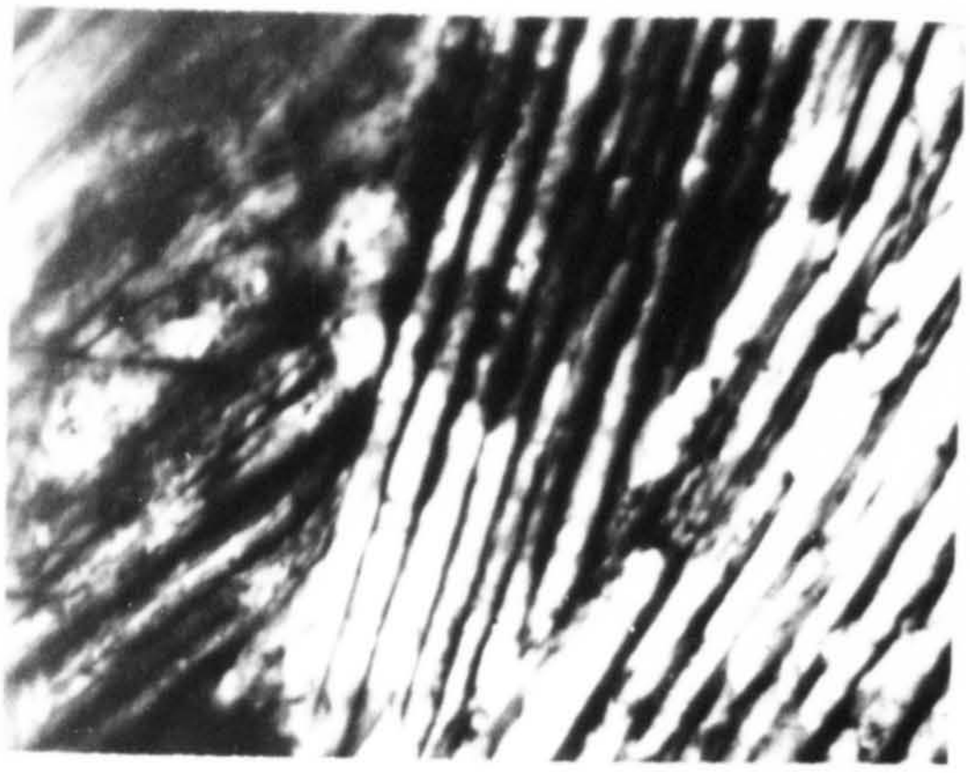

7 days X35,000

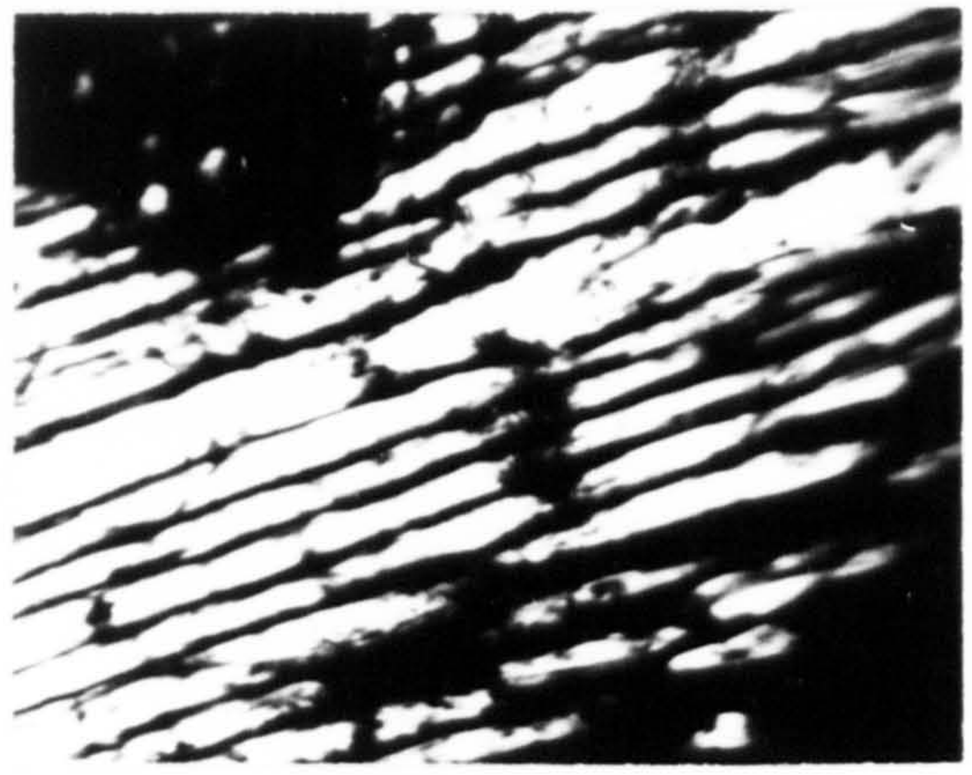

7 days

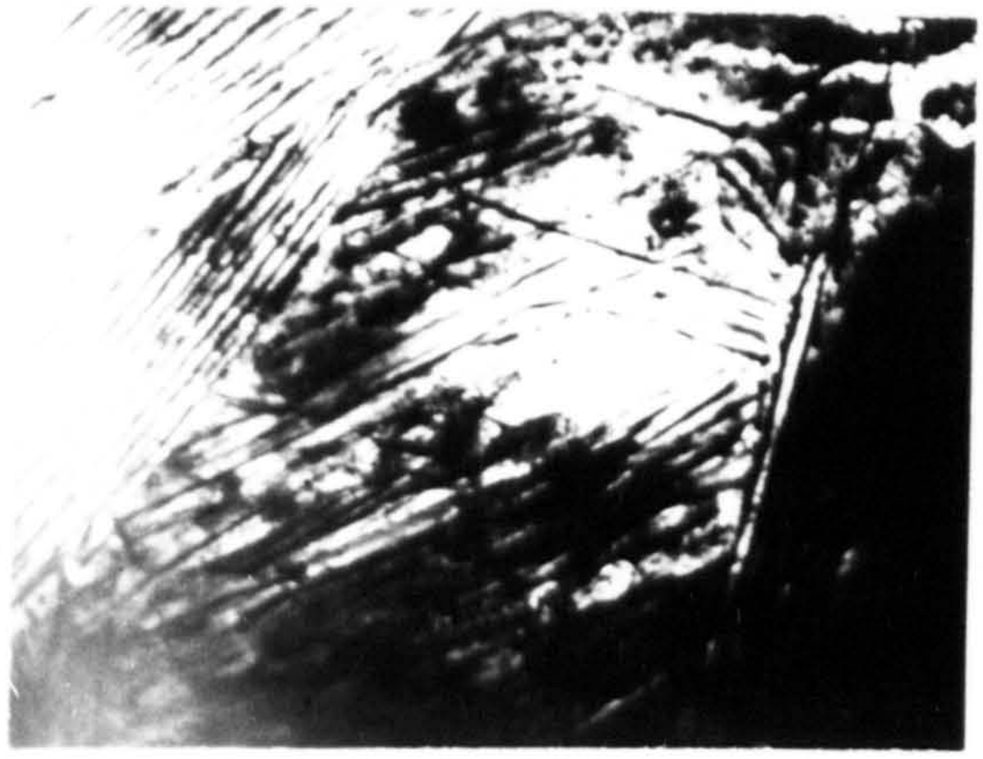

7 days X15,000

THIN FOIL ELECTRON MICROGRAPHS OF TRANSFORMED AREAS IN A Fe-5%Mo ALLOY NITRIDED IN 6% NH_3/H_2 AT 600°C

Fig. VI. 9.

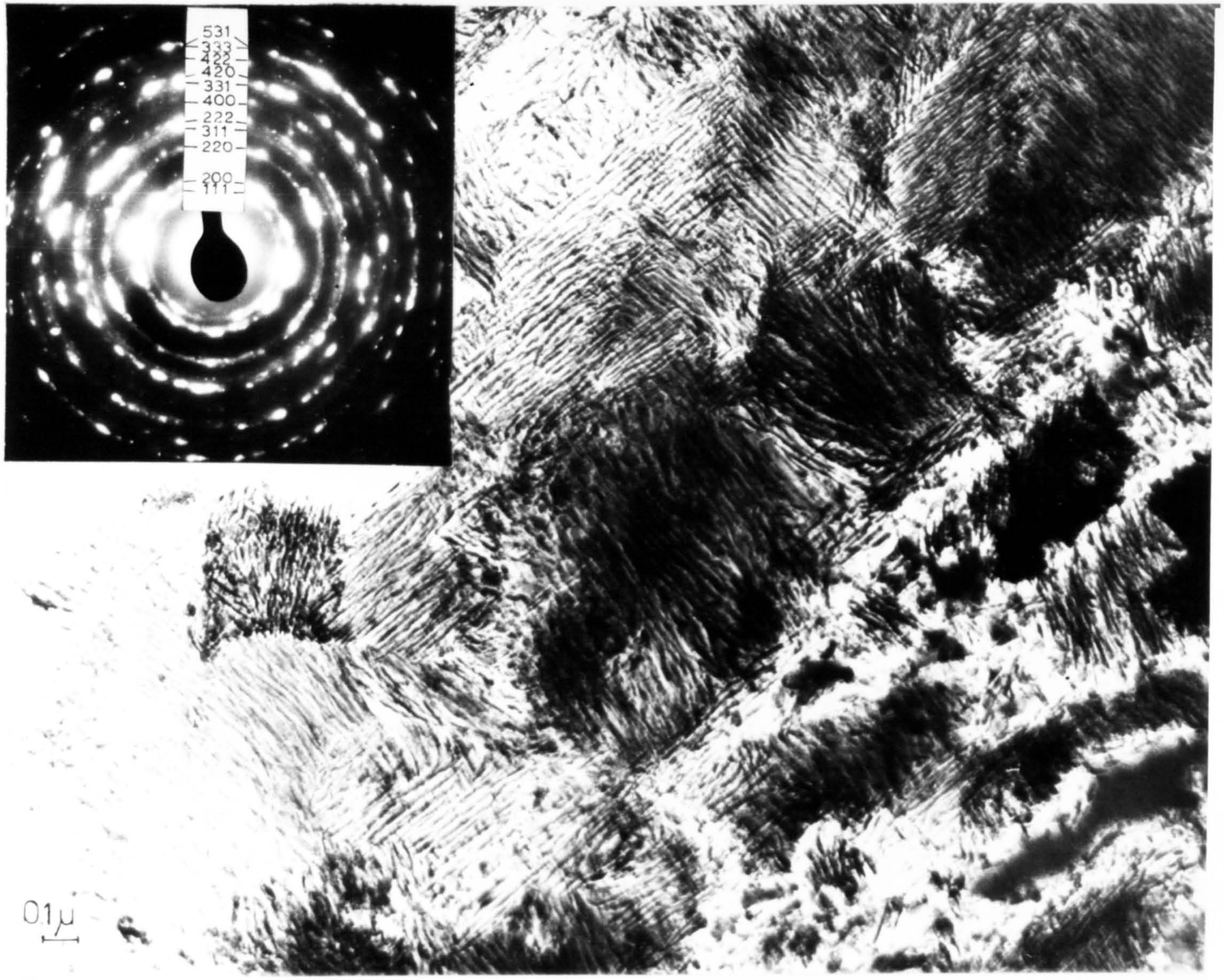

FIBROUS GROWTH OF CrN IN IRON - 9.9% CHROMIUM ALLOY.

(Nitrided 475°C. 19% NH_3-H_2. 242 h.)

high total interfacial energy, to an aggregate of large chromium nitride needles in a ferrite matrix. The driving force for the reaction is probably the reduction in interfacial energy because the precipitated phase is CrN both before and after transformation and so there is no volume free energy change.

VI.4 Discussion of homogeneous precipitation in Fe-Cr-N alloys

The present and other work at Newcastle has established the following general conditions for homogeneous precipitation in Fe-X-N alloys:

(a) Mixed substitution-interstitial solute-atom clusters and metastable species are produced only with alloying elements which decrease the activity coefficient of nitrogen in iron. This increases the solubility of nitrogen in iron, allowing high concentrations of interstitial atoms in solid solution and hence rapid formation of zones or intermediate precipitate. By contrast in iron-silicon alloys where silicon increases the activity coefficient of nitrogen in iron (Roberts, 1970), the nitrogen concentration in equilibrium with a given nitrogen activity is so low that G.P. zones are never observed.

(b) Nitriding must be carried out below a critical temperature and a critical nitrogen potential must be exceeded. The interstitial atom supersaturation above that of the G.P. zone solvus (see Figure VI.10) must also be maintained by "constant activity aging".

Previous work established that precipitation occurred in Fe-X-N alloys where X is niobium or molybdenum and more recent investigations with alloys containing vanadium, titanium and tungsten has shown the general nature of these phenomena. Once formed, the G.P. zones are remarkably stable and the material remains hard even after several hours over-aging at temperatures approaching 700°C. The precipitation goes through each of the stages recognised in the classical work on aluminium alloys: (i) coherent G.P. zones on $\{100\}$ ferrite matrix planes; (ii) formation of at least one intermediate metastable phase becoming partly or wholly incoherent; (iii) precipitation

Fig. VI.10

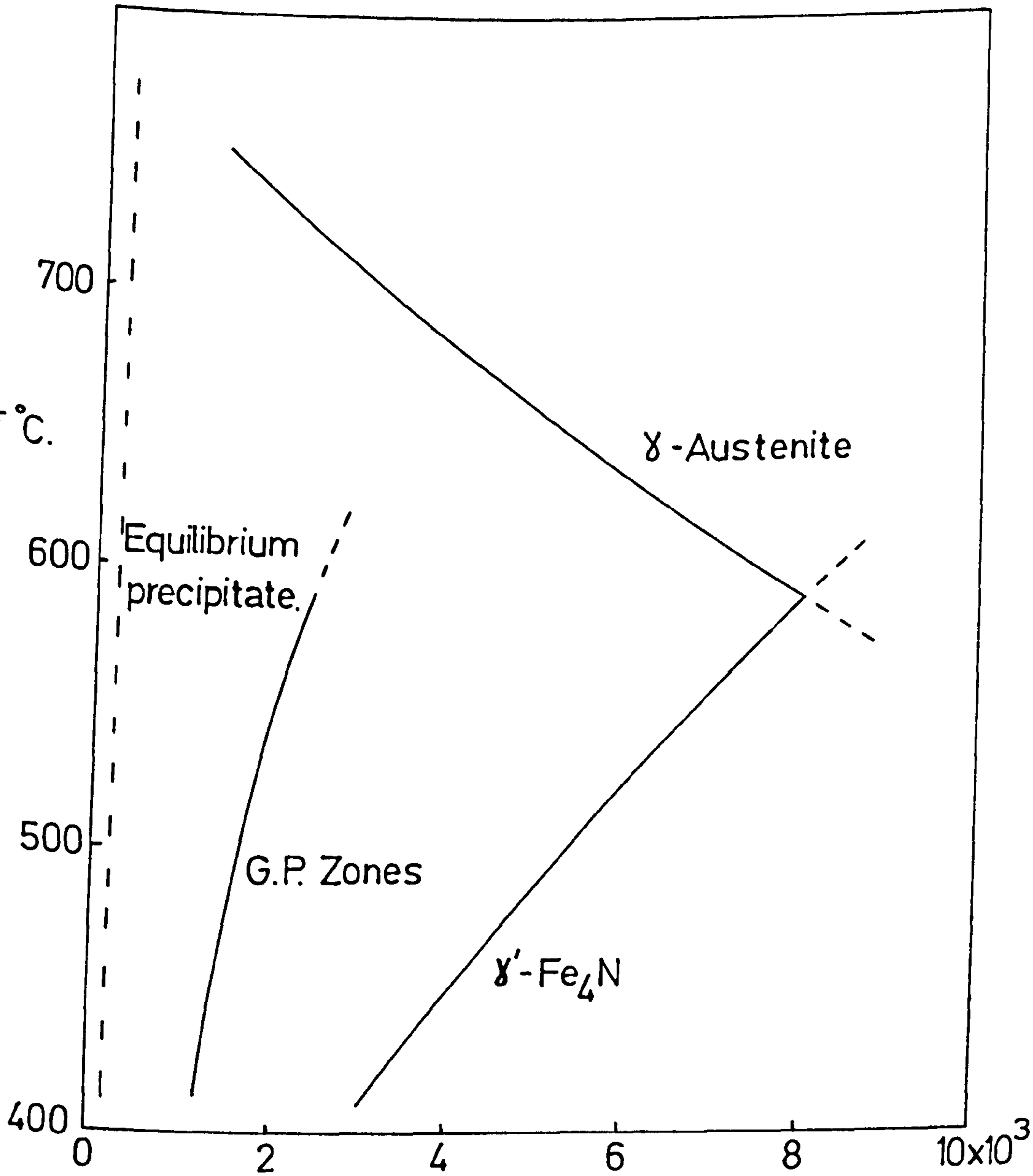

SCHEMATIC DIAGRAM OF CONDITIONS FOR

G.P. ZONE FORMATION

of the final stable phase.

Electron micrographs and electron diffraction patterns from nitrided 5.0wt.%Mo alloy and 1.0wt.%Nb alloy are shown in Figures VI.11 to 13. Figure VI.11 is slightly below peak hardness but is similar to the "tweed" microstructure observed in Cu-Be alloys (Tanner, 1966); there is pronounced $\langle 100 \rangle_{\alpha}$ diffraction streaking. Figures VI.12 and 13 are at about peak hardness and show continuous streaking between matrix diffraction spots in $\langle 100 \rangle_{\alpha}$ directions. They are almost identical to electron micrographs of 4wt.%Cu:Al showing the intermediate precipitate θ' (see Nicholson et. al.;1958).

The zones can be regarded as disc-like clusters of an α''-$Fe_{16}N_2$--type atomic arrangement but with a smaller N:Fe ratio, with some iron atoms substituted and with both substitutional and interstitial solute atoms disordered. The similarity of Figure VI.14 - an electron micrograph of pure iron supersaturated with 0.07wt.%N and aged at room temperature - and Figures VI.12 and 13 suggests that although they occur at quite different temperatures the structural changes during the first stages of nitrogen precipitation are the same for pure iron as for the alloy irons.

The metastable transition phase is essentially an ordered alloy-substituted α''- phase formed initially as coherent plates but eventually becoming incoherent as it grows. Figure VI.13 shows discrete diffraction spots from this precipitate occurring near to matrix spots because its tetragonal structure (see Figure L.4) is only slightly different from that of the body-centred cubic matrix and because it is precipitated on $\{100\}$ matrix planes. The formation of the α''- type transition phase is independant of the structure and composition of the final equilibrium precipitate; the latter is η- Fe_3Mo_3N in 5wt.%Mo and γ- NbN in 1.0wt.%Nb alloys.

In the present investigation, at temperatures as low as 475°C, only the equilibrium precipitate CrN has been observed even after very short nitriding times when the particles are extremely small. This indicates that if precipitation occurs in Fe-Cr-N the zones and/or

Fig.VI.11

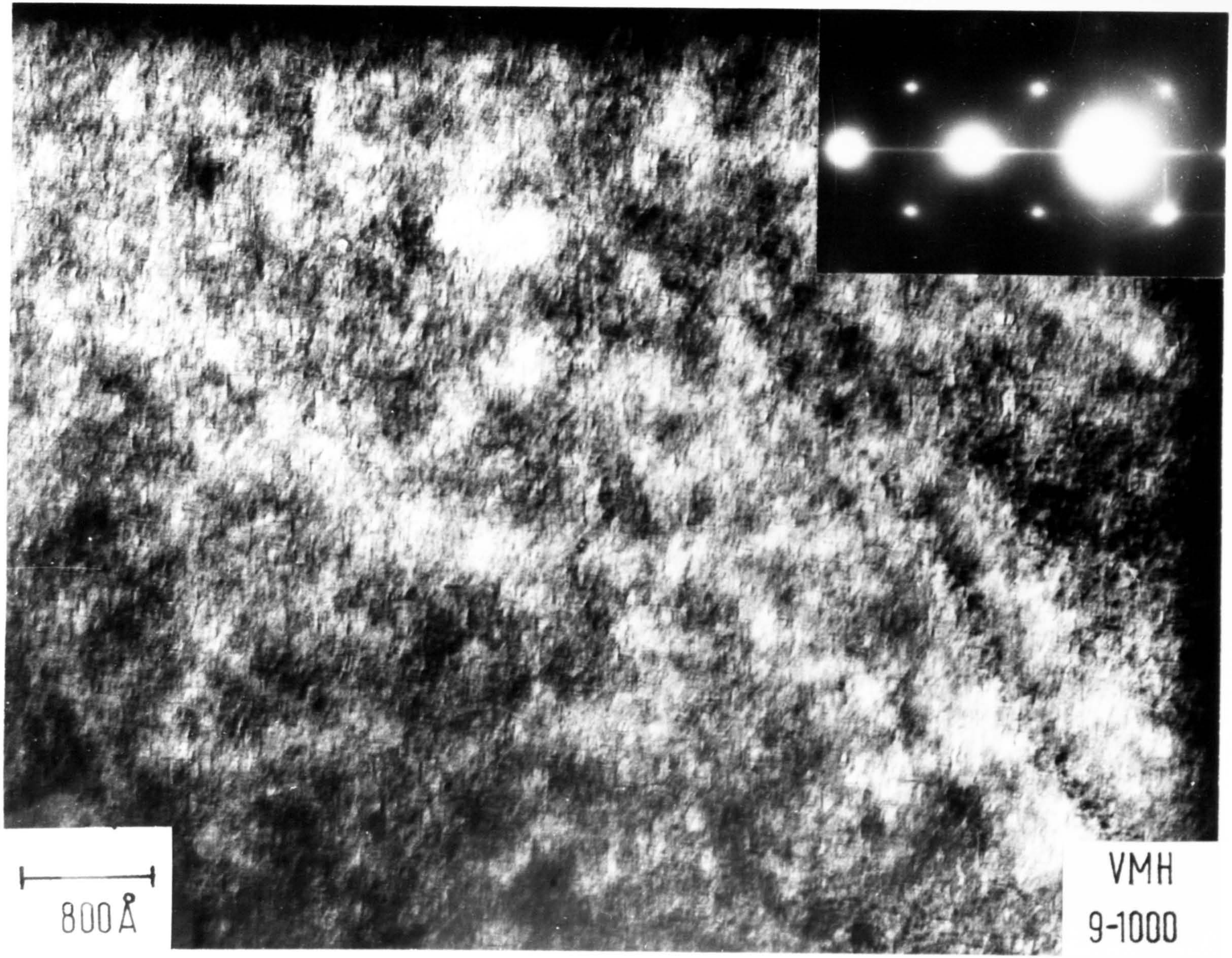
800 Å
VMH
9-1000

Fig.VI.12

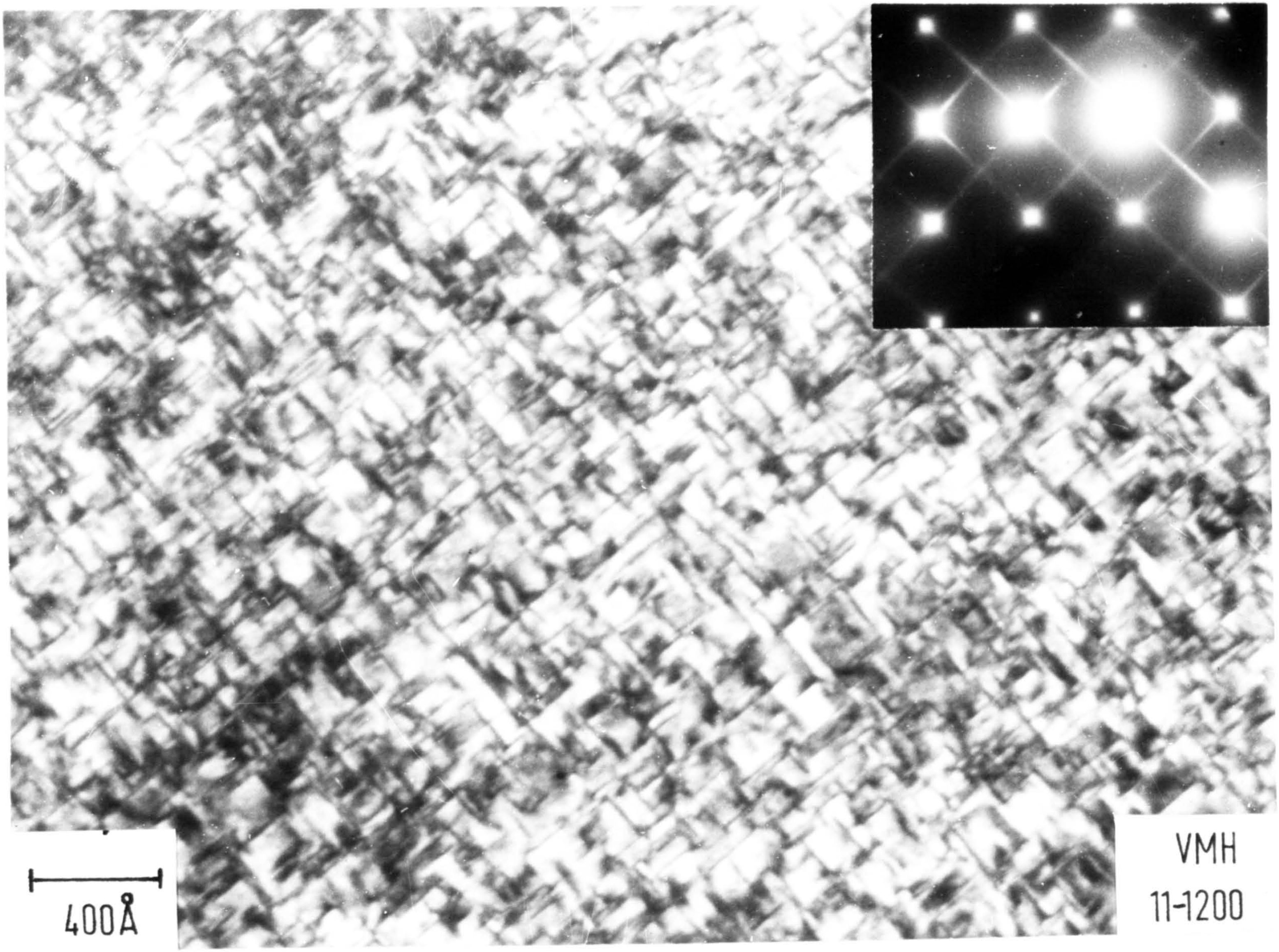
400Å
VMH
11-1200

Fig.VI.13

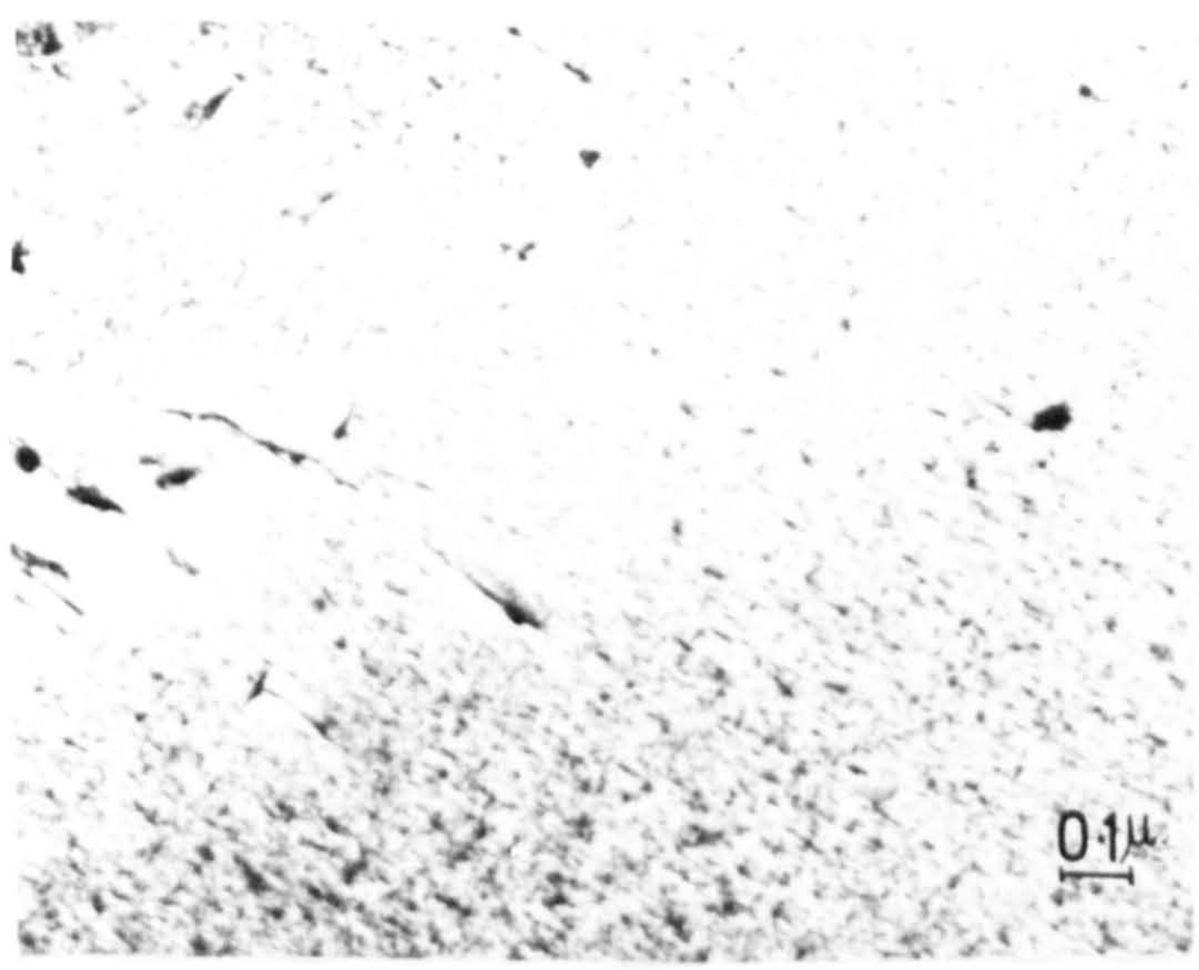

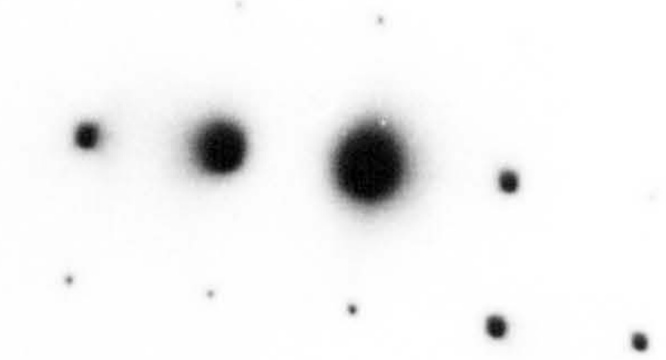

a) 0·99%Nb . 15%NH_3 550°C
241h.
⟨100⟩M Zone

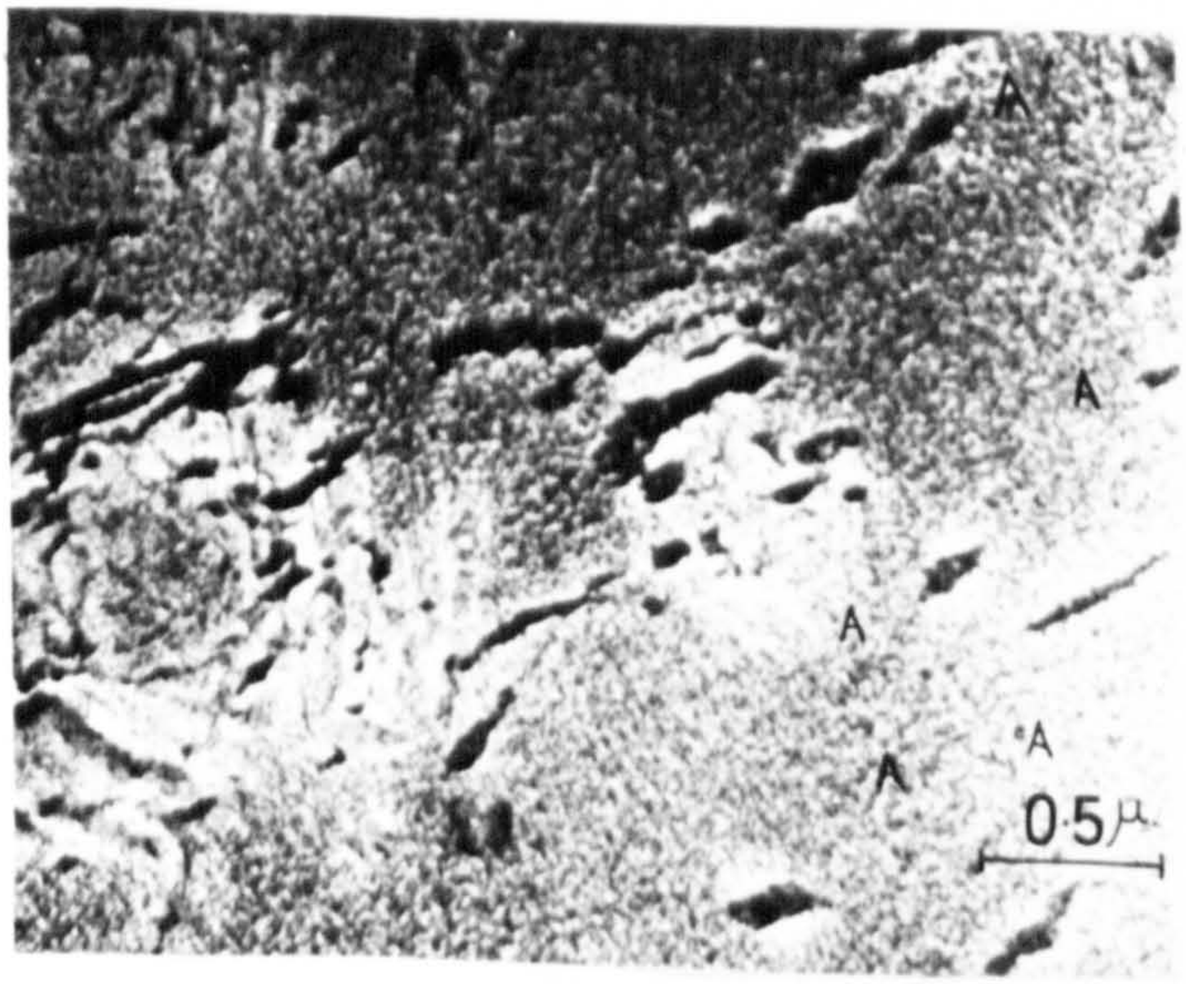

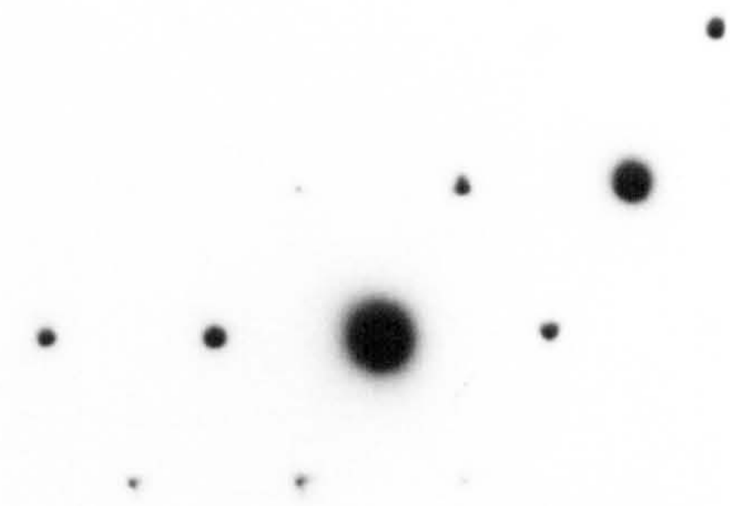

b) 0·99%Nb. 14·8%NH_3 550°C
303h.
⟨111⟩M. Zone.

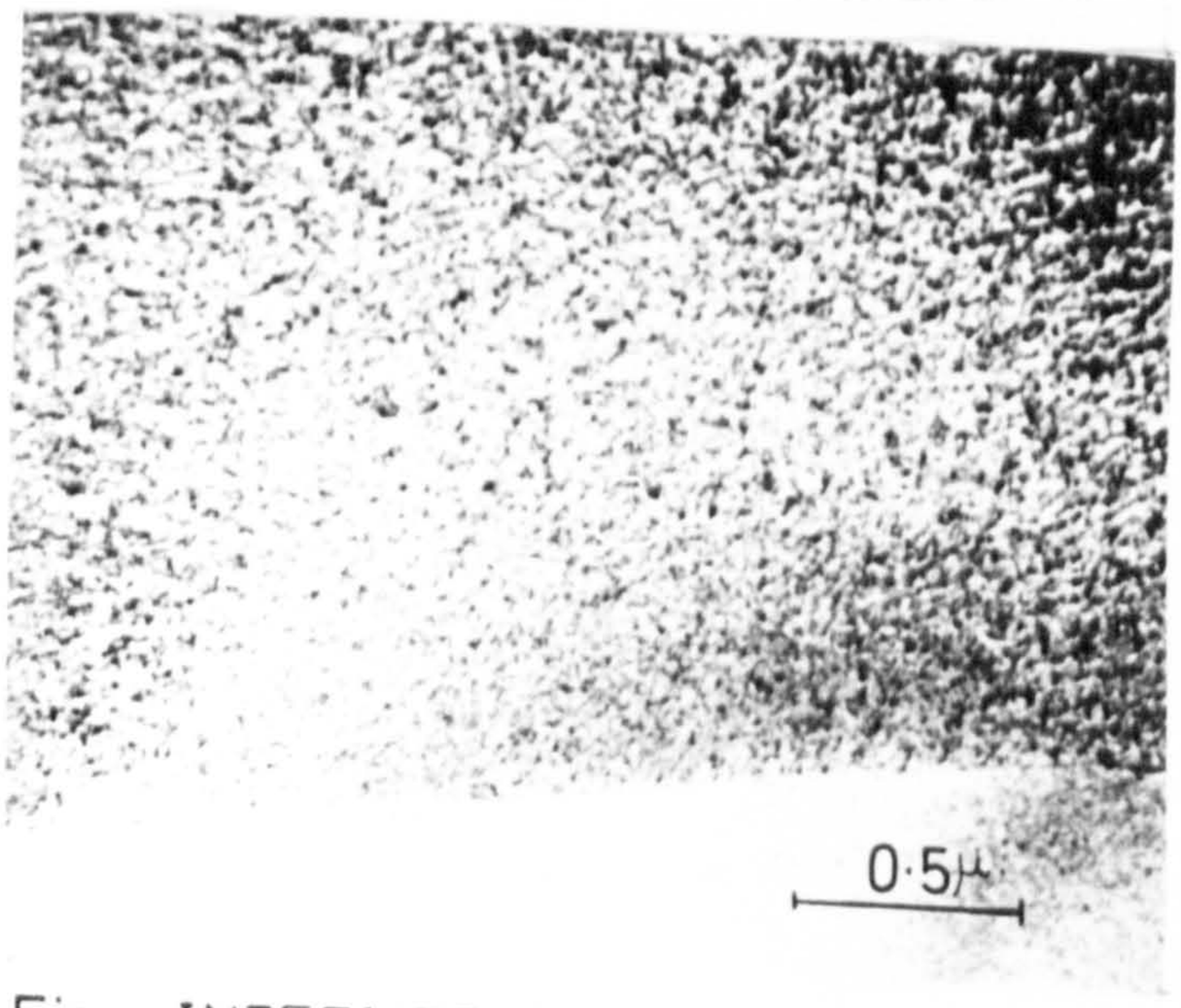

c) details as (b) above

Fig. INTERMEDIATE PRECIPITATES IN Fe-Nb-N ALLOYS PRODUCED BY CONSTANT ACTIVITY AGEING.

Fig.VI.14

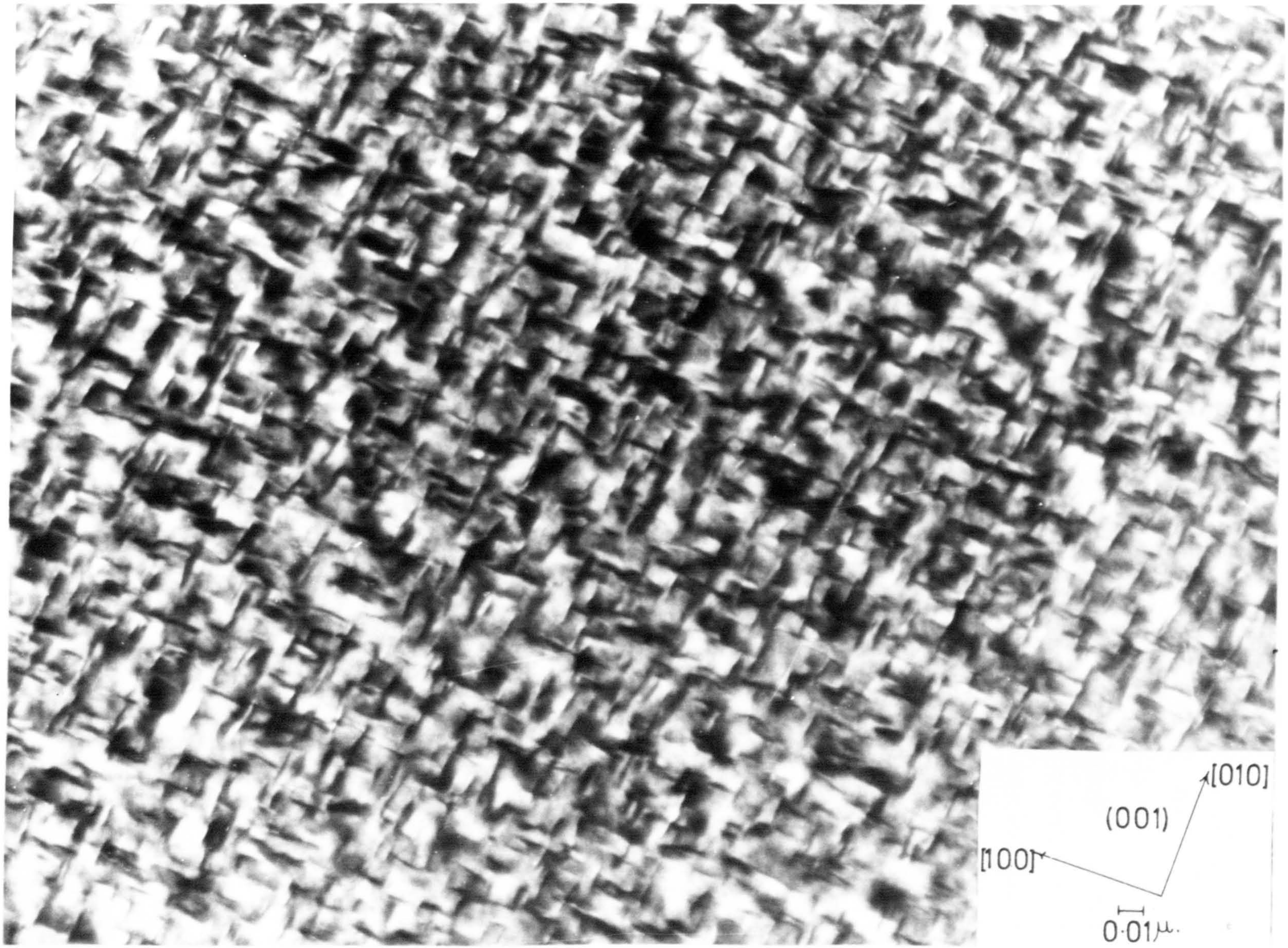

Fig. COHERENT PLATELETS IN IRON–0·072% NITROGEN AGED 16h. AT 21°C.

intermediate precipitate are transient species which exist only during the very earliest stages of clustering of chromium and nitrogen atoms.

Precipitation stages are usually observed in alloy systems at low temperatures where there is limited diffusion of the precipitating species and where zones or metastable precipitates can form more rapidly than the more stable equilibrium phase. At higher temperatures, when diffusion rates become faster, nucleation of the more stable precipitate becomes much more probable. A possible reason for the absence of zones and intermediate precipitates in Fe-Cr-N alloys is the higher diffusivity of chromium in α- iron compared to the other substitutional alloying elements (see Kunitake & Paxton, 1960) with the resultant easier formation of equilibrium phase CrN.

Chapter VII

The kinetics of nitriding of iron-chromium alloys

VII.1 Introduction

Roberts (1970) concluded (see Figure VII.1) that the rate of hardening correlated approximately with the rate of diffusion of nitrogen into a 0.99wt.%Nb - Fe alloy during "constant activity aging" in ammonia-hydrogen mixtures at 550°C. Darken & Smith (see Grieveson & Turkdugan, 1964) support the view that the diffusion of nitrogen in iron is the rate-controlling process when such gas mixtures are used for nitriding pure iron.

Apart from these investigations there is little published data on the kinetics of nitriding with ammonia-hydrogen mixtures at 400-600°C and so the present investigation attempts to elucidate the mechanism of nitriding of iron-chromium alloys at 575°C.

VII.2 The preparation of iron-chromium-nitrogen alloys

The as-received iron-chromium alloys were cold-rolled to 0.5 and 1.5mm. strip and specimens weighing approximately 2g were cut from this stock material. All alloys were annealed in hydrogen at 850°C for 18 hours before "constant activity aging" in ammonia-hydrogen mixtures. The uptake of nitrogen was measured by periodically removing the specimen from the furnace, weighing it and then continuing the nitriding. At each interruption, a small sample was cut from a duplicate specimen to measure the hardness profile after the same successive intervals. To ensure that removal of the specimen from the furnace had negligible effect on the measured rate of nitriding, runs were repeated, but specimens were removed after completely different time intervals.

Fig. VII. 1

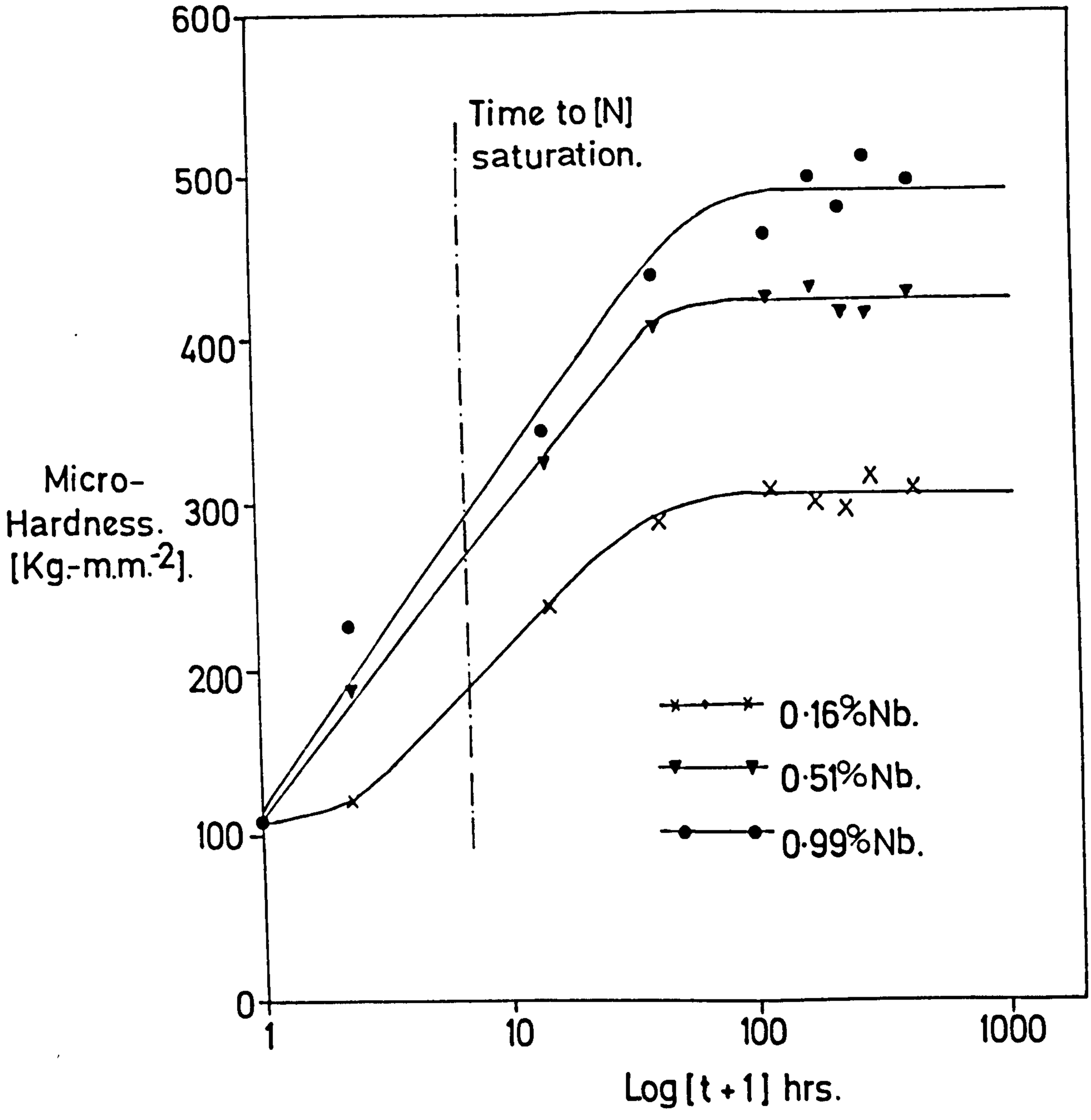

Fig. MICROHARDNESS–TIME CURVES FOR CONSTANT ACTIVITY AGEING OF IRON–NIOBIUM ALLOYS IN $12\%NH_3$–H_2 AT 550° C.

VII.3 Results and discussion

"Constant activity aging" of iron-chromium alloys in ammonia-hydrogen mixtures below 600°C produces appreciable hardness. The rate and manner of hardening is shown in Figures VII.2 to 4 for alloys nitrided in $10NH_3:90H_2$ at 575°C. Those alloys containing not less than 5wt.%Cr nitrided by forming a hard subscale which advanced progressively into the bulk material with the latter retaining its as-annealed hardness. Optical micrographs of case-hardened specimens are shown in Figure VII.5.

Hepworth et. al. (1965) considered the analogous oxidation of a 0.1wt.% aluminium-iron alloy using hydrogen-water mixtures. Applying a similar treatment in the present investigation the following simplifying assumptions must be made:

(a) in internally nitrided specimens the nitrogen concentration varies linearly with penetration depth through the case;

(b) at the surface the nitrogen in solution is in equilibrium with the gas phase; and

(c) nitrogen and chromium are in equilibrium with CrN at the interface between the case and the unnitrided core.

Since the diffusivity of chromium in iron is far less than that of nitrogen, the following diffusion equation may be written for the flux of nitrogen across the nitrided layer under the boundary conditions stated below:

$$\frac{dn}{dt} = D\frac{C - C'}{X} \qquad \ldots.(17)$$

where $\frac{dn}{dt}$ is the rate of nitriding, g.atoms N/cm^2.sec. ,

X is the thickness of the nitrided layer,

C is the nitrogen concentration in iron in equilibrium with the ammonia-hydrogen gas mixture,

C' is the nitrogen concentration in iron at the inner interface in equilibrium with CrN, and

D is the diffusivity of nitrogen in iron.

Fig. VII.2.

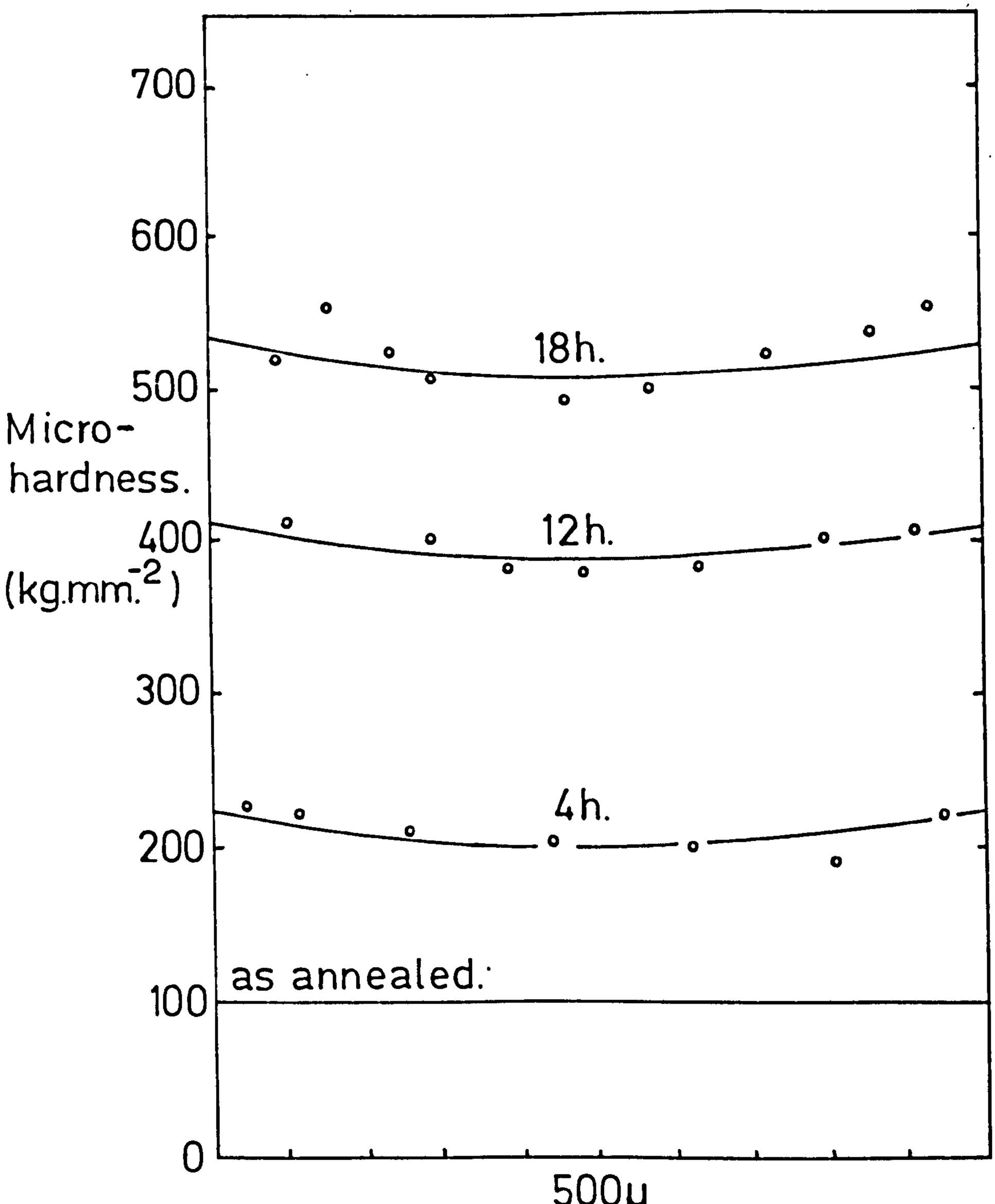

MICROHARDNESS PROFILES FOR 1.2wt%Cr-Fe.

NITRIDED IN 10%NH_3-H_2 AT 575°C.

Fig. VII. 3.

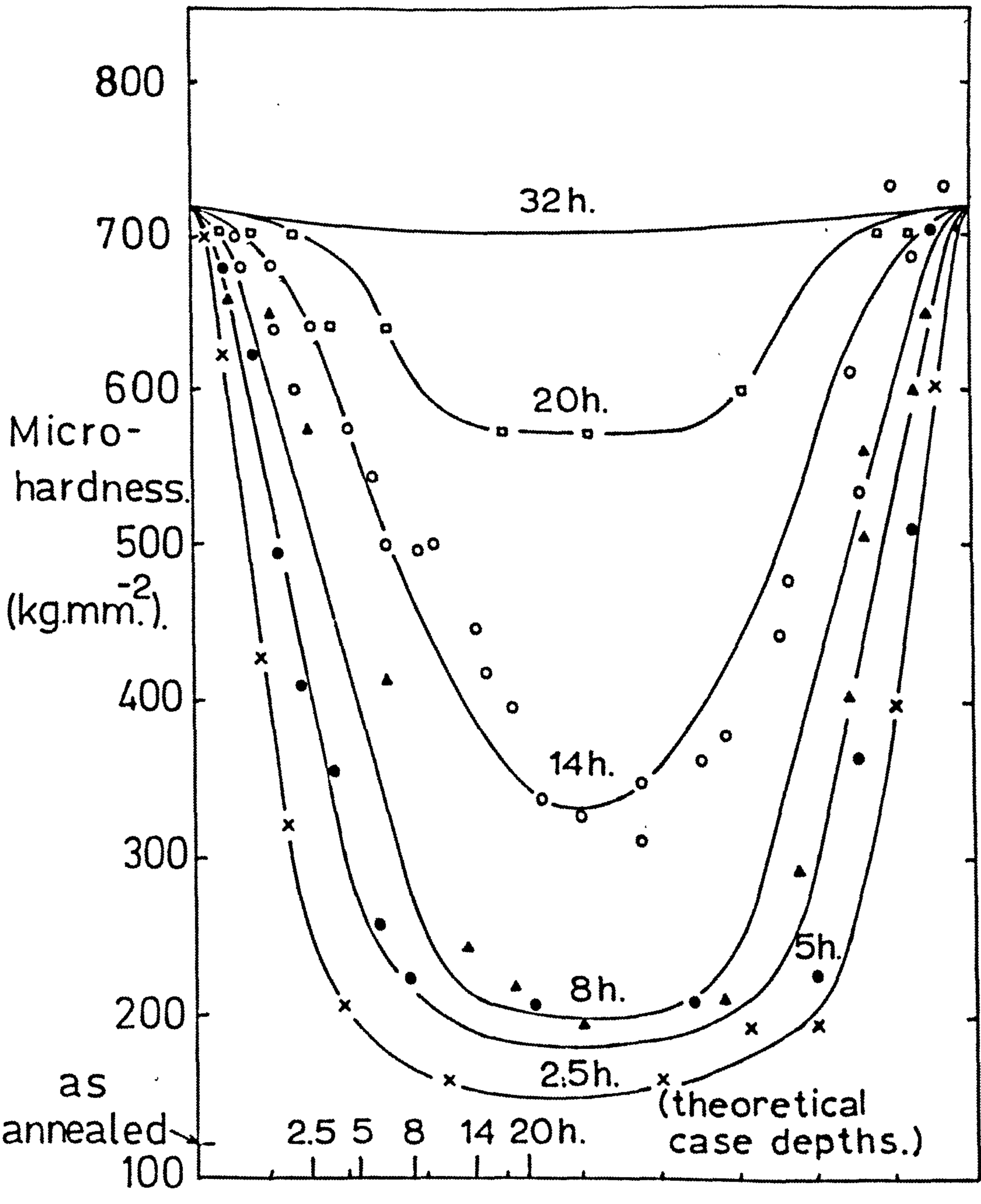

MICROHARDNESS PROFILES FOR 2.3wt.%Cr-Fe

NITRIDED IN 10%NH_3-H_2 AT 575°C.

Fig. VII. 4.

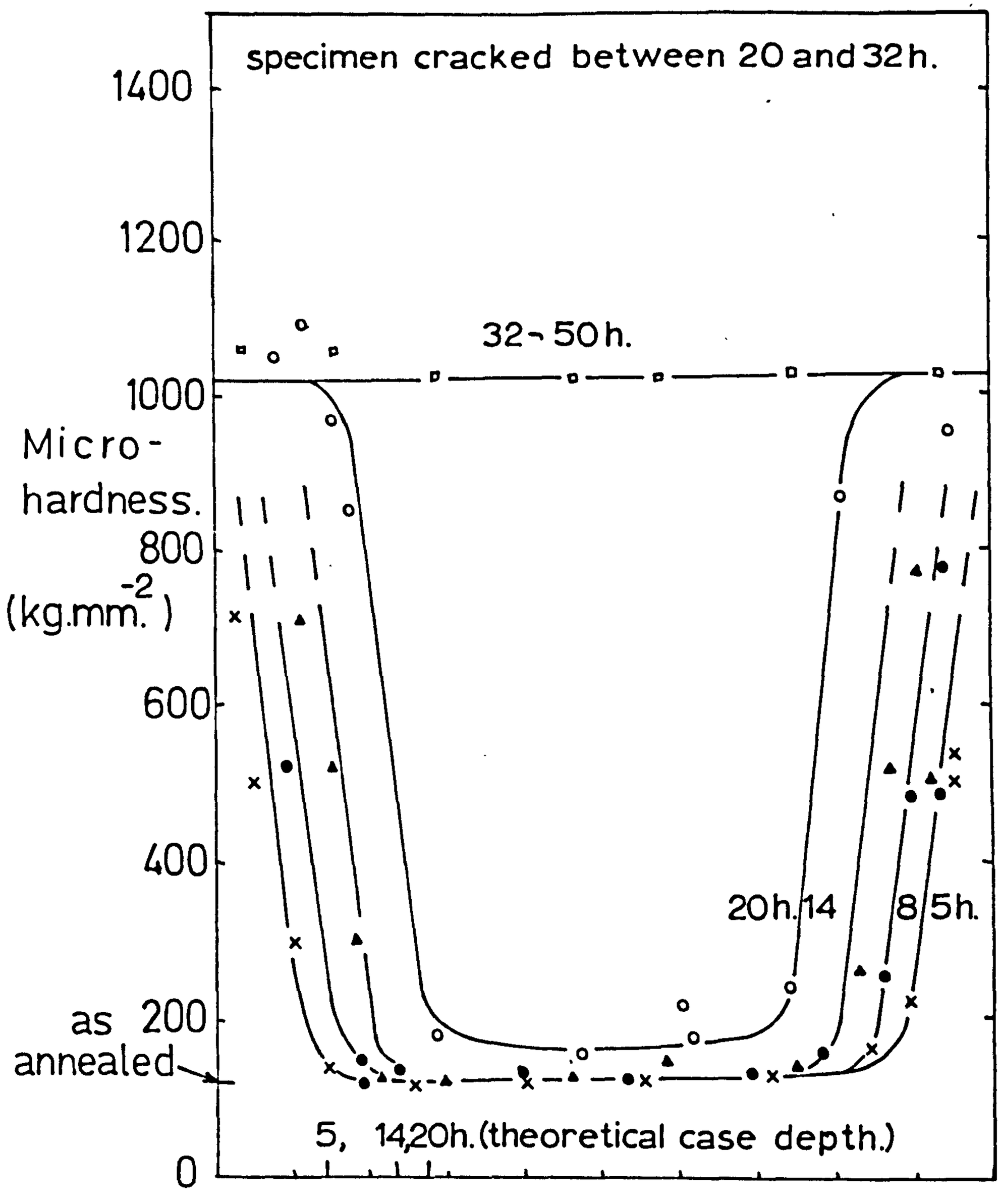

MICROHARDNESS PROFILES FOR 5.6wt.%Cr-Fe.

NITRIDED IN 10%NH_3-H_2 AT 575°C.

Fig. VII. 5.

V.M.H. 800. V.M.H. 140.

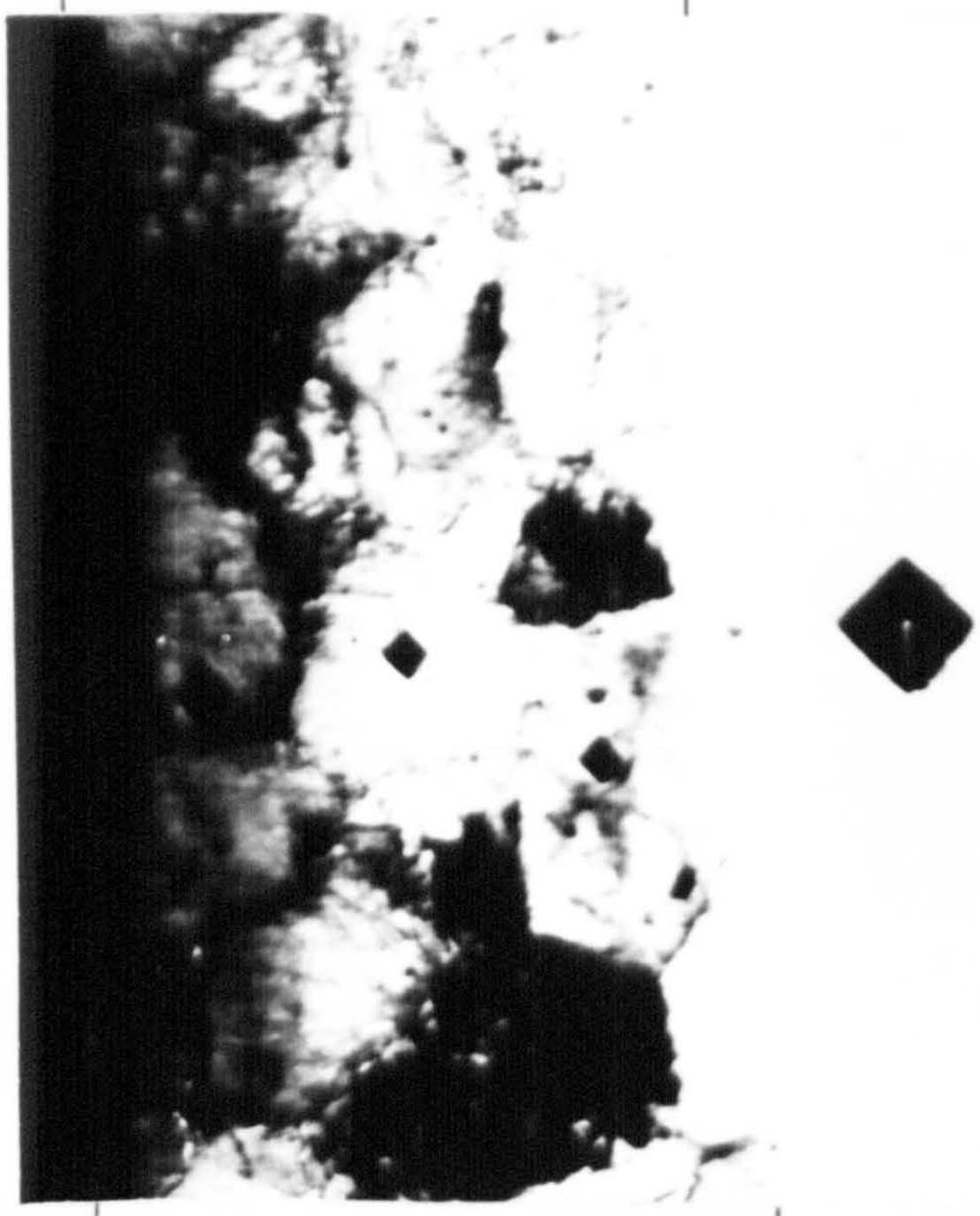

surface nitriding front.

Fe - 9.9% Cr.
Nitrided 575°C.
10%NH_3-H_2. 45h.

X 300.

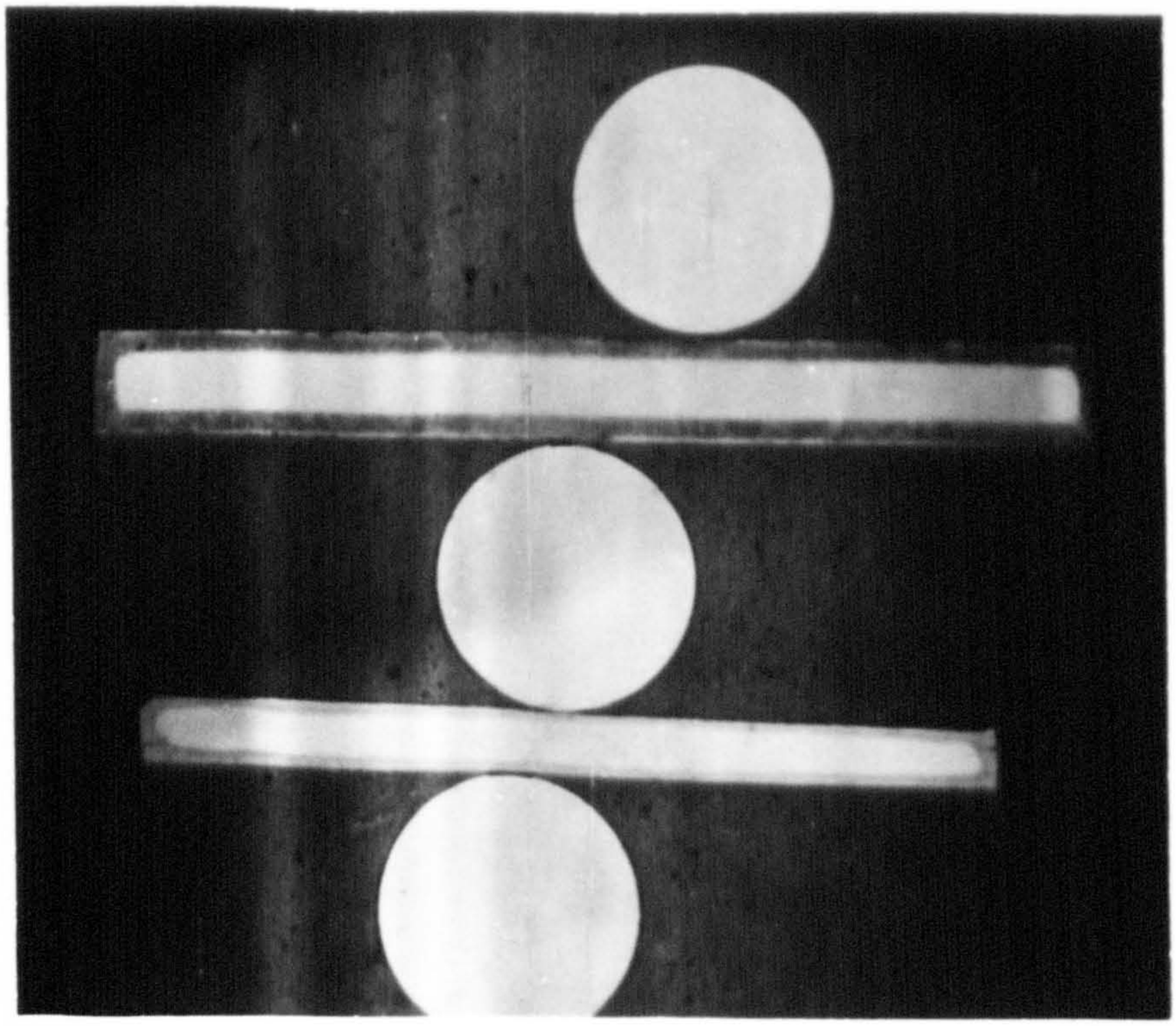

Fe - 7.4% Cr.

X 7.

Fe - 14.0% Cr.
Nitrided 575°C.
6%NH_3-H_2. 97h.

PHOTOMICROGRAPHS OF IRON-CHROMIUM ALLOYS SHOWING "CASED" NATURE OF NITRIDING.

C' is a few orders of magnitude smaller than C as a result of the reasonably strong interaction between chromium and nitrogen and so it may be omitted in Equation.17. The amount of nitrogen transferred across unit area of the sample may be represented in terms of the thickness, (X), the ratio (r) of alloy element to nitrogen, and the chromium concentration (%Cr):

$$n = \frac{\rho}{52} \cdot r\,[\%Cr] \cdot 10^{-2} X, \quad \text{g.atom/cm}^2. \qquad \ldots.(18)$$

where ρ is the density of iron. By combining Equations.17 and 18, taking C' = 0 and converting concentration C to wt.%N, the following rate equation is obtained:

$$\frac{dX}{dt} = \frac{52}{14} \cdot \frac{1}{r} \cdot \frac{[\%N]}{[\%Cr]} \cdot \frac{D}{X} \qquad \ldots.(19)$$

Integrating gives the parabolic equation:

$$X^2 = \frac{52}{7} \cdot \frac{1}{r} \cdot \frac{[\%N]}{[\%Cr]} \cdot Dt \qquad \ldots.(20)$$

The square of the subscale depth, X, is plotted against time in Figure VII.6 for the 0.9wt.%Cr alloy nitrided at 575°C in various nitrogen potentials. The slopes calculated using the above equations are also illustrated and the data can be seen to correlate approximately with the internal nitriding theory. The calculated slopes have not been drawn through the origin as the experimental data appear to indicate that with low nitrogen potentials some "incubation period" occurs before the onset of steady state subscale kinetics. The experimentally observed case depths are generally smaller than the theory predicts, especially with low nitrogen potentials. This could possibly be due to the effect of trace impurities in the gases causing large errors under the experimental conditions where low nitrogen potentials are used. In addition, the high chromium content of this alloy means that it is more susceptible to oxidation than alloys containing less chromium.

The weight increases obtained on nitriding 1.2, 2.3 and 5.6wt.% chromium alloys at 575°C are shown in Figure VII.7 and

Fig. VII. 6.

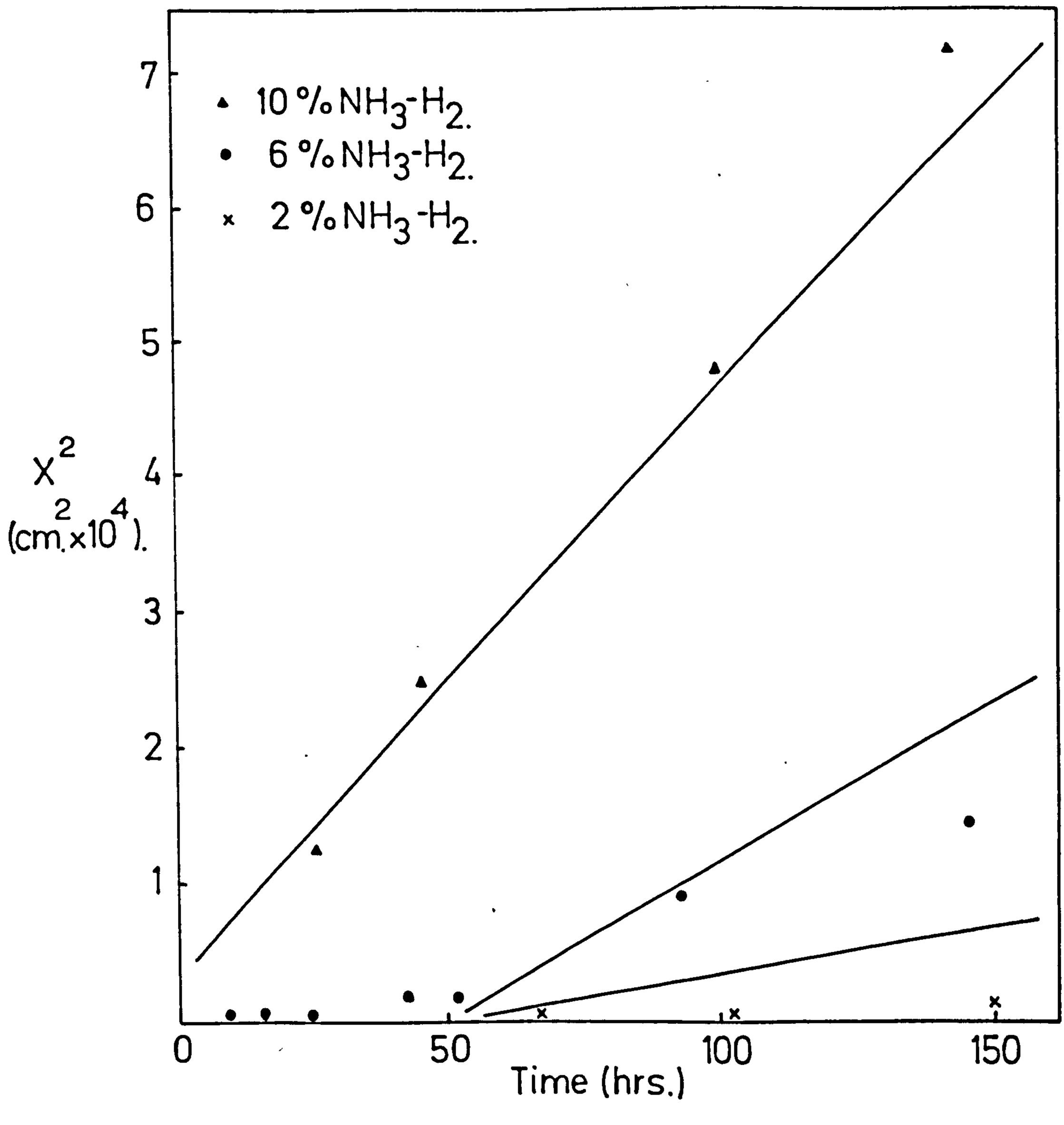

THE SQUARE OF THE SUB-SCALE DEPTH vs. TIME

FOR CONSTANT ACTIVITY AGED 9.9wt.%Cr-Fe ALLOY

AT 575°C.

Fig.VII.7.

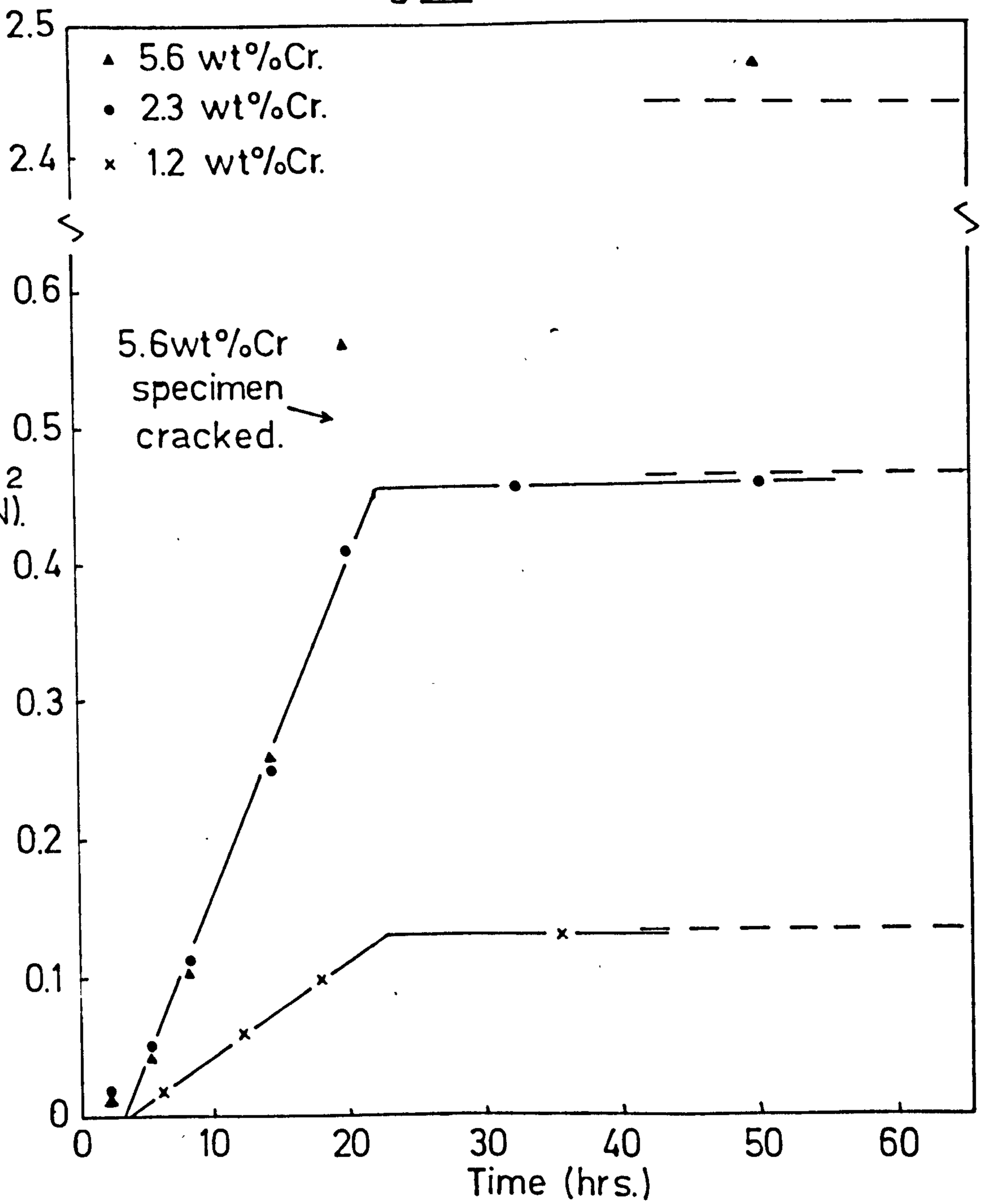

THE PARABOLIC NATURE OF NITRIDING DURING CONSTANT ACTIVITY AGEING OF IRON-CHROMIUM ALLOYS IN $10\%NH_3$-H_2 AT 575°C.

correlate well with the hardness profiles. By measuring the areas under the hardness curves an apparent case depth, X_{app}, has been calculated and with the data of Figure VII.6 the function $\frac{X_{app}^2}{t} \cdot \frac{7}{52} \cdot \frac{1}{D[\%N]}$ is plotted in Figure VII.8 and is in reasonable agreement with the 1:1 slope expected from theory. The value assumed for D, ($2.5 \times 10^{-8} cm^2 sec^{-1}$), gives the best fit with the experimental data but differs somewhat from the accepted value for nitrogen diffusion in pure iron ($1 \times 10^{-7} cm^2 sec^{-1}$; see Grieveson & Turkdugan, 1964). However, because diffusivities obtained by different workers often varies by order of magnitude this four-fold difference is acceptable. The strain induced in the lattice by small particle precipitation could possibly explain the change in diffusion rate.

Calculated case depths for the experimental conditions used are shown in Figures VI.3 and 4 and agree with the observed depths.

The nitriding of 1.2wt.%Cr alloy obviously differs from that observed with higher chromium concentrations. The formation of a hard subscale is not observed and the rate of nitriding is slower than would be expected from the internal nitriding theory applied to higher alloys. The absence of a case indicates that all the nitrogen does not react with chromium on entering the specimen but some diffuses inwards leaving some unreacted chromium which combines with nitrogen at a later stage. As a result, CrN can nucleate inside the specimen before growth of CrN precipitates has absorbed all the chromium in the surface layer. This produces the profile observed in Figure VII.2 where the rate-controlling step is probably diffusion of chromium over small distances around the nucleating and growing CrN particles.

The 1.2wt.%Cr alloy was also nitrided at 575°C in 2, 6, 17 and 25% ammonia:hydrogen mixtures to observe the change in profile with nitrogen potential. The results are shown in Figures VII.9 and 10 and, as expected, the rates of nitriding in 17 and 25% ammonia are identical. The maximum nitrogen activity possible in ferrite is that in equilibrium with Fe_4N and is produced with $14NH_3:86H_2$ at 575°C. Below this critical

Fig. VII.8

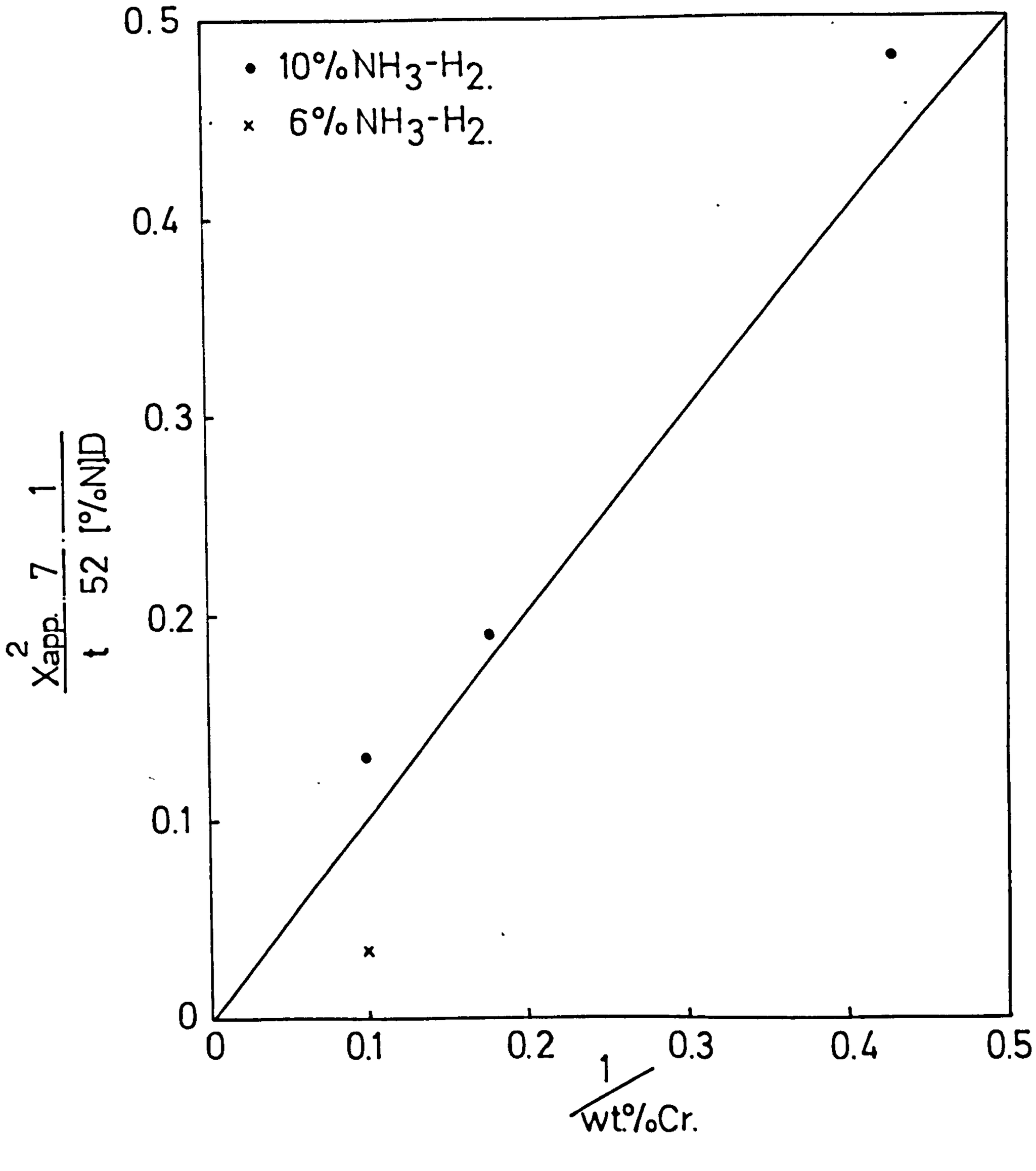

COMPARISON OF EXPERIMENTAL DATA WITH THAT PREDICTED BY INTERNAL NITRIDING THEORY.

Fig. VII. 9.

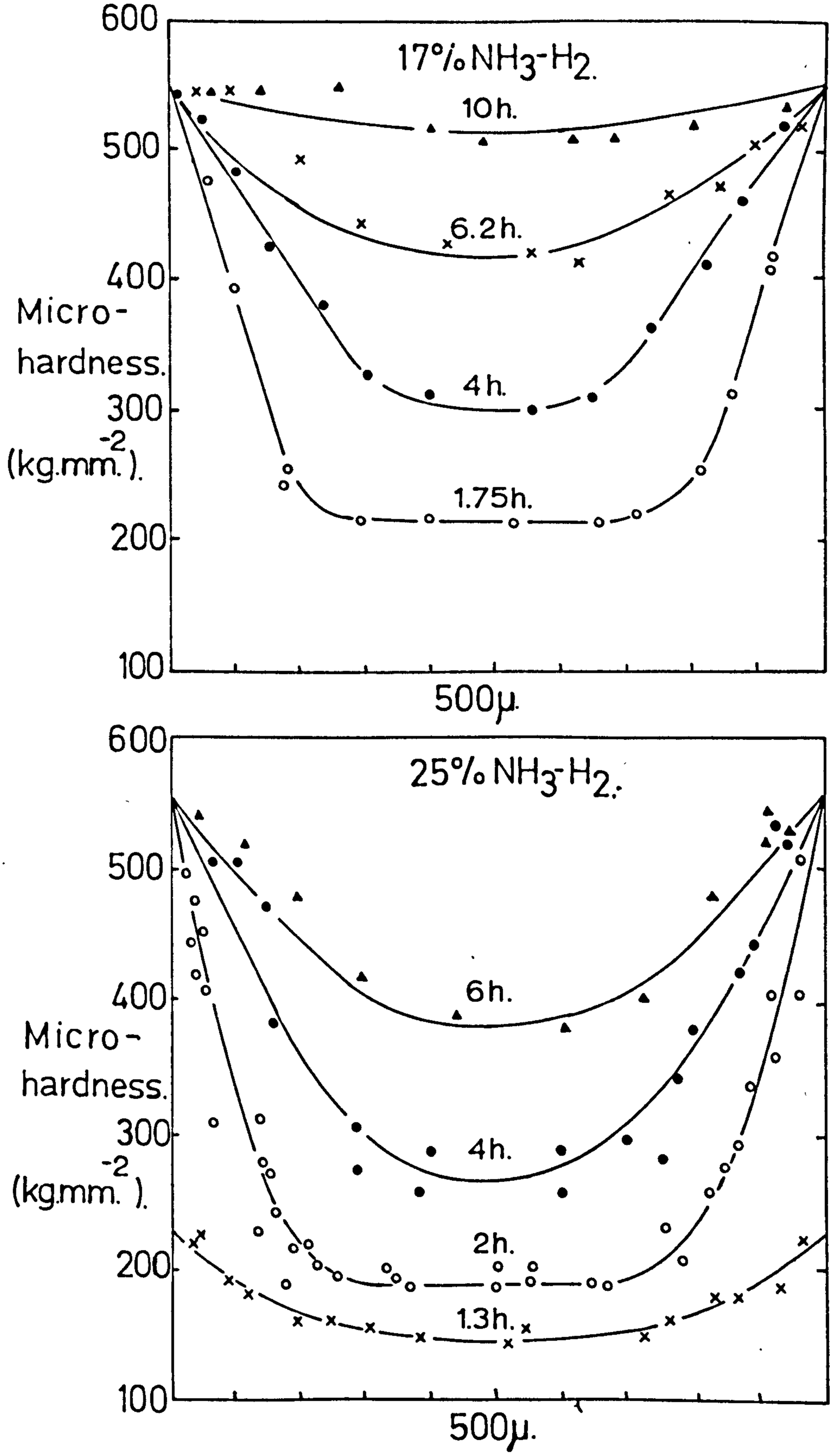

MICROHARDNESS PROFILES OF 1.2wt.%Cr-Fe NITRIDED AT 575°C.

Fig. VII.10.

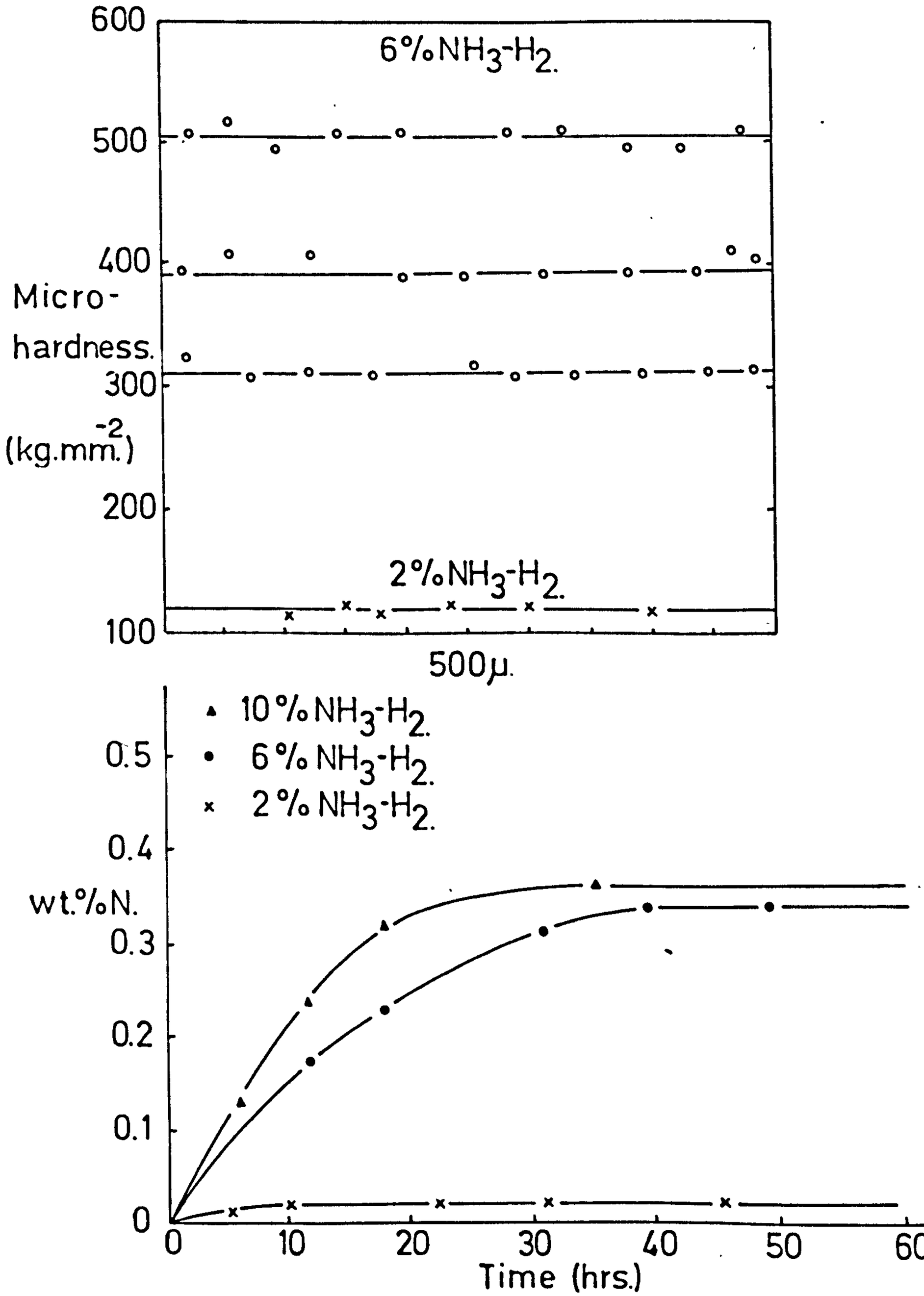

WEIGHT GAIN DATA AND MICROHARDNESS PROFILES FOR 1.2wt% Cr-Fe

potential, the rate at which surface hardness is attained with increasing nitrogen potential is no doubt due to the effect of nitrogen in solution on the rate and density of nucleation i.e. the higher nitrogen concentration produces a larger number of CrN nuclei, and chromium atoms in solution then have smaller average diffusion distances to the nearest nucleus thus giving a faster overall chromium-nitrogen interaction.

A second and perhaps less plausible explanation of the change in hardness profile with nitrogen potential is that at low potentials the specimen does not take up nitrogen as fast as would be expected due to some surface inhibiting effect, whereas above the 14%NH_3 critical limit Fe_4N is formed on the surface and acts as a nitrogen source overcoming the surface inhibiting effect.

On nitriding 1.2%Cr alloy at 575°C in 6NH_3:94H_2 the results correspond with those obtained in 10NH_3:90H_2; the reaction rate is slower and the profiles slightly shallower. With 2NH_3:98H_2 the observations appeared initially to be anomolous as very little gain in weight and virtually no hardness increase was observed but this was subsequently found to be due to the change in character of the precipitation at very low nitrogen potentials. Micrographs from thin foils of 1.2wt.%Cr, in 2%NH_3 are given in Figures VII.11 and 12 which show precipitation of CrN in grain boundaries and on dislocations and demonstrate that a critical nitrogen activity must be exceeded to produce homogeneous precipitation in 1.2wt.% chromium-iron alloy. The equilibrium solubility of CrN in ferrite (see Figure VII.13 from Leslie, 1964) calculated from the solubility product

$$\log [\%Cr][\%N] = \frac{-7480}{T} + 4.86$$

is only about 3×10^{-3} of that observed for homogeneous precipitation of CrN at 575°C, that is, the supersaturation is approximately 300 times the normal solubility. Such observations suggested further experiments to decide whether the initial homogeneous precipitate is the equilibrium CrN phase or whether it is a metastable precursor. If a metastable

Fig.VII.11.

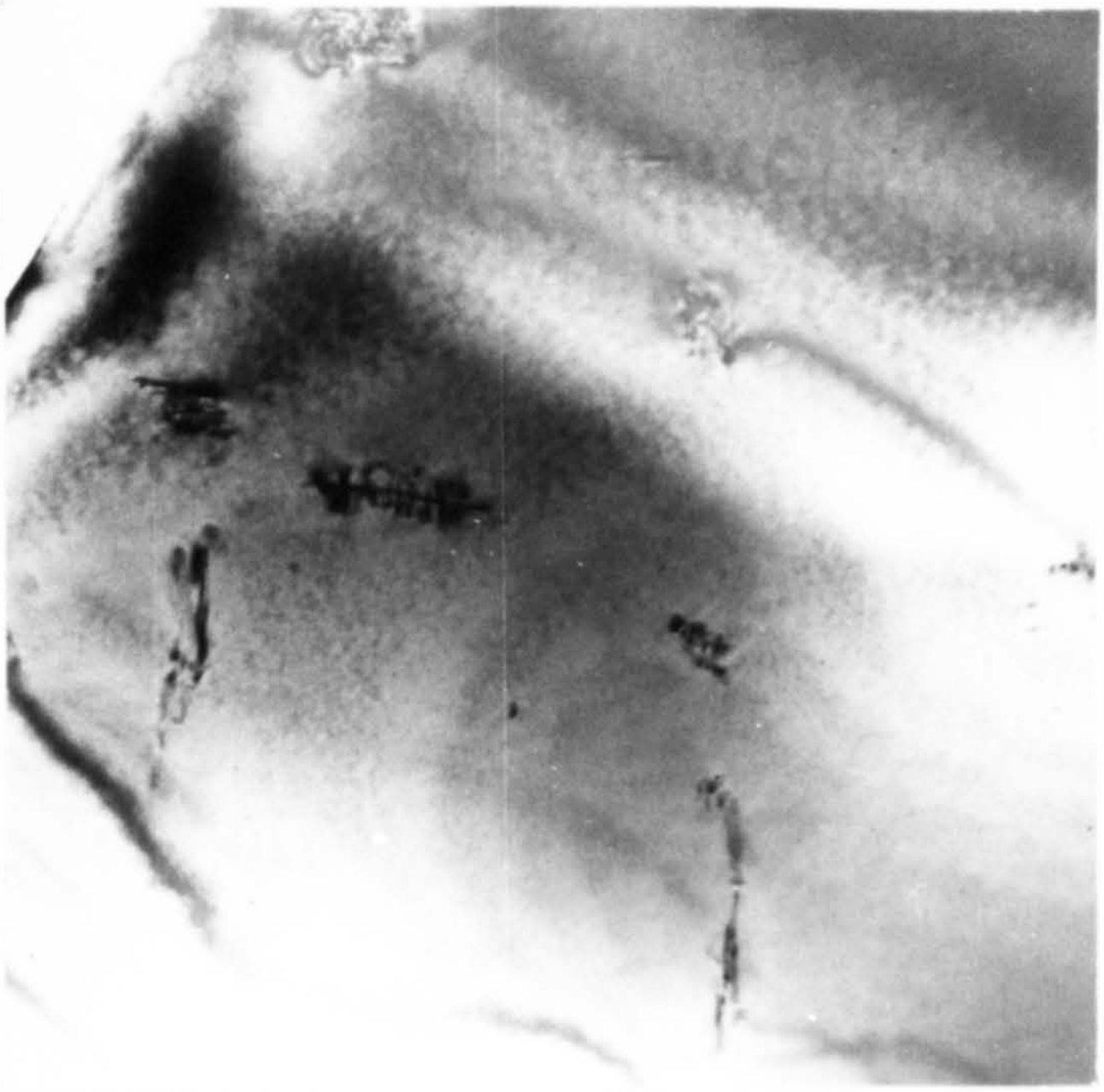

0.2μ

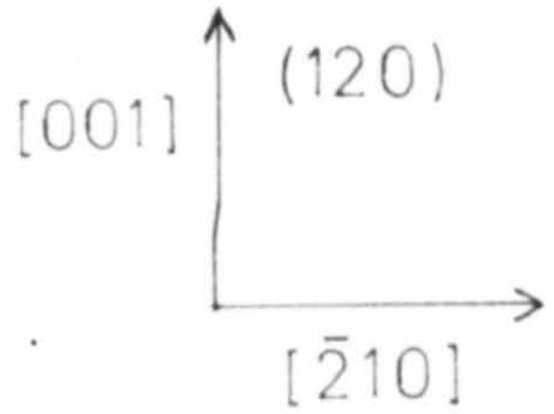

0.2μ

HETEROGENEOUS PRECIPITATION OF CrN

IN IRON - 1.2% CHROMIUM ALLOY

(Nitrided 575°C. 2% NH_3-H_2 67h.)

Fig. VII. 12.

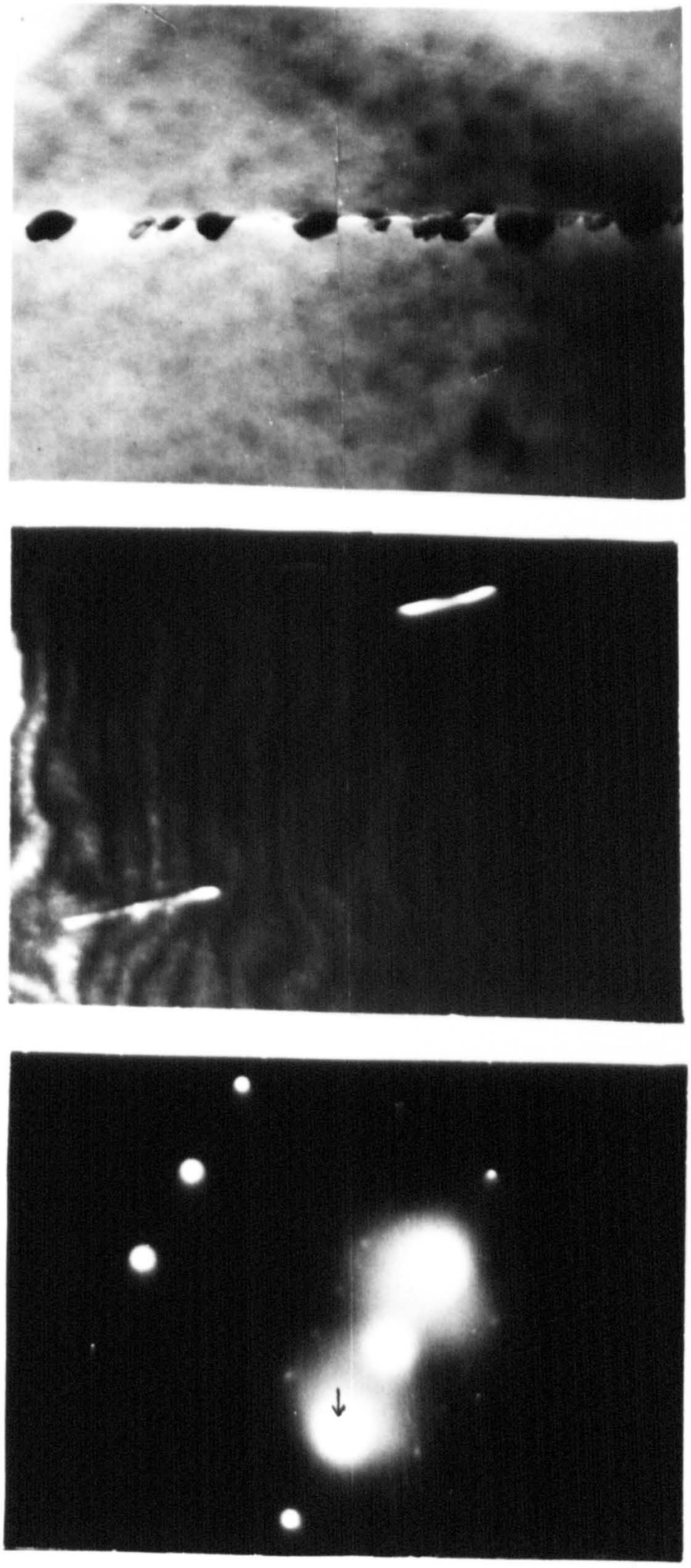

CrN precipitates
in grain boundary.

0.1μ

centred dark field

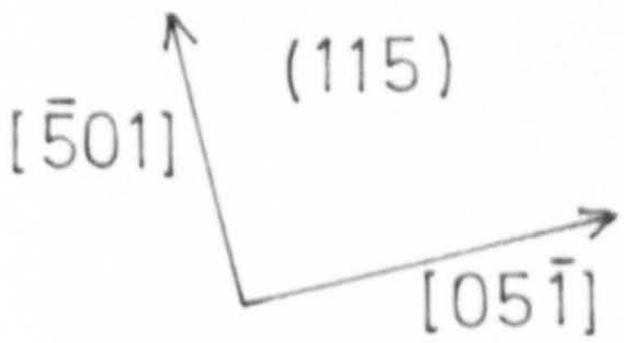

0.1μ

[115]$_m$ zone.
indicating (111) CrN
spot used for
dark field.

HETEROGENEOUS PRECIPITATION OF CrN
IN IRON-1.2%CHROMIUM ALLOY.
(Nitrided 575°C. 2%NH_3-H_2. 67h.)

Fig. VII. 13.

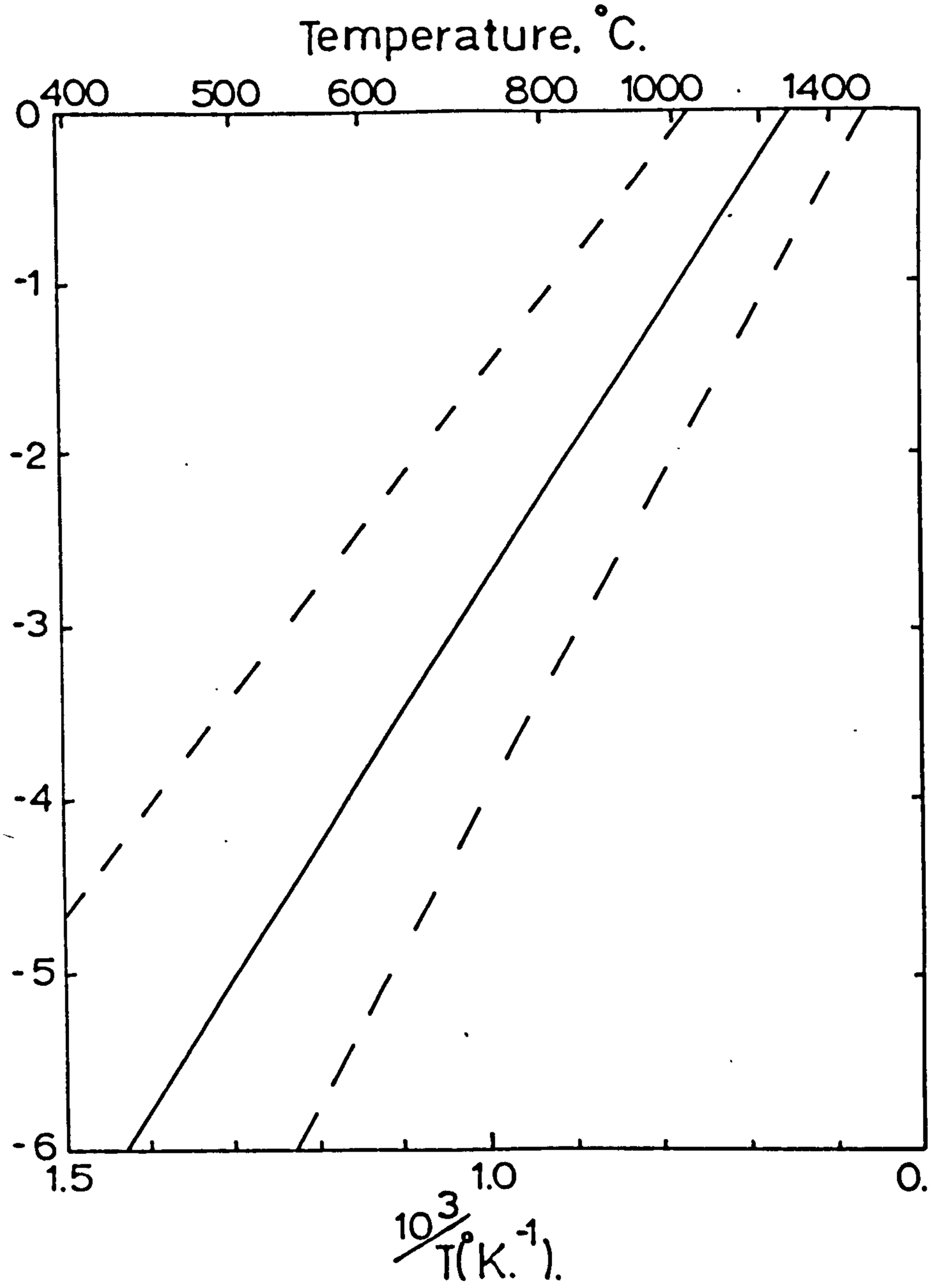

CALCULATED SOLUBILITY PRODUCT OF CrN IN FERRITE.

(after Leslie, 1958)

phase forms in the early stages of nitriding at a high nitrogen potential and the nitrogen potential is then reduced to a level below that in equilibrium with this phase, the metastable precipitate should then dissolve. However, if CrN is nucleated in the initial period of nitriding this will continue to grow even on reducing the nitrogen potential because the potential in equilibrium with CrN is extremely low. Also, on subsequent treatment in hydrogen an unstable preprecipitate would be expected to decompose more readily than CrN. The results shown in Figure VII.14 suggest that even after 4 hours at 575°C the precipitates are stable and continue to grow in a $2NH_3:98H_2$ gas mixture. Moreover, on treating in hydrogen the weight loss is equivalent to the nitrogen in solution in equilibrium with the gas without requiring any decomposition of precipitate.

VII.4 The effect of oxygen on the nitriding of iron-chromium alloys

Metallographic examination of nitrided Fe-Si-N alloys (Roberts, 1970) showed that the precipitated silicon nitride is much coarser in specimens which have previously been annealed in hydrogen. This difference was thought to be due to the reduced oxygen concentration in the hydrogen-treated materials. Subsequent nitriding of alloys pre-treated in hydrogen-water gas mixtures to a selected oxygen activity, proved that oxygen adsorption at the precipitate-matrix interface retards the growth rate.

The rate of nitriding of iron-chromium alloys in ammonia-hydrogen gas mixtures was slower for specimens removed intermittently from the furnace than for specimens nitrided continuously. The effect is shown in curves (a) and (c) in Figure VII.15. It is thought that this difference in rate is related to the oxidation of the specimen each time it is removed from the furnace, to the time required for steady state nitriding conditions to be set up on returning the specimen to the furnace, and to the prevailing oxygen activity in the gas. The linear nature of the weight gain - time plot (a) supports the view that some surface reaction is inhibiting the normal parabolic rate of nitriding.

Fig. VII. 14.

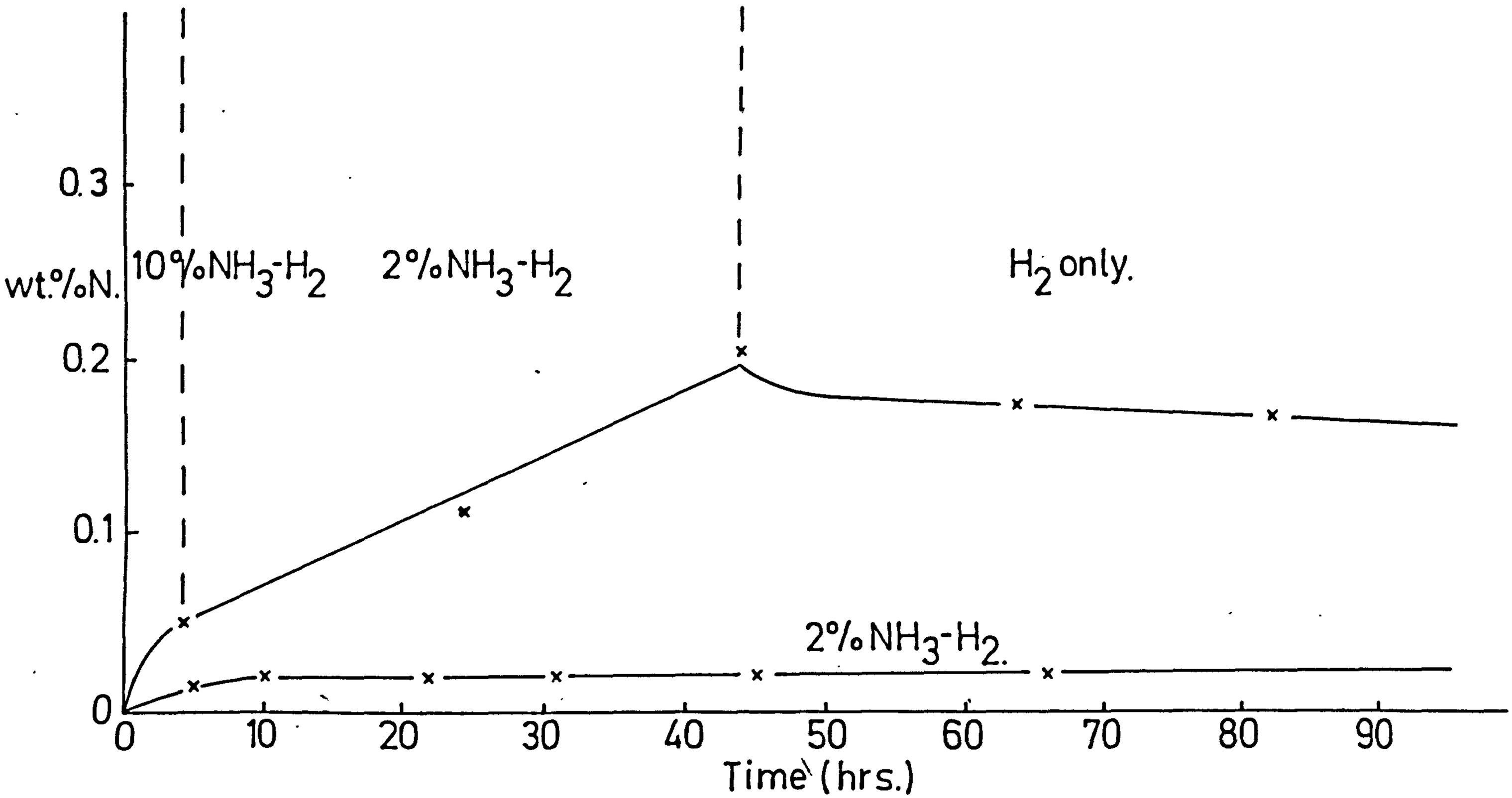

WEIGHT GAIN DATA FOR HOMOGENEOUS AND HETEROGENEOUS PRECIPITATION OF CrN.

Fig.VII. 15.

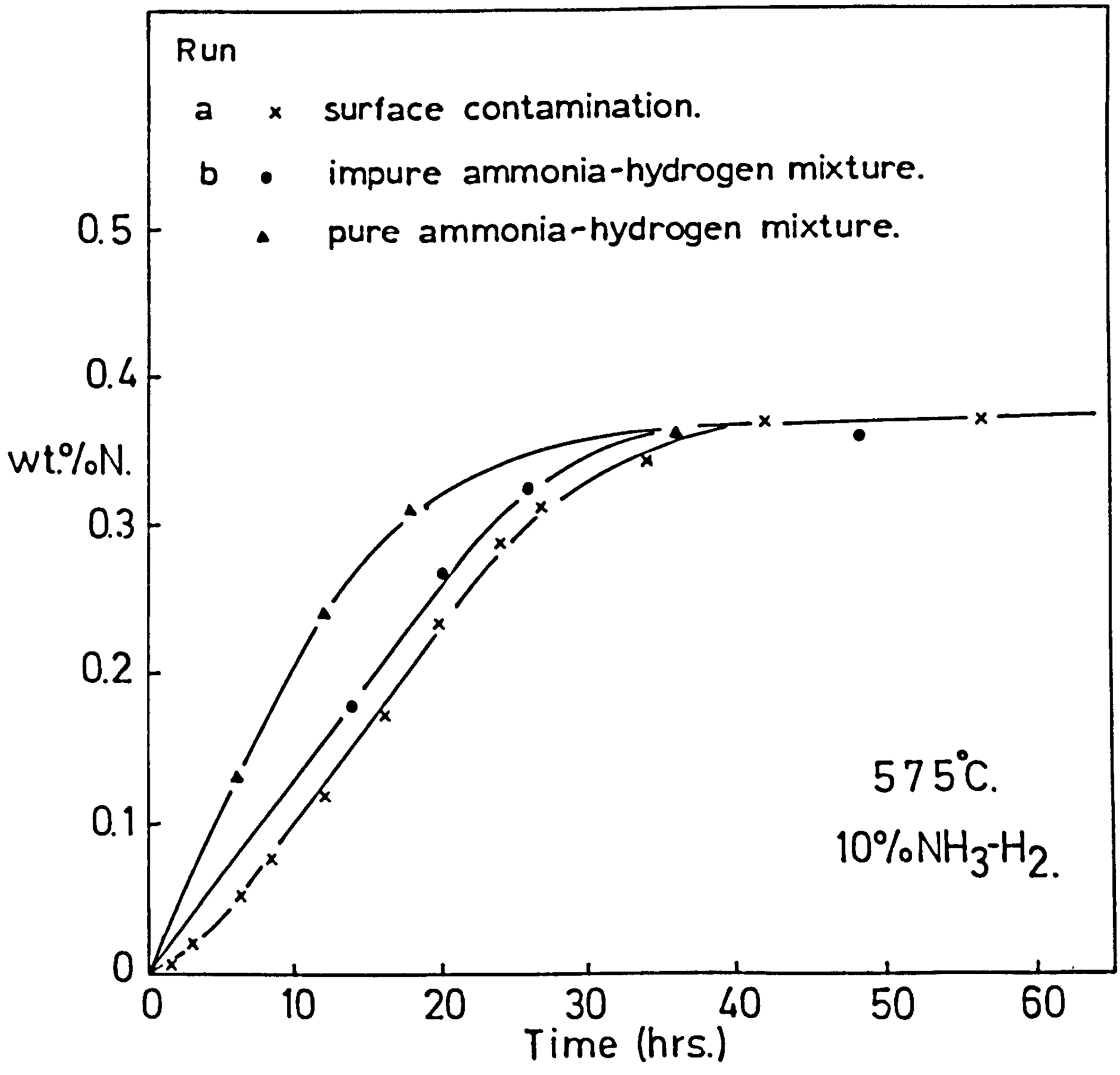

WEIGHT GAIN-TIME CURVES FOR 1.2wt%Cr-Fe SHOWING

THE EFFECTS OF OXYGEN ON NITRIDING RATE.

The effect of increasing the oxygen activity in the gas mixture by using "wet" hydrogen, direct from the cylinder, is shown in curve (b) of Figure VII.16 and illustrates that the traces of water vapour and possibly carbon dioxide, although not causing any observable oxidation, obviously decreases the rate of nitriding with respect to the rate obtained using purified gas.

Surface mechanisms are known to control reaction rates in other systems, as for example in the graphitisation of high-sulphur aluminium-killed steel (Smith et. al., 1951), and so the present observations and their interpretation are perhaps not too unusual.

VII.5 Conclusions

(a) A critical substitutional solute concentration exists above which the rate determining step during the nitriding of a ferritic alloy is the diffusion of nitrogen through the ferrite; for chromium this critical concentration is approximately 2wt.%. The kinetics of the subscale advance in such alloys is the same as applied to internal nitriding in other systems. The square of the subscale depth is:

(i) proportional to the time of nitriding;

(ii) proportional to the surface nitrogen activity;

and (iii) inversely proportional to the alloy content.

(b) With less than the critical 2wt.% chromium, the rate determining step is the diffusion of chromium if the nitrogen potential is sufficiently high for homogeneous precipitation.

(c) The rate of nitriding is reduced by oxidation of the alloy surface and so the nitriding kinetics are affected by oxidising impurities in the nitriding gas mixtures.

(d) No attempt has been made in the present work to study the mechanical properties of iron-chromium-nitrogen alloys in terms of dislocation-particle interactions and this would be an interesting

field for future work. Figure VII.16 illustrates the "pinning" of dislocations by disc-shaped precipitates.

Fig.VII.16.

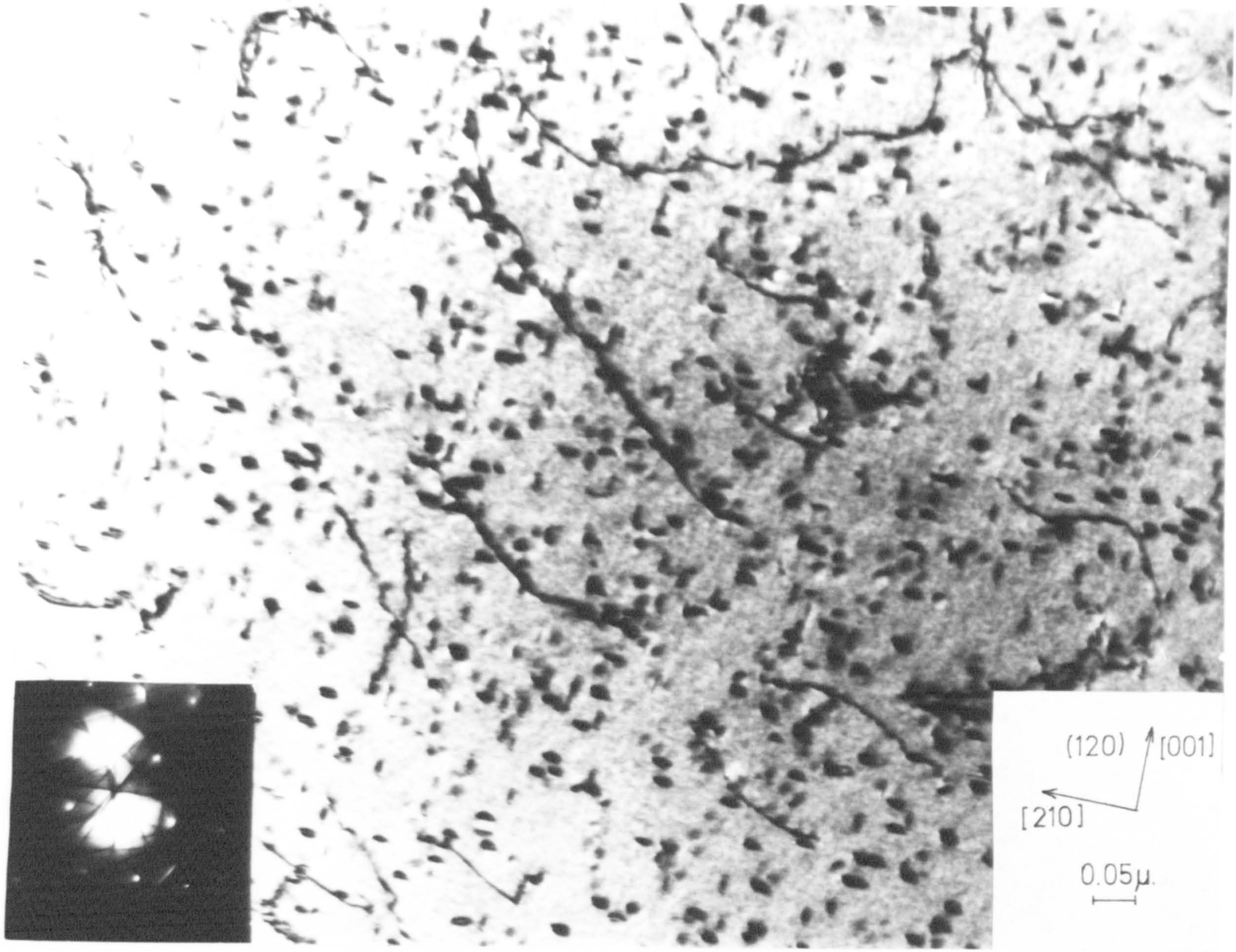

DISLOCATIONS IN CONSTANT ACTIVITY AGED IRON-5.6% CHROMIUM ALLOY.

(Nitrided 575°C. 6%NH_3-H_2 25h.)

Chapter VIII

General Conclusions

A detailed study of precipitation reactions in a ternary system requires knowledge of the component binary systems and the interpretation of the results of the present work would not have been possible without such background information.

In iron-chromium-nitrogen alloys the phases precipitated under given experimental conditions are those predicted by the thermodynamic data for the system and the present results are self-consistent and in agreement with previous observations.

Low temperature aging of nitrogen-ferrites containing chromium demonstrates the effect of chromium on the activity coefficient of dissolved nitrogen and hence on the morphology and kinetics of precipitation.

Six different phases are observed in aged Fe-Cr-N alloys in the range 450 - 1050^{o}C. The composition and mode of precipitation of the nitride formed is dependant not only on the temperature but also on the activities of chromium and nitrogen in solid solution. Previous observations of homogeneous precipitation in Fe-Mo-N, Fe-Nb-N and Fe-N alloys are extended to the Fe-Cr-N system in the present work which contributes to the knowledge of these new technologically-important precipitation processes.

Substitutional-interstitial mixed solute zones must precede the precipitation of alloy-element nitrides and carbides in many systems. For example, the Fe-Mo-C electron micrographs of Irani & Honeycombe (1965) show homogeneous precipitation in localised regions but their quench-aging does not allow the large-scale homogeneous precipitation which is possible by "constant activity" equilibration. Similarly, the electron micrographs of Fe-Mn-N alloys (Baird, 1966) show some evidence of zones but also show that once heterogeneous

nucleation occurs, further homogeneous precipitation is impossible.

These investigations together with current work at Newcastle on Fe-V-N, Fe-Ti-N and Fe-W-N alloys indicate that two of the most important controlling factors affecting homogeneous precipitation in Fe-X-N systems in the range 400 -650°C are (i) the degree of interaction between the substitutional and nitrogen atoms, and (ii) relative fluxes of the substitutional and interstitial solutes.

As a result, small concentrations of niobium, vanadium and titanium, which interact very strongly with nitrogen, give appreciable increases in hardness after nitriding due to the precipitation of a high density of small zones. These structures are extremely stable and transform only after over-aging or prolonged annealing at temperatures above 650°C. On nitriding chromium and manganese alloys containing similar concentrations of substitutional element the precipitation is coarser and over-ages more readily. This is consistent with the weaker, although not inappreciable, affinity of these elements for nitrogen which, in turn, must result in a higher chromium and manganese concentration in solution in equilibrium with the precipitated species and so facilitates particle coarsening. The high diffusivity of chromium is the probable reason for the transient nature or absence of preprecipitation stages in chromium alloys. Compared to other nitrides, the free energies of formation of molybdenum and tungsten nitrides are small and the effect of these elements on the activity coefficient of nitrogen in ferrite (see Figure V.4) is also small. These effects together with the low diffusivities of these elements in iron, due to their relatively large size, suggest that these are the alloys in which preprecipitation processes can more readily be observed. This is amply verified by the work of Spiers (1969) on molybdenum alloys and by more recent investigation of the Fe-W-N system (Stephenson, 1970).

Electron diffraction observations and volume fraction measurements on 5wt.%W alloys provide conclusive evidence of an

- $Fe_{16}N_2$ - type intermediate precipitate.

The observations of Roberts (1970) in Fe-Si-N alloys fit into the general model of precipitation because the effect of silicon on the activity coefficient of nitrogen in ferrite reduces the nitrogen concentration to such a low level that homogeneous precipitation is not observed.

Appendix

A. 1 Introduction

Interstitial alloys, that is those compounds with small non-metal atoms occupying interstices between larger transition metal atoms, were first classified by Hägg (1930) who concluded that the structure type depended upon the radius ratio $R = r_X/r_M$ where r_X and r_M are the radii of the non-metal and metal atoms respectively. If R is less than 0.59, the metal atom arrangement is one of the following four simple types, or can be derived from it by simple distortion:

(i) face-centred cubic;
(ii) close-packed hexagonal;
(iii) body-centred cubic;
and (iv) simple hexagonal with an axial ratio near unity.

For R greater than 0.59 the structures are "complex" and have less pronounced metallic properties than "normal" interstitial alloys.

Hägg postulated that non-metal atoms occupy those interstices in which they can remain in contact with their metal-atom neighbours. Subject to this condition, which imposes a minimum value for the radius ratio of each type of normal structure, the non-metal atoms achieve maximum co-ordination with their surrounding metal atoms by occupying the largest available holes. In the face-centred cubic, the close-packed hexagonal, and the body-centred cubic metal lattices, there are two kinds of interstices, tetrahedral with a co-ordination number 4 and octahedral with a co-ordination number 6. In the two close-packed structures (f.c.c. and c.p.h.) the octahedral hole is perfectly regular, but in the body-centred cubic lattice it posesses tetragonal symmetry. In the simple hexagonal unit cell the only interstices are the large 6 - fold co-ordinated sites at the centres of trigonal prisms of metal atoms.

In an interstitial structure it is not necessary that all the holes of one type be occupied. As a consequence, many homogeneous phases show a wide range of composition. It is common, however, to find that

the range of homogeneity of a phase includes, or is very near to, some simple stoichiometric composition which corresponds to the filling of a definite fraction of the available interstices.

Geometrical principals, whilst being a necessary condition for interstitial alloy formation, are not the only determining factors. As interstitial alloys are formed only by metal atoms with an inner incomplete electron shell an "electronic" factoris implied. It is also accepted (Seitz, 1943) that the electronegativity difference between the metal and the non-metal plays a part in determining the possibility of interstitial alloy formation Thus oxides with relatively high oxygen concentrations are usually ionic or covalent and not metallic.

Radius ratios calculated for different interstitial-alloy systems are listed in Table A.1 (from Schwarzkopf & Kieffer, 1953) and that for manganese and carbon, 0.60, exceeds the critical value of 0.59. Thus in accordance with observations manganese carbides are expected to have complex structures.

Manganese is one of the commonest alloying elements used in the iron and steel industry. All steels contain at least 0.2wt.%Mn and some special steels contain much more e.g. Hadfield's steel with 13wt.%Mn. Its general function is as a de-oxidant and to increase hardenability. An understanding of the Fe-Mn-C ternary system and of manganese steels in general is technologically important but a prerequisite for this is a thorough knowledge of the component binary systems. Although the iron-manganese and iron-carbon equilibrium diagrams are well established, a number of incompletely characterized phases have recently been claimed in the manganese-carbon system but because there is little agreement between different observations there seems to be doubt about the validity of such claims.

The phases shown in Figure A.1 were reported by Kuo & Persson (1954) who reviewed all previous work on the system. Their unit cell dimensions are given in Table A.2. Each of the four characterized carbides has a crystal structure which frequently occurs in other

Table 1. Radius ratios in interstitial alloy systems (after Schwarzkopf & Kieffer, 1953)

	Sc	Ti	V	Cr	Mn	Fe	Co	Ni
r_{Me} =	1.62	1.47	1.34	1.27	1.26	1.26	1.25	1.24 Å
B	0.54	0.59	0.65	0.69	0.69	0.69	0.70	0.70
C	0.47	0.52	0.57	0.60	0.60	0.60	0.61	0.62
N	0.44	0.48	0.53	0.56	0.56	0.56	0.57	0.57
O	0.37	0.41	0.45	0.47	0.48	0.48	0.48	0.48
H	0.19	0.20	0.22	0.24	0.24	0.24	0.24	0.24

	Y	Zr	Nb	Mo	Tc	Ru	Rh	Pd
r_{Me} =	1.80	1.60	1.46	1.39		1.34	1.34	1.37 Å
B	0.48	0.54	0.60	0.63		0.65	0.65	0.64
C	0.42	0.48	0.53	0.55		0.57	0.57	0.55
N	0.39	0.44	0.49	0.51		0.53	0.53	0.52
O	0.33	0.38	0.41	0.43		0.45	0.45	0.44
H	0.17	0.19	0.20	0.22		0.22	0.22	0.22

	La-Lu	Hf	Ta	W	Re	Os	Ir	Pt
r_{Me} =	1.87–1.74	1.59	1.46	1.39	1.37	1.35	1.36	1.39 Å
B	0.47–0.50	0.55	0.60	0.63	0.64	0.64	0.64	0.63
C	0.41–0.43	0.48	0.53	0.55	0.55	0.56	0.56	0.55
N	0.38–0.41	0.44	0.49	0.51	0.52	0.53	0.52	0.51
O	0.32–0.34	0.38	0.41	0.43	0.44	0.44	0.44	0.43
H	0.16–0.17	0.19	0.20	0.22	0.22	0.22	0.22	0.22

	Th	U	
r_{Me} =	1.80	1.52 Å	
B	0.48	0.57	r_B = 0.87 Å
C	0.42	0.50	r_C = 0.76 Å
N	0.39	0.47	r_N = 0.71 Å
O	0.33	0.39	r_O = 0.60 Å
H	0.17	0.20	r_H = 0.30 Å

Fig. A. 1.

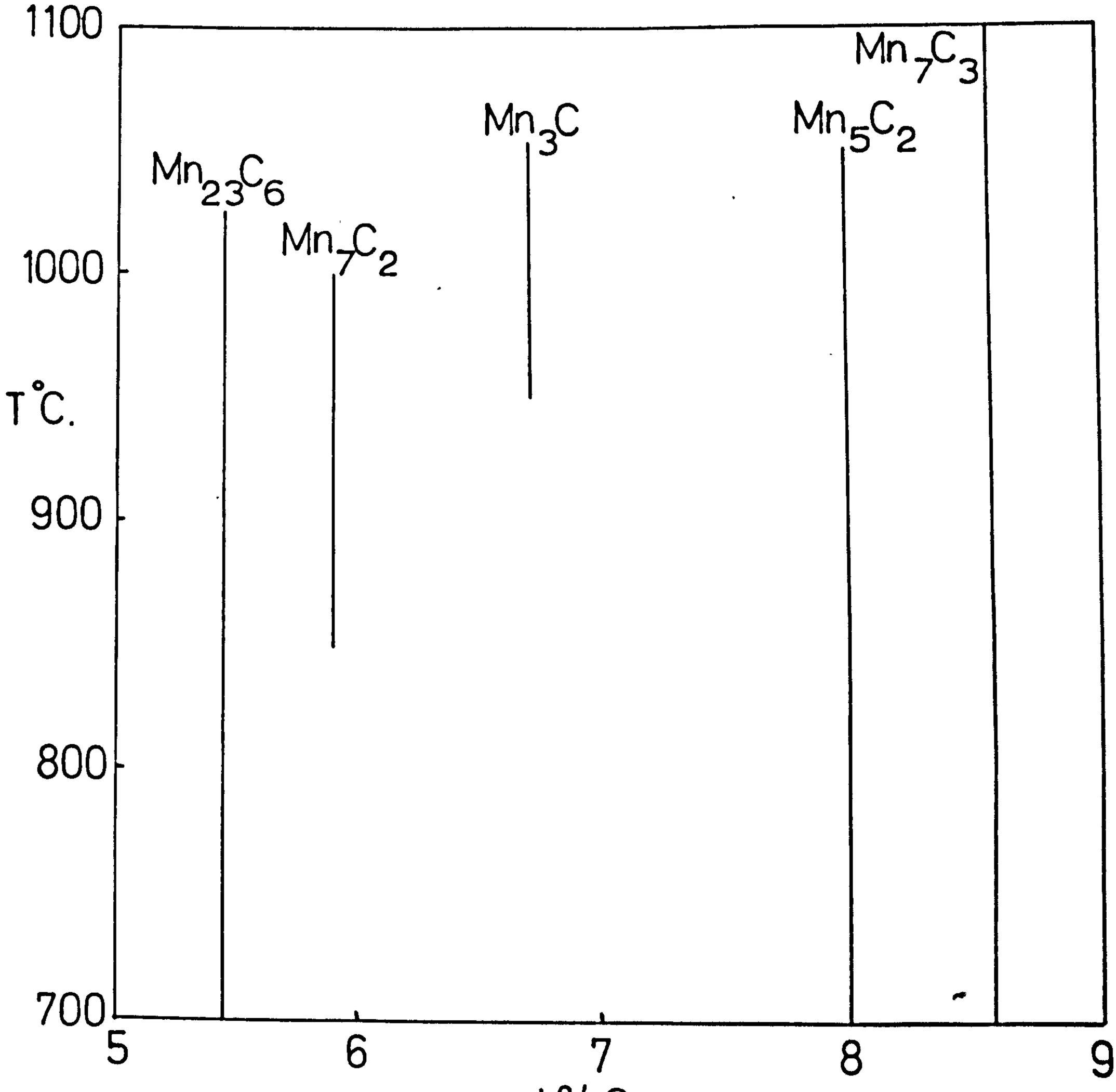

STABILITY RANGE OF MANGANESE CARBIDES

(from Kuo and Persson, 1954.)

Table A.2

Unit cell dimensions of manganese and manganese carbides

phase	crystal structure	unit cell dimensions, Å			
		a	b	c	
α-Mn	b.c.c.	8.917			*
β-Mn	b.c.c.	6.313			*
$Mn_{23}C_6$	f.c.c.	10.598			*
$Mn_{22}C_6$ (Mn_7C_2)	hexagonal	7.492		12.070	:
Mn_3C	orthorhombic	4.545	5.103	6.787	*
Mn_5C_2	monoclinic	11.563	4.573	5.058	*
			β = 97° 45'		
Mn_7C_3	orthorhombic	4.546	6.959	11.976	*

* from Bouchaud (1967)

: from this investigation.

carbide systems, and so it seems possible that the unknown phase "Mn_7C_2" might also be an example of a widely found structure type. The present investigation aimed at establishing the exact structure of the new phase.

An investigation by Picon & Flahaut (1957) suggested the existence of the carbides listed in Table A.3 but, in general, these results contradict previous observations and few of their findings have been corroborated. Jack & Wild (1965) showed that a complete range of solubility exists between Mn_5C_2 and Fe_5C_2 and determined the exact crystal structures of these materials. Duggin (1966) confirmed these results and later (Duggin, 1967) reported the following manganese-rich iron-manganese-carbon phases analogous to the Mn_4C and Mn_6C_2 found by Picon & Flahaut:

carbide	dimensions, Å	
	a	c
tetragonal	6.772	9.427
hexagonal	5.77	6.98

These phases have not been observed in any other investigation and the strongest X-ray reflexions (see Table A.4) from Duggin's phases were indexed by Jack as $Mn_{23}C_6$ and α-Mn respectively; there is therefore no experimental basis for the existence of these or any uncharacterized manganese carbides other than "Mn_7C_2".

In his summary of work on the manganese-carbon system, Bouchaud (1967) reaches a similar conclusion. The "Mn_7C_2" phase, first reported by Kuo & Persson, to contain about 5.9wt.%C and existing between 850 and 1,000°C, was indexed by Jack (1964) on the basis of a hexagonal unit cell:

$$a = 7.492 \quad ; \quad c = 12.070 \text{ Å}.$$

He noted the approximate coincidence of many strong reflexions in the X-ray diffraction patterns of $Mn_{23}C_6$ and "Mn_7C_2" which indicated that they had similar structures. It was further noted that the unit cell dimensions and volume were related to those of cubic $Mn_{23}C_6$

Table A.3

Manganese carbides observed by Picon & Flahaut (1957)

formula	crystal structure	unit cell dimensions, Å		
		a	b	c
Mn_4C	totragonal	7.66		10.57
Mn_6C_2	hoxagonal	5.48		6.71
Mn_6C_2	orthorhombic	4.53	5.11	6.76
Mn_8C_3	triclinic		———	
Mn_8C_3	cubic	8.14		
Mn_8C_3	hexagonal	13.90		4.55

Table A.4

Manganese carbides observed by Duggin (1967)

(a) Tetragonal carbide.

a=6.772; c=9.427 Å

intensity	{hkl}	$\sin^2\theta$ obs. (FeKα)
w	113	0.1348
vw	212	0.1469
ms	004	0.1683
vw	104	0.1885
m	213	0.2018
vw	311	0.2157
vs	302	0.2266
ms	214	0.2689
s	313	0.2940
m	322	0.3028
vw	323	0.3615
m	314	0.3692
m	511	0.5377
m	512	0.5694
s	503	0.6025
	433	
w	217	0.6154
s	335	0.6274
m	425	0.6696
m	108	0.6940

$Mn_{23}C_6$ a=10.580 Å

$\sin^2\theta$ calc. (FeKα)	{hkl}
0.1341	400
0.1676	420
0.2011	422
0.2263	{511, 333}
0.2682	440
0.2933	533
0.3017	{600, 442}
0.3603	533
0.3687	622
0.5363	800
0.5698	820
0.6034	{822, 660}
0.6285	{555, 751}
0.6704	840
0.6955	911

Table A.4 (continued)

(b) Hexagonal carbide

a=5.77; c=6.98 Å			∝-Mn a=8.957 Å	
intensity	{hkl}	$\sin^2\vartheta$ obs. (FeK∝)	$\sin^2\vartheta$ calc. (FeK∝)	{hkl}
vvw	003	0.1742		
vw	112	0.1899	0.1871	400
vs	103	0.2112	0.2105	330
m	210	0.2574	0.2573	332
w	211	0.2813	0.2806	422
w	312	0.5604	0.5613	444
w	115	0.5837	0.5847	710
vs	205	0.6296	0.6314	721
w	304	0.6442		
w	313	0.6550	0.6548	642
vw	402	0.6752		

(a = 10.61 Å) as follows:

$$a_h \approx a_c / \sqrt{2}$$
$$c_h \approx 2a_c / \sqrt{3}$$
$$V_h \approx V_c / 2$$

which suggested that the hexagonal phase is related to the cubic phase in the same way that close-packed hexagonal and face-centred cubic metal atom arrangements are related or as wurtzite is related to zinc blende.

This indexing, but not the suggested structure, was independently reported by Bouchaud & Fruchart (1964) and they proposed, from density measurements and analysis, that the composition was $Mn_{15}C_4$ with three of these formula weights ($Mn_{45}C_{12}$).per unit cell.

Duggin (1969) incorrectly interpreted the diffraction pattern of "$(Mn,Fe)_7C_2$" on the basis of a mixture of two phases:

(i) hexagonal a = 7.471 ; c = 12.044 Å
(ii) tetragonal a = 6.772 ; c = 9.427 Å .

His reported X-ray data with the suggested indexing is shown in Table A.5; most of the reflexions can be indexed on the basis of the hexagonal cell without any need for a mixture of phases.

A.2 Specimen preparation

Manganese is a volatile reactive element, easily oxidised, and its carbides decompose slowly in moist air. The new phase has been prepared in the present and other work only as powders and so the structural investigation is by X-ray powder diffraction techniques. Weighed powder mixtures of manganese and carbon were pelletised and heated in vacuo in silica tubes between 900 and 1,000°C for various times. Little reaction with the silica tube was observed and heating times greater than 24 hours were sufficient to establish equilibrium.

Table A.5

X-ray data for "Mn_7C_2" from Duggin (1969)

intensity	{hkl} tet.	{hkl} hex.	$\sin^2\theta$ obs. (FeKα)	{hkl}* "Mn_7C_2"
vvw	212	203	0.1483	203
w		211	0.1641	211
w	004		0.1716	114
vw		105	0.1832	105
vw		212	0.1843	212
vvw	104		0.1890	
vw		204	0.1934	204
mw	213		0.2022	300
m	311		0.2158	213
s	302		0.2278	302
mw		006	0.2333	006
m		205	0.2523	106 205
vw		303	0.2609	303
		214		214
m	214		0.2691	220
w	313		0.2947	222
w		311	0.2977	311
w	322		0.3008	116
mw		304	0.3056	304
w		215	0.3185	215
		312		312
vvw		206	0.3238	206
vvw	323		0.3646	401
w	314		0.3724	224

* indexing from this investigation.

tet. = tetragonal phase ; hex. = hexagonal phase.

Table A.5 (continued)

intensity	{hkl} tet.	{hkl} hex.	$\sin^2\theta$ obs. (FeKα)	{hkl*} "Mn_7C_2"
w		405	0.5201	{405 307
vw	511	109	0.5466	109
vvw		501	0.5654	501
w	512		0.5725	414
w		227	0.5863	{502 325
		502		
s	503		0.6030	{330 317
	433			
vvw		330	0.6071	
s	217	209	0.6140	{209 308
mw	335		0.6284	{420
mw		332	0.6311	{332
vw	425		0.6731	00,10
				422
mw		219	0.6806	{228 219 423
vw	514		0.6984	511
	108			
m		511	0.7008	{318 416

A.3 X-ray methods

Preliminary X-ray examination of reacted materials was carried out using filtered FeK_α radiation in a 11.46cm. Philips camera but detailed structural investigation used monochromatic FeK_α and CrK_α radiations from a LiF plane-crystal monochromator together with Unicam 19cm. cameras.

A.4 Crystal structure determination

The positions of the X-ray reflexions were measured with a direct-reading vernier scale (Gibson, 1946) and the unit cell dimensions were determined from the resolved high angle doublets. The intensity of each reflexion was measured using a direct-reading microdensitometer (Taylor, 1951), plotting the line profile on graph paper, and measuring the area under the peak with a planimeter. The mean values from both sides of each film were taken as the "observed intensities".

The intensity of any X-ray powder reflexion (hkl) is given by:

$$I_{hkl} = \text{constant} \cdot F^2_{hkl} \frac{1 + \cos^2 2\alpha \cos^2 2\theta}{\sin^2\theta \cos\theta} \cdot p \cdot A \qquad \ldots\ldots(A1)$$

and $$F^2_{hkl} = \left[\Sigma f \cos 2\pi(hx + ky + lz)\right]^2 + \left[\Sigma f \sin 2\pi(hx + ky + lz)\right]^2 \qquad \ldots\ldots(A2)$$

where F is the structure amplitude;

θ is the Bragg angle for reflexion from a family of planes (hkl);

α is the Bragg angle of the beam reflected from the monochromator;

p is the number of co-operating planes reflecting at the same angle;

A is the absorption factor.

A temperature correction is applied to the scattering factor, , of an atom with general co-ordinates x, y, z:

$$f = f_o \exp.\left(\frac{-B\sin^2\theta}{\lambda^2}\right) \qquad \ldots\ldots(A3)$$

and $$B = 8\pi^2\bar{\mu}^2 \qquad \ldots\ldots(A4)$$

where λ is the wavelength of the X-rays;

f_o is the scattering factor for an atom at rest;

and $\bar{\mu}^2$ is the mean square amplitude of thermal vibration.

The observed structure amplitudes, F_o, calculated from equation A1 were compared with those calculated for the postulated structure and, when relevant, structure refinement was carried out with an English Electric KDF9 computer using a structure factor-least squares refinement programme (Cruikshank, 1964). The input data required for the SFLS programme is contained in three tapes:

Data Tape (1) includes the symmetry elements for the structure, the scattering factors for each of the atoms in the structure, and the refining instructions for these atoms;

Data Tape (2) contains the parameters to be refined and the isotropic or anisotropic temperature factor for these atoms;

Data Tape (3) contains the indices of the reflexions and their observed structure factor.

Refinement of the parameters was carried out until the best agreement between the observed and calculated intensities was reached. Since many reflexions consisted of superimposed components (e.g. 212 and 105 in "Mn_7C_2") resolution was obtained by dividing the total observed intensity of the multiple reflexion in the ratio of the calculated intensities of the components. This re-division was repeated successively as refinement proceeded. Refinement was carried out until the residual R' reached a minimum value.

$$R' = \frac{\Sigma |F_o - F_c|^2}{\Sigma F_o^2}$$

where F_o and F_c are the observed and calculated structure amplitudes.

A.5 Line broadening measurements

In addition to the structure determination, stacking disorder in the specimen was also studied by X-ray methods. Such disorder

gives a mixture of sharp and diffuse reflexions on X-ray photographs and it is necessary to carry out line broadening measurements in order to characterize it. Since both sets of lines were produced under the same instrumental conditions, the sharp lines were used as standards for broadening measurements. Instrumental broadening and "α- doublet" corrections (Jones, 1938) were applied to the integral line widths to give the diffraction broadening, β. The crystallite size, t, is related to the diffraction broadening by the Scherrer formula:

$$t = \frac{K\lambda}{\beta \cos\theta} \qquad \ldots.(A5)$$

where the constant K is taken as unity.

For plate-like crystallites which are small in only one direction, equation A5 is modified and the plate thickness becomes:

$$t = \frac{K\lambda \cos\Psi}{\beta \cos\theta} \qquad \ldots.(A6)$$

where Ψ is the angle between the plate normal and the normal to the reflexion plane (hkl). In hexagonal crystals and for plates that are thin in the [001] direction (see Figure A.2):

$$\cos\Psi = \frac{\sin\theta_{001}}{\sin\theta_{hkl}} . \qquad \ldots.(A7)$$

A.6 Results and discussion

X-ray photographs of the types of phases observed in this investigation are shown in Figures A.3, A.4 and A.5; the mixtures formed under different experimental conditions are summarised in Table A.6 and the unit cell dimensions of the manganese carbides are listed in Table A.2. The results are in agreement with the data of Kuo & Persson except for runs 5, 11, 18, 23 and 29 - 32. The three runs, 5, 11 and 18, in which $Mn_{23}C_6$ and Mn_5C_2 are the only phases observed, are inconsistent with Kuo & Persson's suggested phase diagram (see Figure A.1) where the "Mn_7C_2" phase occurs between $Mn_{23}C_6$ and Mn_5C_2 at the experimental

Fig. $\overline{A}$.2

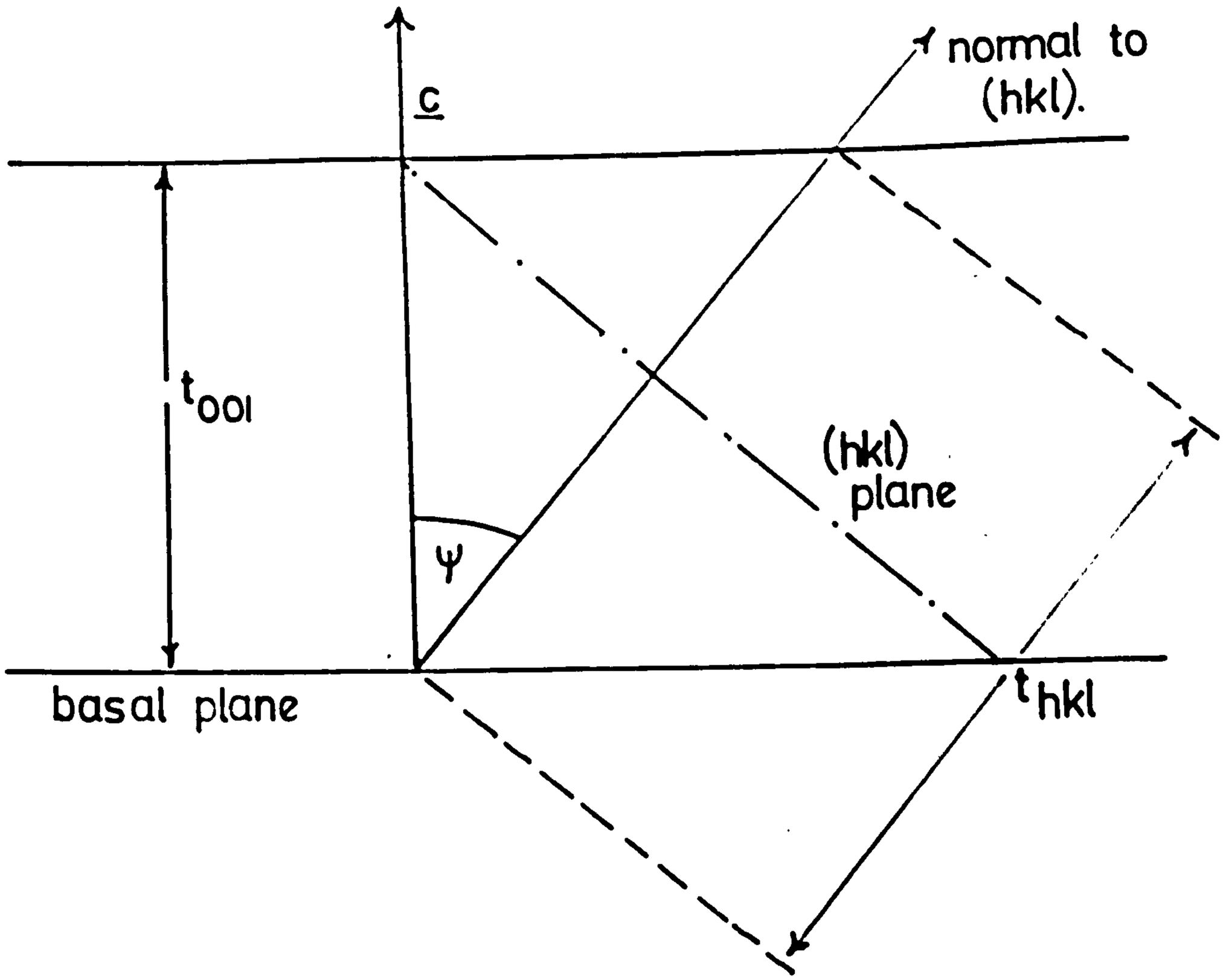

(i) $t_{hkl} = \frac{\lambda}{\beta_{hkl} \cos\theta_{hkl}}$.

(ii) $t_{001} = \frac{\cos\psi \times \lambda}{\beta_{hkl} \cos\theta_{hkl}}$ where $\cos^2\psi = \frac{\sin^2\theta_{001}}{\sin^2\theta_{hkl}}$

Calculation of thickness of plate-like crystallites from the broadening of powder lines.

Fig. $\overline{A}$. 3.

i) Cubic $Mn_{23}C_6$. $a_o = 10.61$ Å.

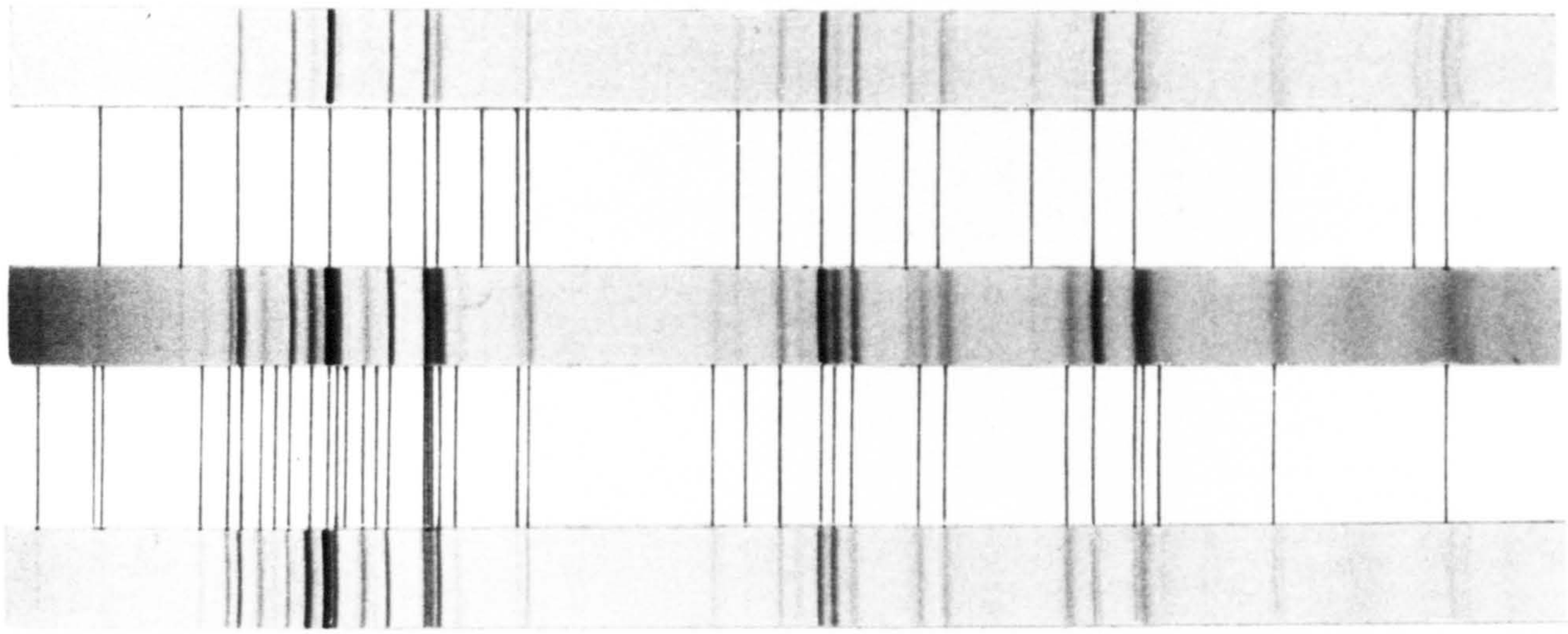

i).

i + ii).

ii).

ii) Hexagonal $Mn_{23}C_6$. $a_o = 7.492$ Å.

$c_o = 12.070$ Å.

X-RAY POWDER PHOTOGRAPHS OF $Mn_{23}C_6$ PHASES.
(Fe Kα radiation.)

Fig. $\overline{\underline{A}}$.4.

α-Mn.

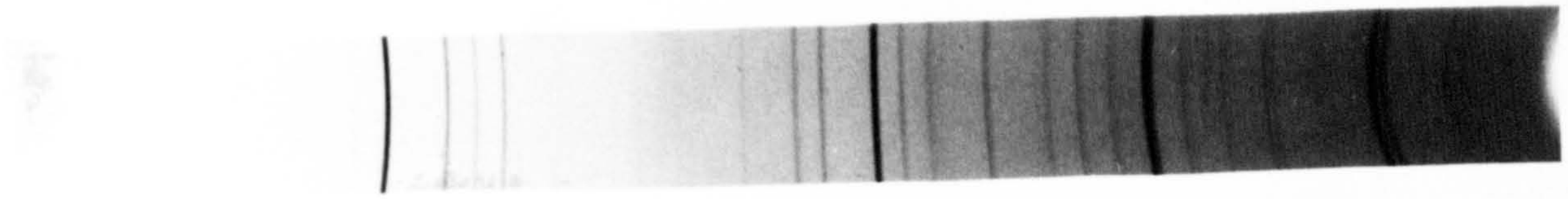

β-Mn.

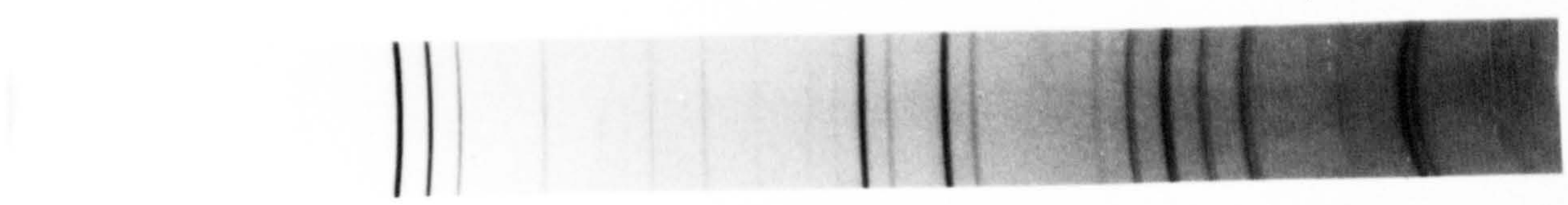

Mn_7C_3.

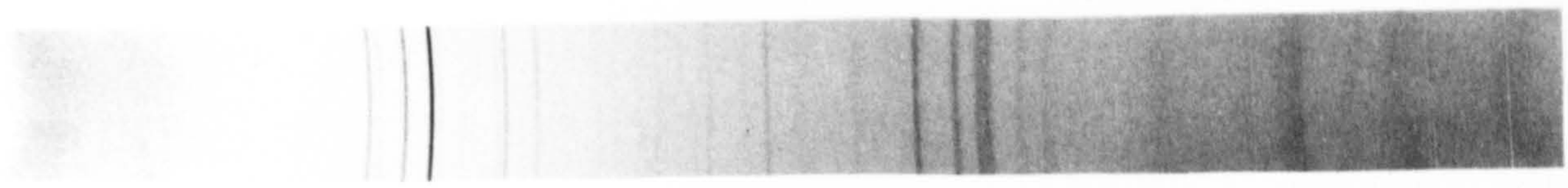

X-RAY PHOTOGRAPHS OF PHASES OBSERVED

IN THE MANGANESE-CARBON SYSTEM.

Fig. $\overline{A}$.5.

Mn_3C

Mn_5C_2

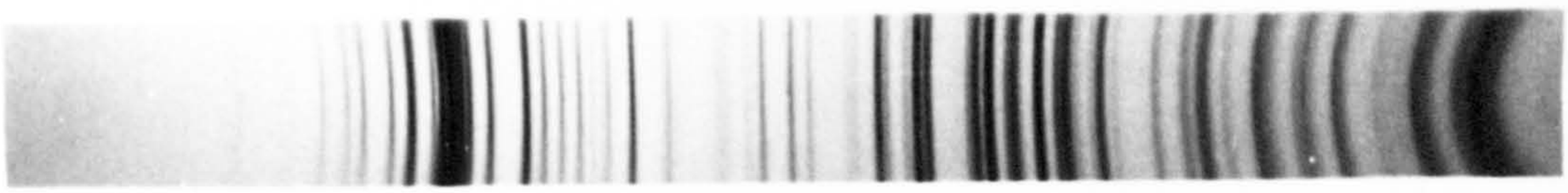

X-RAY PHOTOGRAPHS OF PHASES OBSERVED IN THE MANGANESE-CARBON SYSTEM.

Table A.6

Heat-treatment of manganese-carbon mixtures

(X-major phase x-other phases)

run	initial composition (wt.%C)	temp. °C.	time hrs.	phases observed					
				α-Mn	$Mn_{23}C_6$	"Mn_7C_2"	Mn_3C	Mn_5C_2	Mn_7C_3
1	3.0	910	48	X	x				
2	5.0	"	"		X	x			
3	7.0	"	"					X	
4	4.93	960	96				x	X	
5	4.93	950	140		x			X	
6	5.21	960	92				x	X	
7	5.41	"	"					X	
8	5.59	"	"						X
9	"	"	48					X	x
10	"	"	72					X	x
11	5.28	950	44		x			X	
12	"	"	72					x	x
13	"	"	72				x	X	
14	5.04	"	44			X			
15	"	"	72			x		x	
16	"	"	72			x		x	
17	5.10	960	44		x	X			
18	"	"	52		X			x	
19	5.07	"	44			X		x	
20	"	"	44			X		x	
21	5.17	"	24		X	x			
22	"	"	48			X			
23	"	run 22 plus 800	24		x	X			
24	5.26	960	30			X	x		

Table A.6 (continued)

Heat-treatment of manganese-carbon mixtures

(X-major phase x-other phases)

run	initial composition (wt.%C)	temp. °C.	time hrs.	phases observed					
				α-Mn	$Mn_{23}C_6$	"Mn_7C_2"	Mn_3C	Mn_5C_2	Mn_7C_3
25	5.26	960	18			X	x		
26	5.22	"	18		X	x			
27	"	"	30		x	X			
28	5.18	"	48		x	X			
29	5.20	800	24	x	X	x			
30	5.35	"	"	x	X	x			
31	5.73	"	"		X	x	x		
32	5.48	"	"		X	x			

temperatures. The remaining five runs (23, 29 - 32) carried out at 800°C indicate that the "Mn_7C_2" phase can exist at lower temperatures than previously suggested. All the observations of this and most other work may be explained if the "Mn_7C_2" phase contains a small amount of oxygen; it is then possible for the resultant ternary phase "$Mn_7(C,O)_2$" to co-exist with α-Mn and $Mn_{23}C_6$ or with Mn_5C_2 and $Mn_{23}C_6$ in different ternary phase fields in accordance with observations. A possible phase diagram is shown by Figure A.6.

The crystal structure of $Mn_{23}C_6$, determined by Westgren (1935), is shown in Figure A.7 with atoms in the positions given in Table A.7. The related hexagonal unit cell has 46 manganese atoms and 12 carbon atoms in positions shown in Figure A.8 and Table A.8. The two structures may be considered schematically to be composed of layers of cubo-octahedra and cubes with single atoms in the interstices between the layers.

The observed and calculated structure amplitudes obtained for this structure are shown in Table A.9. The agreement indicates that the structure is correct in principal but there are several reflexions (201, 202,401) for which F_o and F_c are in poor agreement. The parameters for this structure would not refine to give the expected fit between observed and calculated structure amplitudes and so small changes to the postulated structure were considered.

The cubo-octahedra of atoms were rearranged to form pseudo-cubo-octahedra as shown in Figure A.9 and this improved the agreement between the observed and calculated data although the parameters would still not refine to an accepted level; additional small changes were then explored. The new atomic positions are given in Table A.10.

The transformation of atomic positions in the analogous hexagonal cell and the change from cubo-octahedra to pseudo-cubo-octahedra were considered by Fruchart et. al. (1968) who concluded that the proposed structure gave interatomic distances for two pairs of atoms in special positions (f) which were closer than their radii sum (2.52 Å).

Fig. A. 6.

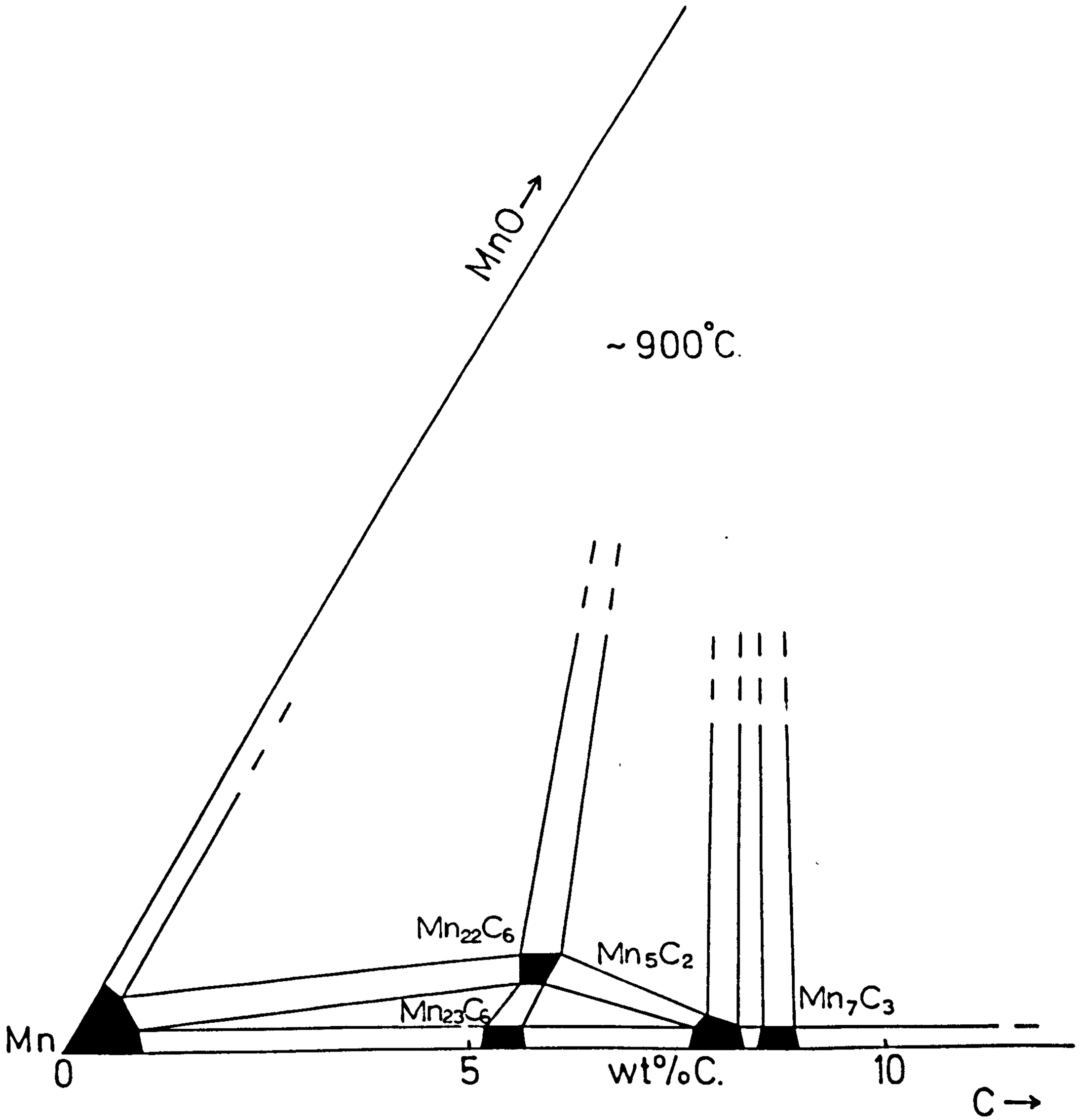

SCHEMATIC TERNARY PHASE DIAGRAM FOR

THE Mn-C-O SYSTEM.

Fig. Ā.7

CUBIC $Mn_{23}C_6$ STRUCTURE.

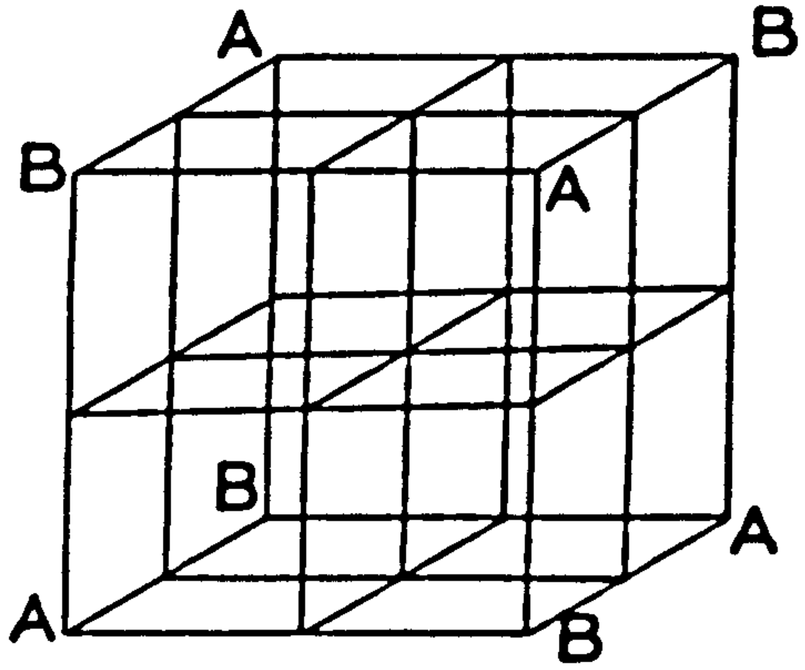

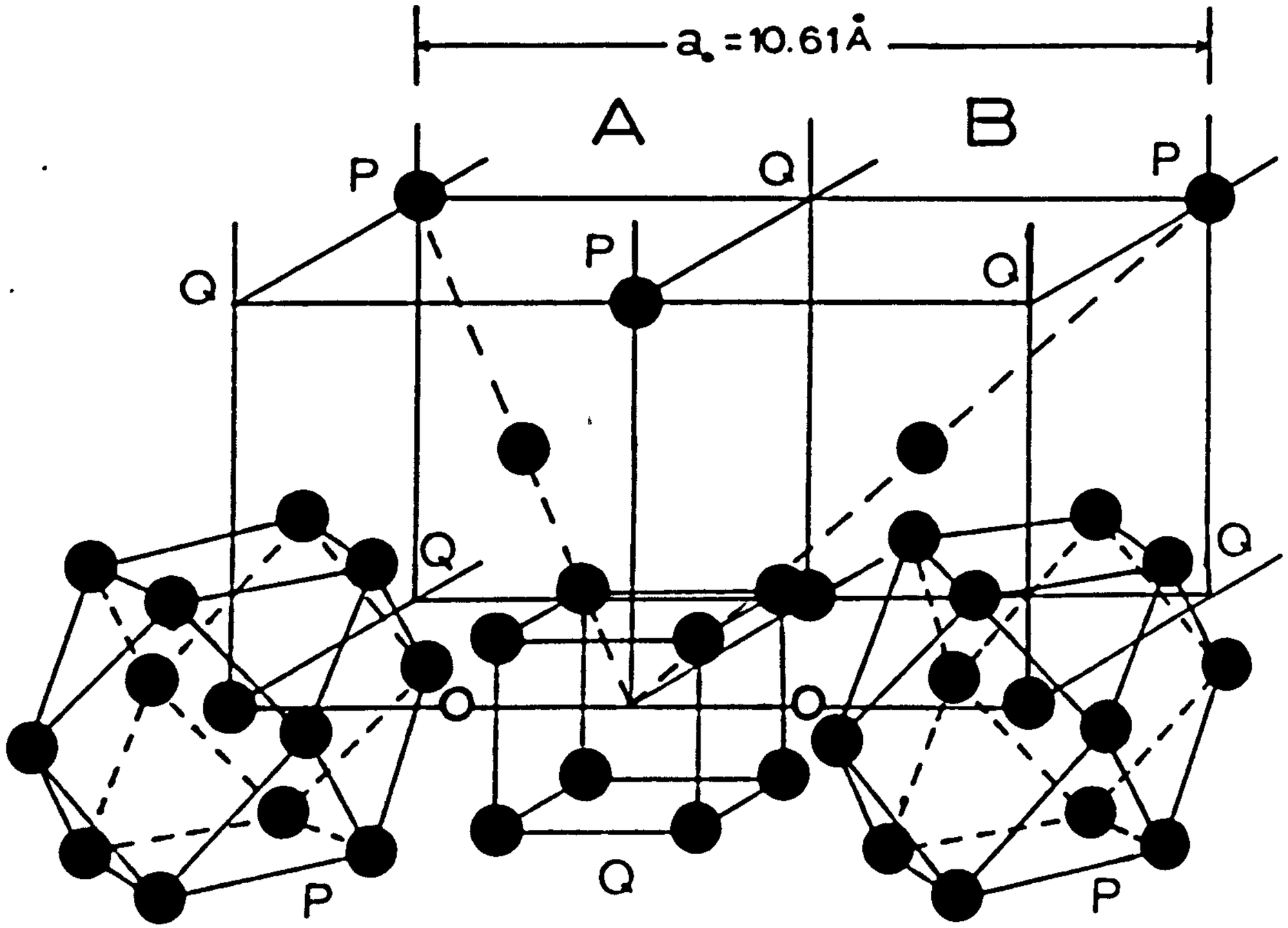

● Manganese

O Carbon.
(in square artiprism interstices.)

Table A.7

Atomic parameters for $Mn_{23}C_6$ (from Westgren, 1935)

space group Fm3m; 4formula units per unit cell.

(see International Tables 1962; No.225)

Atom	x	y	z
4Mn in (a)	0.000	0.000	0.000
8Mn in (c)	0.250	0.250	0.250
32Mn in (f)	0.385	0.385	0.385
48Mn in (h)	0.165	0.835	0.000
24C in (e)	0.275	0.000	0.000

Fig. Ā.8

HEXAGONAL $Mn_{23}C_6$ STRUCTURE.

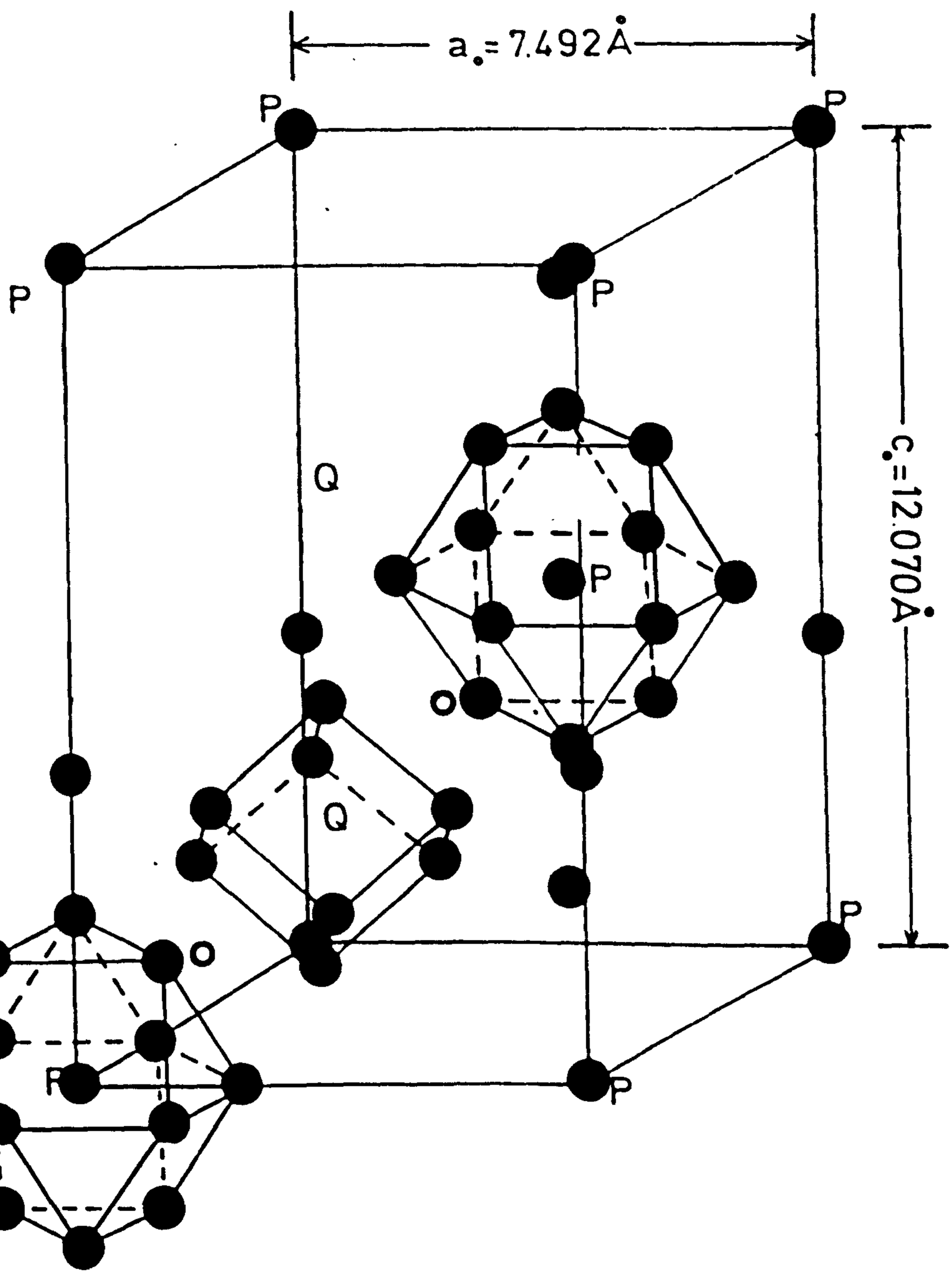

● Manganese. O Carbon.
(in square antiprism interstices.)

Table A.8

Atomic parameters for initial transformed structure ($Mn_{23}C_6$)

Space group P3ml; 2 formula units per unit cell.

(see ›International Tables, 1962; No.164)

Atom	x	y	z	$\frac{U_{iso.}}{\mu^2}$ * ($Å^2$)
2Mn in (d)	0.333	0.666	0.250	0.02
2Mn in (d)	0.333	0.666	0.875	0.02
2Mn in (d)	0.333	0.666	0.625	0.02
2Mn in (c)	0.000	0.000	0.172	0.02
2Mn in (c)	0.000	0.000	0.328	0.02
6Mn in (i)	0.222	0.778	0.083	0.02
6Mn in (i)	0.444	0.556	0.417	0.02
6Mn in (i)	0.153	0.847	0.559	0.02
6Mn in (i)	0.153	0.847	0.059	0.02
12Mn in (j)	0.333	0.000	0.250	0.02
6C in (i)	0.150	0.850	0.112	0.01
6C in (i)	0.150	0.850	0.612	0.01

* isotropic temperature factors are assumed.

Table A.9

Observed and calculated structure factors for initial transformed structure ($Mn_{23}C_6$)

CrKα radiation

Line No.	{hkl}	$F_{obs.}$	$F_{calc.}$
1	110	5.40	1.49
2	103	2.02	1.84
	$10\bar{3}$	2.48	2.27
3	200	3.70	8.21
4	201	5.13	15.17
	$20\bar{1}$	1.69	4.77
5	$20\dot{2}$	3.43	28.32
	$20\bar{2}$	1.28	10.85
6	203	7.27	11.76
	$20\bar{3}$	8.10	13.10
7	210	2.93	3.95
8	211	13.62	9.86
	$21\bar{1}$	2.57	1.86
9	114	17.01	16.08
10	105	12.52	12.41
	$10\bar{5}$	10.27	10.17
11	212	9.51	9.39
	$21\bar{2}$	8.09	7.98
12	204	8.46	21.60
	$20\bar{4}$	7.32	18.84
13	300	18.94	17.24
14	213	20.08	11.78
	$21\bar{3}$	19.17	11.25
15	302	28.12	23.28
	$30\bar{2}$	49.43	40.95

Table A.9 (continued)

Line No.	{hkl}	$F_{obs.}$	$F_{calc.}$
16	006	52.54	43.16
17	106	7.61	5.16
	$10\bar{6}$	18.60	12.61
	205	18.77	12.73
	$20\bar{5}$	3.79	2.57
18	214	7.50	11.41
	$21\bar{4}$	5.14	7.73
	303	0.02	0.02
	$30\bar{3}$	0.23	0.27
19	220	22.46	21.38
20	310	7.39	6.92
21	222	19.71	12.99
22	311	12.43	8.07
	$31\bar{1}$	5.49	3.55
23	116	16.09	12.90
24	304	30.11	20.78
	$30\bar{4}$	11.72	8.07
25	312	0.26	0.17
	$31\bar{2}$	5.63	3.62
	215	11.43	7.35
	$21\bar{5}$	2.89	1.86
26	206	0.42	0.99
	$20\bar{6}$	8.32	17.95
27	107	1.49	0.99
	$10\bar{7}$	4.92	3.27

Table A.9 (continued)

Line No.	{hkl}	$F_{obs.}$	$F_{calc.}$
28	313	3.57	7.79
	$31\bar{3}$	3.31	7.22
29	400	7.43	3.51
30	401	17.12	7.36
	$40\bar{1}$	1.77	0.72
31	224	14.43	10.86
32	402	0.06	0.15
	$40\bar{2}$	3.74	9.60
33	216	0.32	0.58
	$21\bar{6}$	4.25	7.56
34	207	5.95	8.55
	$20\bar{7}$	1.43	2.05
35	403	4.67	9.47
	$40\bar{3}$	4.28	8.68
36	321	5.25	4.84
	$32\bar{1}$	2.06	1.79
	306	1.38	1.27
	$30\bar{6}$	4.22	3.99
37	322	0.18	0.45
	$32\bar{2}$	1.46	3.69
	315	3.18	8.01
	$31\bar{5}$	0.55	1.39
38	412	1.03	2,57
	$41\bar{2}$	1.64	3.96
39	226	0.89	0.89
	208	0.57	0.57
	$20\bar{8}$	2.88	2.88

Table A.9 (continued)

Line No.	{hkl}	$F_{obs.}$	$F_{calc.}$
40	307	0.24	0.07
	$30\bar{7}$	0.46	0.13
	$40\bar{5}$	19.27	5.47
	$40\bar{5}$	3.41	0.97
41	109	6.35	6.04
	$10\bar{9}$	6.62	6.30
43	501	2.73	1.83
	$50\bar{1}$	8.96	5.98
44	414	6.29	4.83
	$41\bar{4}$	13.73	11.96
45	502	5.87	4.70
	$50\bar{2}$	11.12	8.91
	325	9.19	7.36
	$32\bar{5}$	6.27	5.02
46	330	33.11	27.84
47	308	16.20	10.78
	$30\bar{8}$	35.28	27.28
48	420	3.00	5.79
	332	5.01	9.67
	415	1.22	2.26
	$41\bar{5}$	0.35	0.64
49	421	1.30	2.50
	$42\bar{1}$	0.39	0.76
50	00,10	3.06	14.46
	422	2.08	9.68
	$42\bar{2}$	0.09	0.59

Fig. A.9

HEXAGONAL $Mn_{22}C_6$ STRUCTURE.

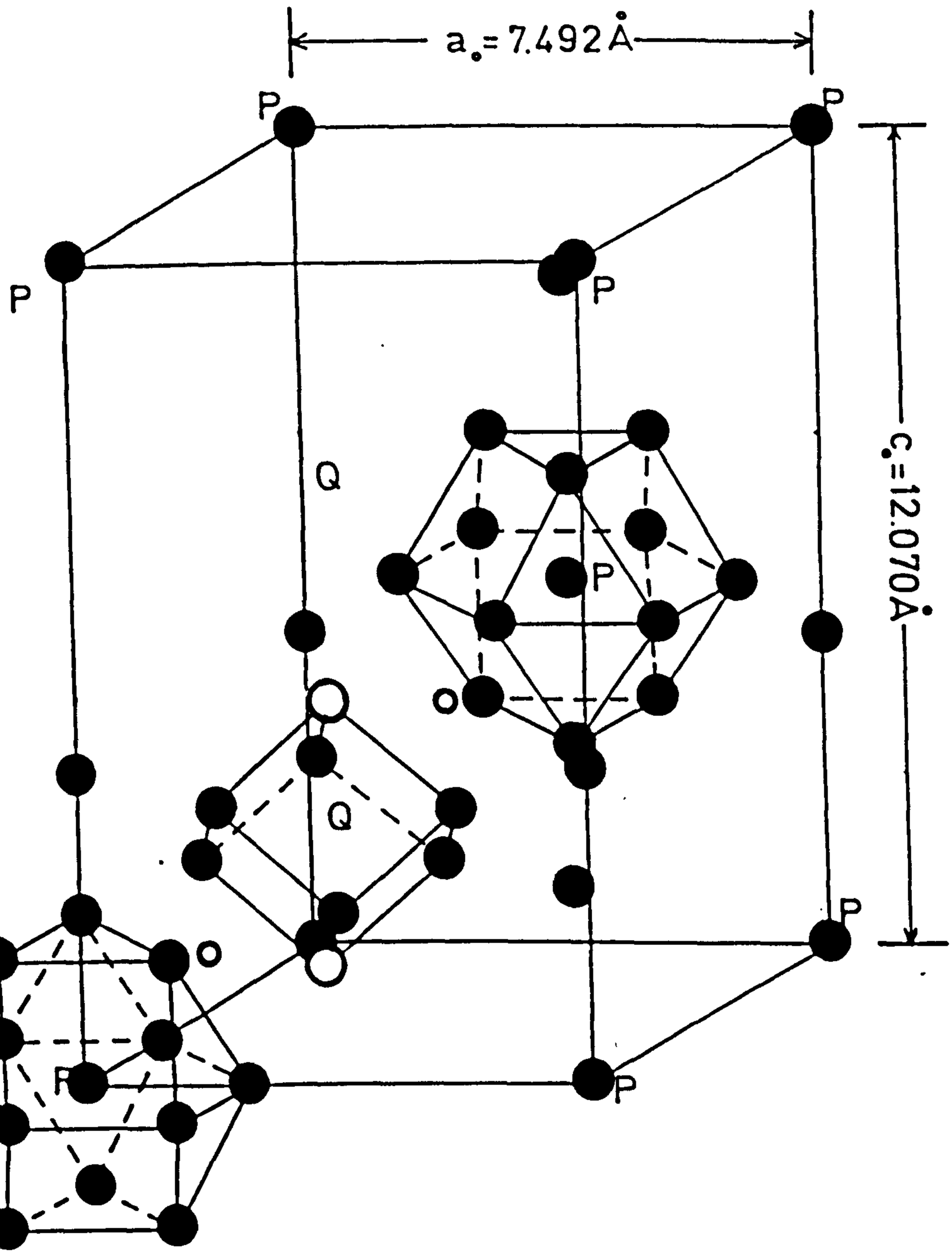

○● Manganese. O Carbon.
(in square antiprism interstices.)

Table A.10

Initial atomic parameters for $Mn_{23}C_6$ hexagonal structure

Space group $P6_3/mmc$; 2 formula units per unit cell.

(see International Tables, 1962; No.194)

Atom	x	y	z	$U_{iso}^{*} = \bar{\mu}^{2}$ ($Å^2$)
2Mn in (c)	0.333	0.667	0.250	0.02
4Mn in (e)	0.000	0.000	0.172	0.02
4Mn in (f)	0.333	0.667	0.635	0.02
12Mn in (j)	0.333	0.000	0.250	0.02
12Mn in (k)	0.444	0.889	0.417	0.02
12Mn in (k)	0.153	0.307	0.559	0.02
12C in (k)	0.150	0.300	0.112	0.01

* isotropic temperature factors are assumed.

With this evidence, together with the smaller observed c-dimension of the actual cell compared to that calculated from the unit cell dimension of cubic $Mn_{23}C_6$, they suggested that two of the four sites (f) were vacant giving a composition $Mn_{22}C_6$. The basis of this conclusion is in fact in error because the manganese atoms in the special positions (f) are an acceptable distance apart, 3.02 Å, whereas the two pairs of atoms in special positions (e) i.e. those atoms at the top and bottom of the "transformed"cubes" are apparently much closer (1.88 Å) than their radii sum.

Possible structures have been considered by placing manganese atoms in each set of sites (e) and (f) in three ways:

(i) as four atoms in four sites,

(ii) "collapsed" to give two atoms in two sites,

and (iii) removed from the structure.

Where initial agreement between observed and calculated structure amplitudes was reasonable, refinement of the parameters was attempted and the R-factors for these possible structures are shown in Table A.11. Structures (i), (ii) and (iii) give the lowest R, but as discussed above, (i) and (iii) are less feasible structures due to the overlapping of manganese atoms in the 4-fold positions (e). The structure is therefore probably that shown in Figure A.9 with the two of the four manganese atoms shown as open circles removed and the remaining two atoms moved to the 2-fold positions (0,0,0.25) and (0,0,0.75). The resultant $Mn_{22}C_6$ structure is in reasonable agreement with the observed analytical, metrical and density measurements shown in Table A.12.

The X-ray data for $Mn_{22}C_6$ is given in Table A.13 followed by the atomic parameters (Table A.14) and the observed and calculated intensities in Table A.15. Although the R-factor is large, the comparison of observed and calculated intensities shown in Figure A.10 indicates that the suggested atomic arrangement must be near to, if not exactly the same as, the actual crystal structure.

The diffuse nature of the reflexions, together with the resultant

Table A.11

R-factors for different postulated structures

(for all structures, carbon atoms not refined)

composition	changes from parameters shown in Table A.5.	R (all planes)		R (sharp lines)	
		initial	after refinement	initial	after refine-ment
(i) $Mn_{23}C_6$	none	0.29	0.22	0.18	0.13
(ii) $Mn_{22}C_6$	4Mn in (e) removed 2Mn added in (d)	0.28	0.26	0.23	0.15
(iii) $Mn_{22}C_6$	4Mn in (f) removed 2Mn added in (b)	0.31	0.33	0.21	0.18
(iv) $Mn_{21}C_6$	as (ii) plus 2Mn in (c) removed	0.36	———	———	———
(v) $Mn_{21}C_6$	as (iii) plus 2Mn in (c) removed	0.44	———	———	———
(vi) $Mn_{20}C_6$	as (ii) plus 4Mn in (f) removed 2Mn added in (b)	high R-factor			
(vii) $Mn_{21}C_6$	4Mn in (e) removed	0.31	———	0.29	———
(viii) $Mn_{21}C_6$	4Mn in (f) removed	high R-factor unlikely on packing considerations			
(ix) $Mn_{22}C_6$	2Mn in (c) removed	high R-factor			
(x) $Mn_{21}C_6$	12Mn in (k) at (0.444,0.889, 0.417) etc. moved to (0,111,0.889,0.417); etc. - 4Mn in (f) removed	0.60 corresponds to conversion of cubic atomic arrangement to octahedra.			

Table A.12

Observed and calculated data for $Mn_{22}C_6$

	Observed	Calculated
Unit cell dimensions, Å	a = 7.492; c = 12.090	a = 7.503; c = 12.252[+]
Density, $g.ml^{-1}$	7.30 + 0.05[*]	7.29
Composition, wt.%C	5.48 + 0.01[*]	5.62

+ calculated from f.c.c. $Mn_{23}C_6$ a = 10.61 Å.

* from Bouchaud and Fruchart (1964).

Table A.13

X-ray data for $Mn_{22}C_6$

(corrected for absorption)

Hexagonal a = 7.492; c = 12.070 Å

FeKα radiation: $K\alpha_1$ = 1.9360; $K\alpha_2$ = 1.9399; Kα = 1.9373.

Line No.	I obs.	$\sin^2\theta$ obs.	$\sin^2\theta$ calc.	{hkl}
1	m	0.0665	0.0669	110
2	w	0.0803	0.0802	103
3	vw	0.0924	0.0926	200
4	vw	0.0955	0.0956	201
5	w	0.1144	0.1149	202
6	m	0.1465	0.1471	203
7	vw	0.1561	0.1560	210
8	ms	0.1622	0.1624	211
9	s	0.1696	0.1698	114
10	m	0.1823	0.1817 0.1830	212 105
11	mw	0.1920	0.1921	204
12	m	0.2002	0.2006	300
13	vw	0.2046	0.2070	301
14	s	0.2140	0.2139	213
15	vs	0.2259	0.2263	302
16	s	0.2314	0.2315	006
17	m	0.2502	0.2499 0.2538	205 106
18	w	0.2591	0.2585 0.2589	303 214
19	s	0.2671	0.2675	220
20	w	0.2895	0.2898	310

Table A.13 (continued)

Line No.	I obs.	$\sin^2\theta$ obs.	$\sin^2\theta$ calc.	{hkl}
21	s	0.2929	0.2932	222
22	m	0.2960	0.2962	311
23	m	0.2984	0.2984	116
24	s	0.3035	0.3035	304
25	vw	0.3162	0.3155	312
			0.3167	215
26	mw	0.3205	0.3207	206
27	vw	0.3385	0.3374	107
28	vw	0.3479	0.3477	313
29	vw	0.3558	0.3566	400
30	w	0.3629	0.3630	401
31	ms	0.3699	0.3684	224
32	vw	0.3815	0.3820	117
			0.3823	402
33	vw	0.3877	0.3875	216
34	mw	0.4048	0.4043	207
35	mw	0.4141	0.4145	403
36	mw	0.4301	0.4299	321
			0.4321	306
37	vw	0.4502	0.4492	322
			0.4505	315
38	vw	0.4936	0.4938	412
39	vw	0.5005	0.4990	226
			0.5007	208
40	m	0.5176	0.5157	307
			0.5173	405

Table A.13 (continued)

Line No.	I obs.	$\sin^2\theta$ obs.	$\sin^2\theta$ calc.	{hkl}
41	vw	0.5441	0.5431	109
42	vw	0.5569	0.5573	500
43	vw	0.5629	0.5637	501
44	m	0.5710	0.5710	414
45	mw	0.5845	0.5830	502
			0.5842	325
46	s	0.6018	0.6018	330
			0.6049	317
47	s	0.6128	0.6100	209
			0.6121	308
48	vw	0.6239	0.6241	420
			0.6275	332
49	vw	0.6314	0.6288	415
			0.6305	421
50	vw	0.6439	0.6430	00,10
51	vw	0.6508	0.6498	422
52	vw	0.6593	0.6550	326
			0.6597	333
			0.6602	504
53	vw	0.6649	0.6653	10,10
54	w	0.6721	0.6717	407
55	ms	0.6795	0.6790	228
			0.6820	423
56	ms	0.6995	0.6996	416
			0.7013	318
57	vw	0.7100	0.7099	11,10
58	vw	0.7179	0.7180	505

Table A.13 (continued)

Line No.	I obs.	$\sin^2\theta$ obs.	$\sin^2\theta$ calc.	{hkl}
59	vw	0.7265	0.7270	424
60	vw	0.7324	0.7322	20,10
61	vw	0.7378	0.7386	327
62	vw	0.7495	0.7489	513
63	vw	0.7684	0.7681	408
64	ms	0.7860	0.7832	417
			0.7848	425
65	s	0.8024	0.8024	600
66	vw	0.8114	0.8106	319
67	m	0.8280	0.8281	602
68	m	0.8312	0.8311	431
69	s	0.8337	0.8333	336
70	m	0.8448	0.8449	11,11
71	w	0.8692	0.8672	20,11
72	s	0.9055	0.9053	604

Table A.14

Atomic parameters for $Mn_{22}C_6$-

Space group $P6_3/mmc$; 2 formula units per unit cell.
(see International Tables, 1962; No.194)

Atom	x	y	z	$= \frac{U_{iso}}{\mu^2}$ * $(\text{Å})^2$
2Mn in (c)	0.333	0.667	0.250	0.02
2Mn in (d)	0.000	0.000	0.250	0.02
4Mn in (f)	0.333	0.667	0.625	0.02
12Mn in (j)	0.333	0.000	0.250	0.02
12Mn in (k)	0.444	0.889	0.417	0.02
12Mn in (k)	0.153	0.307	0.559	0.02
12C in (k)	0.150	0.300	0.112	0.04

* isotropic temperature factors are assumed.

Table A.15

Observed and calculated intensities for $Mn_{22}C_6$.

CrKα radiation. S=sharp; D=diffuse; -=weak or overlapping lines.

Line No.	{hkl}	line breadth	I obs.	I calc.
1	110	S	5.91	9.93
2	103	-	2.00	0.41
3	200	-	2.60	0.89
4	201	-	5.59	5.17
5	202	-	2.49	8.47
6	203	D	21.59	32.47
7	210	-	2.07	17.06
8	211	D	104.22	78.66
9	114	S	69.35	48.84
10	105	-	96.68	14.74
	212	-		17.68
11	204	D	22.29	0.12
12	300	S	64.55	40.86
13	301	-	22.35	21.18
14	213	D	279.06	410.93
15	302	S	588.38	502.65
16	006	S	168.12	223.53
17	106	-	161.80	1.00
	205	-		214.39
18	214	-	30.45	39.40
	303	-		56.30
19	220	S	129.28	96.47
20	310	S	20.71	74.27
21	222	S	148.06	106.14
22	311	-	70.70	1.96

Table A.15 (continued)

Line No.	{hkl}	line breadth	I obs.	I calc.
23	116	S	99.15	22.23
24	304	S	200.97	191.58
25	312	-	66.77	30.03
	215	-		30.81
26	206	-	13.72	14,47
27	107	-	5.30	9.64
28	313	-	9.62	28.79
29	400	-	11.40	72.84
30	401	-	41.00	2.97
31	224	S	87.54	40.61
32	402	-	5.82	35.60
33	216	-	7.63	2.89
34	207	-	8.86	41.88
35	403	-	9.05	7.39
36	321	-	16.05	1.86
	306	-		33.49
37	322	-	6.12	3.08
	315	-		8.09
38	412	-	2.05	0.01
39	226	-	2.96	18.01
	208	-		4.44
40	307	-	111.63	46.36
	405	-		71.34
41	109	-	26.80	26.50
42	500	-	8.60	17.28
43	501	-	30.10	30.80

Table A.15 (continued)

Line No.	{hkl}	line breadth	I obs.	I calc.
44	414	S	161.53	63.78
45	502	D	152.52	18.83
	325	D		46.69
46	330	S	497.61	384.60
	317	-		1.04
47	308	S	658.18	623.31
	209	-		18.73
48	420	-		103.29
	332	-		115.00
49	415	-	344.54	26.63
	421	-		30.06
50	00,10	-	65.75	58.27

Fig A. 10

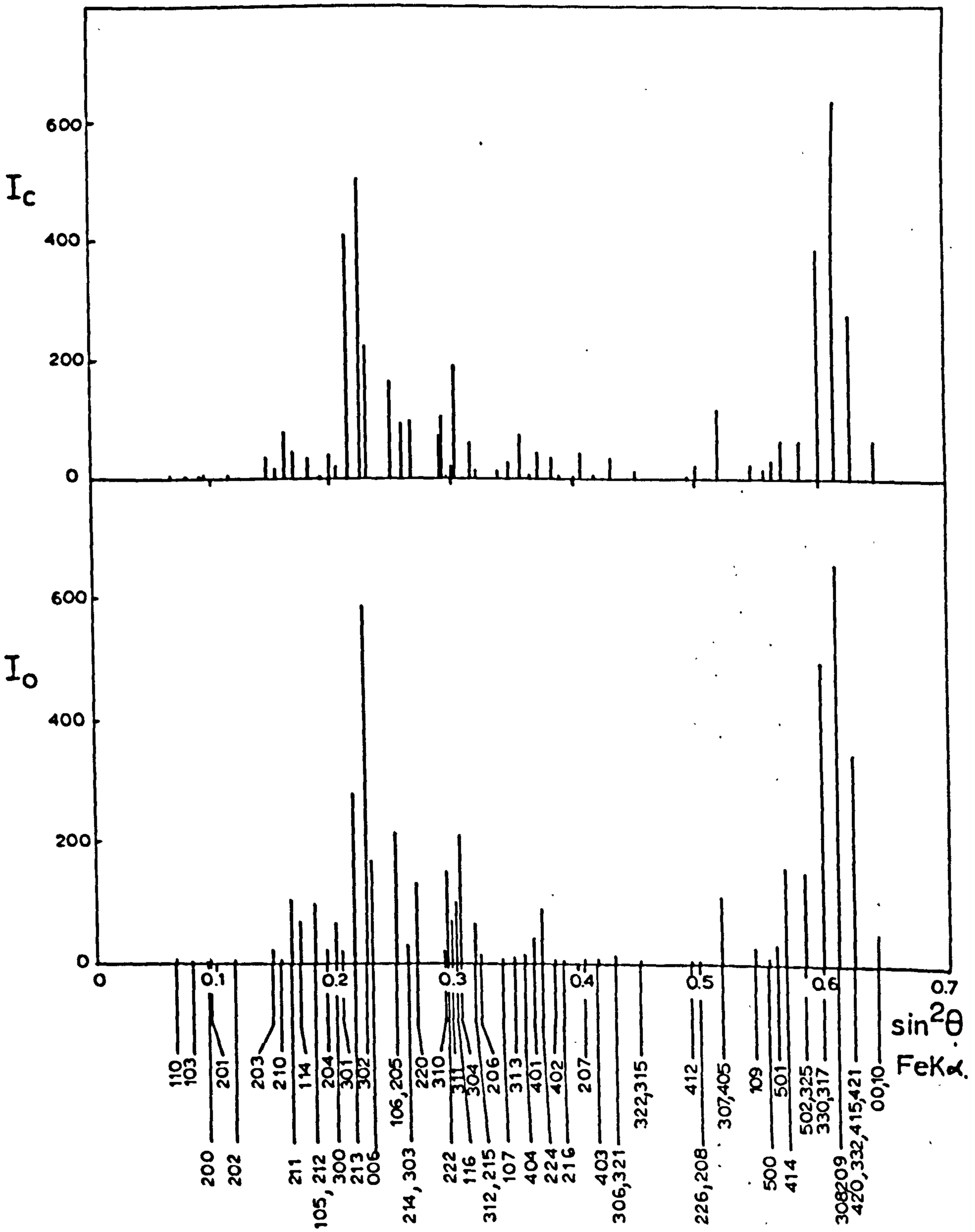

COMPARISON OF OBSERVED AND CALCULATED

INTENSITIES FOR $Mn_{22}C_6$

overlapping lines, introduces larger errors than usual in the measurement of intensities. An additional possible contribution to the error may be the presence of interstitial oxygen.

A.7 Characterization of stacking disorder

The mixture of sharp and diffuse reflexions observed on X-ray powder photographs of $Mn_{22}C_6$ suggest some kind of stacking disorder. The indices of the diffuse reflexions are:

$$(h - k) \neq 3n \qquad \text{when} \qquad l \neq 0$$

where n is zero or any integer; this is consistent with successive blocks of crystal with different stacking sequences along the c-axis

ABAB...., ACAC.... and BCBC....

where A, B and C are layers containing half the unit cell contents. The resultant regions of perfect crystallinity are then plate-like in character, but reflexions of the type 00l are not affected since the atomic layers along [00l] are perfectly regular over the whole crystal. The diffuse reflexions arise because in specific directions the faults break up the crystal into domains and the broadening can be considered as due to the small size of these regions of perfect order.

The stacking disorder is similar in character to that observed in close-packed hexagonal cobalt metal (Edwards & Lipson, 1942). Many treatments of stacking disorder are known (Warren, 1941; Barrett, 1950; Anantharaman & Christian, 1956; Averbach & Warren, 1949) and the scattering from such faulted crystals is calculated using a statistical method. The probability that any two phases in the stacking sequence are the same, when chosen at random, is calculated and the values are incorporated in the usual expression for scattering from a unit cell (Equation A.2).

Wilson's treatment (1942) gives the integral breadth, M, of a broadened line as:

$$M = 2(1 - p) / (1 + p)$$

p is either p_e for l even or $-p_o$ for l odd, with

$$p_e = \left\{ -\alpha + \sqrt{(4 - 8\alpha + \alpha^2)} \right\} / 2$$

and

$$p_o = -\left\{ \alpha + \sqrt{(4 - 8\alpha + \alpha^2)} \right\} / 2$$

where α is the chance of a fault at any plane.

The even lines are therefore considerably broader than the odd lines, for

$$M_e / M_o = (1 - p_e)(1 - p_o) / (1 + p_e)(1 + p_o) = 3$$

when α is small.

Application of this argument to the present type of fault suggests that the integral breadths of the broadened lines (hkl) where l is even should be 3 times greater than for those reflexions with l odd. This would result in different apparent block sizes (Equation A.6) for l odd and l even reflexions and such values calculated for $Mn_{22}C_6$ and shown in Table A.16 are reasonably consistent with these theoretical predictions.

Table A.16

Block size determination for $Mn_{22}C_6$-

Line No.	hkl	$\cos\theta$	$\cos\psi$	β	t_{app} (Å)
6	203	.0.8914	0.6282	0.00484	338
8	211	0.8781	0.1991	0.00298	175
10^x	105	0.8628	0.9374	0.01061	236
14	213	0.8372	0.5205	0.00762	188
30	401	0.7015	0.1332	0.00232	188
40^x	405	0.5249	0.5578	0.01220	202
45	325	0.4267	0.5246	0.01384	207
11	204	0.8548	0.7314	0.00239	905
18^x	214	0.7984	0.6308	0.00315	586

x possible large error due to overlapping of reflexions.

References

Adcock, F. 1926, J.I.S.I. II, 117.

Adcock, F. 1931, J.I.S.I. 124, 99.

Anantharaman, T.R. & Christian, J.W. 1956, Acta. Cryst. 9, 479.

Averbach, B.L. & Warren, B.E. 1949, J. Applied Phys. 20, 1066.

Baird, J.D. & Jamieson, A. 1963, N.P.L. Symposium No.15.

Baird, J.D. & Jamieson, A. 1966, J.I.S.I. 204, 793.

Baird, J.D. & Mackenzie, C.R. 1964, J.I.S.I. 202, 427.

Barrett, C.S. 1950, Trans. A.I.M.E. 188, 123.

Berry, F.G. & Honeycombe, R.W.K. 1970, Met. Trans. 1, 3279.

Blix, R. 1926, Z. Phys. Chem. B3, 229.

Booker, G.R., Norbury, J. & Sutton, A.L. 1957, J.I.S.I. 187, 205.

Bouchaud, J.-P., Fruchart, R. 1964, Bull. Soc. Chim. Fr., 1579.

Bouchaud, J.-P. 1967, Ann. Chim. 2, 353.

Brunhauer, S., Jefferson, M.E., Emmett, P.H. & Hendricks, S.B. 1931, J. Am. Chem. Soc. 53, 1778.

Colbeck, E.W. & Garner, R.P. 1939, J.I.S.I. 139, 99.

Corney, N.S. & Turkdogan, E.T. 1955, J.I.S.I. 180, 344.

Cook, A.J. & Jones, F.W. 1943, J.I.S.I. 148, 217.

Cruikshank, D.W.J. 1964 unpublished.

Darken, L.S. 1958, N.P.L. Symposium, No.9.

Darken, L.S. & Wriedt, H.A. unpublished work, U.S. Steel Corp. Research Laboratory.

Dijkstra, L.J. 1949, Trans. A.I.M.E. 224, 1119.

Duggin, M.J., Cox, D. & Zwell, L. 1966, Trans. A.I.M.E., 236, 1342.

Duggin, M.J. 1967, Nature 216, 362.

Duggin, M.J. 1969, Trans. A.I.M.E. 245, 1347.

Edwards, O.S. & Lipson, H. 1942, Proc. Roy. Soc. (A), 180, 268.

Eriksson, S. 1934, Jernkont. Ann. 118, 530.

Forrest, P.G. & Hopkins, L.M.T. 1963, N.P.L. Symposium No.15.

Franks, R. 1935, Trans. A.S.M. 23, 968.

Fruchart, R., Audière, J.P. & Michel, A. 1968, C.R.Ac.Sc.Fr. 266, 1691.

Gibson, J. 1946, J.Sci. Instrum. 23, 159.

Grieveson, P. & Turkdogan, E.T. 1964, Trans. A.I.M.E. 230, 1604.

Grozier, J.D., Paxton, H.W. & Mullins, W.W. 1963, National Science Foundation Report No.G19748.1.

Hägg, G. 1930, Z. Physik. Chem. (B), 11, 152.

Hale, K.F. & McLean, D. 1963, J.I.S.I. 201, 337.

Hansen, M. 1958, "Constitution of Binary Alloys", McGraw-Hill.

Heal, T.J. & Hardy, H.K. 1954, Progr. Metal. Phys. 5, 143.

Hepworth, M.T., Smith, R.P. & Turkdogan, E.T. 1965, Trans. A.I.M.E. 236, 1278.

Hopkin, L.M.T. 1965, J.I.S.I. 203, 583.

Hrivnak, I. 1961, Met. Treatment, 28, 175 & 233.

Hume-Rothery, W. & Pearson, W.B. 1949, J. Inst. Metals 76, 722.

Irani, J.J. & Honeycombe, R.W.K. 1965, J.I.S.I. 203, 826.

Jack, K.H. 1948, Proc. Roy. Soc. (A), 195, 34.

Jack, K.H. 1951a, Proc. Roy. Soc. (A), 208, 200.

Jack, K.H. 1951b, Proc. Roy. Soc. (A), 208, 216.

Jack, K.H. 1964, Unpublished work, University of Newcastle.

Jack, K.H. & Maxwell, D. 1952, J.I.S.I. 170, 254.

Jack, K.H. & Wild, S. 1966, Nature 212, 248.

Jeannin, Y., Mannerskantz, C. & Richardson, F.D. 1963, Trans. A.I.M.E. 227, 300.

Jones, F.W. 1938, Proc. Roy. Soc. (A), 166, 16 & 376.

Keh, A.S. & Wriedt, H.A. 1962, Trans. A.I.M.E. 224, 560.

Kindlemann, L.E. & Ansell, G.S. 1970, Met. Trans. 1, 163.

Krivobok, V.N. 1935, Trans. A.S.M. 23, 1.

Kubachewski, O. & Evans, E.H. 1958, "Metallurgical Thermodynamics" Pergamon Press, 240.

Kunitake, T. & Paxton, H.W. 1960, Trans. A.I.M.E. 218, 1003.

Kuo, K. & Persson, L.E. 1954, J.I.S.I. 178, 39.

Lagneborg, R. 1967, Trans. A.S.M. 60(1), 67.

Lehrer, E. 1930, Z.Electrochem. 36, 460.

Leslie, W.C. 1964, "nitrogen in ferrite steels", Unpublished, work, U.S. Steel Corp. Fundamental Research Laboratory.

Mehr, R.F., Barratt, C.S. & Jerabeck, H.S. 1934, Trans. A.I.M.E. 113, 211.

Nicholson, R.B., Thomas, G. & Nutting, J. 1958-59, J. Inst. Metals. 203, 826.

Paranjpe, V.G., Cohen, M., Bevers, M.B. & Floe, C.F. 1950, Trans. A.I.M.E. 188, 261.

Pearson, J. & Ende, U.J.C. 1953, J.I.S.I. 175, 52.

Pipkin, N.J. 1967, Ph.D. Thesis, University of Newcastle upon Tyne.

Picon, M. & Flahaut, J. 1957, Compt. Rend. 245, 534.

Roberts, W. 1970, Ph.D. Thesis, University of Newcastle upon Tyne.

Sano, K. 1937, J. Chem. Soc. Japan 58, 981.

Schönberg, N. 1954, Acta. Chem. Scand. 8, 213.

Schwartzkopf, P. & Keiffer, R. 1953, "Refractory Hard Metals", Macmillan Press.

Seitz, F. 1943, "The Physics of Metals", McGraw-Hill.

Seybolt, A.U. & Oriani, R.A. 1956, Trans. A.I.M.E. 206, 556.

Smith, G.V., Macmillan, J.A. & Dulis, E.J. 1951, Trans. A.S.M. 43, 692.

Spiers, D.L. 1969, Ph.D. Thesis, University of Newcastle upon Tyne.

Stephenson, A. 1970, Unpublished work, University of Newcastle upon Tyne.

Tanner, L.E. 1966, Phil. Mag. 14, 111.

Taylor, A. 1951, J. Sci. Instrum. 28, 200.

Turkdogan, E.T. 1963, Unpublished work, U.S.Steel Corp. Fundamental Research Laboratory.

Turkdogan, E.T. & Ignatowicz, S. 1957, J.I.S.I. 185, 200.

Turkdogan, E.T. & Ignatowicz, S. 1958, J.I.S.I. 188, 242.

Warren, B.E. 1941, Phys. Rev., 59, 693.

Wert, C.A. 1949, J. Appl. Phys. 20, 943.

Westgren, A. 1933, Jernkont Ann. 117, 501.

Wilson, A.J.C. 1942, Proc. Roy. Soc. (A), 180, 277.